Disrupted propionate metabolism evokes transcriptional changes in the heart by increasing histone acetylation and propionylation

Kyung Chan Park[1], Nicholas T. Crump[2#], Niamh Louwman[1], Steve Krywawych[3], Yuen Jian Cheong[4], Iolanda Vendrell[5,6], Eleanor K. Gill[1], Mala Gunadasa-Rohling[1], Kerrie L. Ford[1], David Hauton[7], Marjorie Fournier[8], Elisabete Pires[7], Lydia Watson[1], Gerald Roseman[1], James Holder[8], Andreas Koschinski[1], Ricardo Carnicer[9], M. Kate Curtis[1], Manuela Zaccolo[1], Alzbeta Hulikova[1], Roman Fischer[5,6], Holger Kramer[10∞], James McCullagh[7], Sophie Trefely[4], Thomas A. Milne[2], Pawel Swietach[1]

1. Department of Physiology, Anatomy & Genetics, University of Oxford, Sherrington Building, Parks Road, Oxford, OX1 3PT, UK.
2. MRC Molecular Haematology Unit, MRC Weatherall Institute of Molecular Medicine, Radcliffe Department of Medicine, University of Oxford, Oxford, OX3 9DS, UK.
3. Department of Chemical Pathology, Great Ormond Street Hospital NHS Foundation Trust, Great Ormond Street, London, WC1N 3JH, UK.
4. Epigenetics & Signalling Programmes, Babraham Institute, Cambridge, CB22 3AT, UK.
5. Target Discovery Institute, Nuffield Department of Medicine, Roosevelt Drive, Oxford, OX3 7FZ, UK.
6. Chinese Academy for Medical Sciences Oxford Institute, Nuffield Department of Medicine, University of Oxford, Roosevelt Drive, Oxford, OX3 7FZ, UK.
7. Department of Chemistry, University of Oxford, Mansfield Road, Oxford, OX1 3TA, UK.
8. Department of Biochemistry, Parks Road, Oxford, OX1 3QU, UK.
9. Division of Cardiovascular Medicine, Radcliffe Department of Medicine, University of Oxford, Oxford, OX3 9DU, UK.
10. MRC Laboratory of Molecular Biology, Francis Crick Avenue, Cambridge Biomedical Campus, Cambridge, CB2 0QH, UK.

[#]*Current address:* Hugh and Josseline Langmuir Centre for Myeloma Research, Centre for Haematology, Department of Immunology and Inflammation, Imperial College London, London, W12 0NN, UK.

∞Deceased

**Corresponding author.* Email: pawel.swietach@dpag.ox.ac.uk ; Address: Department of Physiology, Anatomy & Genetics, Sherrington Building, Parks Road, Oxford, OX1 3PT, UK.

Running title: Propionate-sensitive cardiac epigenetic changes

ABSTRACT

Propiogenic substrates and gut bacteria produce propionate, a post-translational protein modifier. Here, we use a mouse model of propionic acidaemia (PA) to study how disturbances to propionate metabolism result in histone modifications and changes to gene expression that affect cardiac function. Plasma propionate surrogates were raised in PA mice, but female hearts manifested more profound changes in acyl-CoAs, histone propionylation and acetylation, and transcriptional changes. These resulted in moderate diastolic dysfunction with raised diastolic [Ca^{2+}], expanded end-systolic ventricular volume, and reduced stroke volume. Propionate was traced to histone H3 propionylation and caused increased acetylation genome-wide, including at promoters of *Pde9a* and *Mme*, genes related to contractile dysfunction through down-scaled cGMP signalling. The less severe phenotype in male hearts correlated with β-alanine build-up. Raising β-alanine in cultured myocytes treated with propionate reduced propionyl-CoA levels, indicating a mechanistic relationship. Thus, we link perturbed propionate metabolism to epigenetic changes that impact cardiac function.

INTRODUCTION

Post-translational modifications (PTMs) of histone lysine residues can change chromatin structure and gene transcription[1]. A well-studied histone modification is acetylation[2], which plays a prominent role in cardiac development[3], responses to environmental triggers[4], and cardiac disease[5,6]. Propionate, the three-carbon homologue of acetate, can also modify histones, but its metabolic supply-lines are more restricted and less is known about its significance in the heart. Sources of propionate include the catabolism of odd-numbered fatty acids and branched-chain amino acids (BCAAs)[7], and the activity of gut bacteria[8], but whether this is sufficient to evoke epigenetic changes in the heart remains elusive. Propionyl-CoA has been shown to propionylate histones in cultured cells[9,10] and in the liver[11] and brain[12] *in vivo*, though its cardiac actions remain unclear. Propionyl-CoA may also increase histone acetylation by activating the acetyltransferase p300[13] or through the inhibitory effect of propionate on histone deacetylases (HDACs), akin to that of butyrate[8,14,15].

The link between propionate and cardiac dysfunction can be interrogated by studying propionic acidaemia (PA), an inborn error of metabolism. In PA, loss-of-function mutations in *PCCA* or *PCCB* genes result in reduced or absent propionyl-CoA carboxylase (PCC) activity[7], which hinders propionyl-CoA catabolism. Increased bio-availability of propionyl-CoA/propionate may potentially act as a substrate for[10,16] or inducer of[14,17,18] histone acylation[13]. PA patients commonly develop cardiac dysfunction, characterised by dilated cardiomyopathy and long-QT arrythmias[19], which have been discussed in terms of toxicity and mitochondrial dysregulation[20], but a role for epigenetic changes cannot be excluded. Establishing a link between propionyl-CoA and gene expression would add a new and important axis to our understanding of cardiometabolic disease, ranging from other inborn errors of metabolism[21] (e.g. methylmalonic acidaemia)[19] to diabetes[22].

We studied mice with genetically-altered PCC activity (FVB *Pcca*$^{-/-}$ A138T)[23], wherein the murine *Pcca* gene was knocked-out and a hypomorphic human mutant (*PCCA* A138T) was inserted. This hypomorphic model maintains an elevated propionyl-CoA load and has been used to study a mild-to-moderate form of PA because, unlike complete knock-outs[24], it supports growth into adult life[23], which is essential for understanding phenotype at organism-level. Previous studies described this mouse as having dysregulated Ca^{2+} handling and diastolic impairment at 8 months of age, attributing these changes to cumulative oxidative damage and micro-RNA dysregulation[25]. We used young adult mice to investigate epigenetic responses because, by this age, PA markers[26] stabilise at an elevated level and epigenetic

changes are expected, but without the confounding effects of oxidative damage that emerge in later life[27]. We find that a global genetic disruption to propionate metabolism raises cardiac propionate and propionyl-CoA to levels that cause histone propionylation and a net increase in acetylation *in vivo*. These PTMs are sufficient to trigger a transcriptional response, including the upregulation of genes previously implicated in cardiac dysfunction. We report a sex-dependence in terms of metabolic disturbance that produced a proportionally greater transcriptional and phenotypic response in females. The smaller propionyl-CoA excess in male PA hearts related to higher levels of β-alanine, a rate-limiting precursor of carnosine which serves as a major anti-oxidant in the heart[28]. We speculate a role for these actions in hearts under metabolic stresses that influence propionate metabolism.

RESULTS

Surrogates of propionate metabolism are raised in PA mice

Propionyl-CoA is generated in mitochondria and can be processed to derivatives, including propionyl-carnitine: a commonly used surrogate[26] (**Figure 1A**). These metabolites can interconvert with free propionate anions, which crosses membranes as the acid. We used plasma [propionate] as a proxy of systemic propionate excess to benchmark the PA mouse against human patients. [Propionate] in decompensated PA patients can reach low millimolar levels[29-31], but those with managed disease have considerably lower levels: 67(±41) μM propionate and 23(±8.5) μM propionyl-carnitine (**Figure 1B**). Mouse plasma was prepared from blood freshly collected after the induction of terminal anaesthesia in 8-week PA mice ("amPA"). Measurements indicated 81(±16) μM propionate, i.e. within the range of PA patients and substantially elevated compared to 12(±2.6) μM in wild-type littermates ("amWT"). Free propionate correlated positively with propionyl-carnitine and negatively with acetyl-carnitine (**Figure 1C**). There was no apparent sex-dependence in plasma metabolites, arguing for an equivalent global propionate-load in male and female PA mice.

Cardiac tissue generates propionate derivatives

We performed biochemical analyses on plasma and snap-frozen hearts and livers harvested from amPA and amWT mice. Metabolomic analyses by ion-exchange mass

spectrometry (IC-MS) confirmed the metabolic signature of PA in amPA mice: elevated 2-methylcitrate and *N*-propionylglycine[32] (**Figure 1D/E**), including in the heart (**Figure 1F**). For example, 2-methylcitrate and cis-2-methylaconitate accumulation indicate that propionyl-CoA becomes conjugated to Krebs cycle intermediates in place of acetyl-CoA, raised 3-acetylpropionate and *N*-propionylglycine levels are evidence for chemical conjugation of excess propionate, and the build-up of the oxidised methionine denotes a backlog of this propiogenic amino acid (**Figure 1G**). These observations indicate that the PA mouse heart processes considerable propionate fluxes, which may trigger biological responses within the myocyte.

Propionate metabolism shows sex-dependent differences

Many of the metabolic pathways for propionate involve amino acids, either upstream (e.g. BCAAs) or downstream (e.g. β-alanine/3-aminopropionate). To measure these, we performed metabolomic analyses on paired plasma and cardiac samples using a semi-targeted method that detects derivatised amino acids plus underivatised acyl-carnitines[33] (**Figure 2A/B**). In plasma, seventeen metabolites were significantly affected by PA genotype of which 5 were also significantly affected by sex (**Figure 2A; Supplementary Table 1**). Notable changes included propionyl-carnitine, methionine, aspartate/valine dipeptide (increase), and acetyl-carnitine (decrease) and asparate (decrease in female only; possibly due to aconitase inhibition by 2-methylcitrate)[34] (**Figure 2C**). In cardiac tissue, 137 metabolites were changed in PA, including twenty-two that were sex-dependent and three that showed a significant interaction between sex and genotype (**Figure 2B; Supplementary Table 2**). amPA hearts had significantly increased carnitine conjugates of three or more carbons (propionyl, C4:0, C5:0, C6:0, C7:0; **Figure 2D**). An elevation of the carnitine conjugate of succinate/methylmalonate was also detected in amPA, which is somewhat counterintuitive given that these mice have impaired ability to convert propionyl-CoA to methylmalonate by PCC. amPA hearts also had elevated lysine, tyrosine, GABA, and various dipeptides (**Figure 2D**). Strikingly, only male amPA hearts had raised β-alanine compared to male amWT (**Figure 2D**). PA was associated with higher levels of β-alanine dipeptides anserine and carnosine, but the extent of this was greater in males. Overall, the total cardiac β-alanine content is raised in PA, but more so males.

We then performed metabolomic analyses on cardiac lysates to measure short-chain acyl-CoA (**Figure 2E**). As expected, propionyl-CoA was greatly elevated in PA hearts but its excess was larger in female mice. Female PA hearts had a higher excess of isovaleryl-CoA and (iso)butyryl-CoA, compared to male PA hearts, which could be a consequence of a bottleneck in BCAA catabolism (isobutyryl-CoA from valine and isovaleryl-CoA from leucine). The PA genotype also associated with higher β-hydroxy β-methylglutaryl-CoA (HMG-CoA), an intermediate of leucine catabolism, as well as ketone and mevalonate pathways. We also observed a decrease in glutaryl-CoA in PA, which could relate to a reduction in lysine metabolism, in agreement with raised lysine levels in PA hearts. Collectively, these data demonstrate that disruption of PCC in PA results in sex-dependent differences in propionate metabolism and acyl-CoA handling.

Raising β-alanine lessens propionyl-CoA build-up

We found that the metabolic disturbance associated with propionyl-CoA is less profound in male PA hearts and associates with a higher build-up of β-alanine. This non-proteinogenic amino acid can be synthesised from propionyl-CoA and is the rate-limiting precursor of carnosine and anserine: dipeptides with well-established antioxidant[35] and pH/Ca^{2+} buffering[36] properties in the heart[28]. The lower propionyl-CoA excess in male PA hearts may be explained by augmented production capacity of carnosine; indeed, overexpression of carnosine synthase in mice reduced cardiac propionate levels[35]. Higher levels of β-alanine dipeptides would, in turn, facilitate mitochondrial function and metabolic flows. If β-alanine conferred such protection, then raising its bioavailability in propionate-stressed cells *in vitro* should reduce the propionyl-CoA excess. If, in contrast, β-alanine were merely an 'endpoint' for propionyl-CoA metabolism, then raising intracellular [β-alanine] experimentally would cause propionyl-CoA to build-up.

We tested these models by ^{13}C-tracing experiments in cultured wild-type neonatal rat ventricular myocytes (NRVMs). To determine the concentration of propionate required to raise propionyl-CoA to the range in PA hearts *in vivo*, acyl-CoAs were quantified as a function of [propionate] (**Figure 3A**). 1 mM propionate *in vitro* was determined to match the mid-range of propionyl-CoA in PA hearts. To trace propionate metabolism, exogenous [1-^{13}C]propionate was used. To trace background propionate metabolism without exogenous propionate, isoleucine and valine were replaced with ^{13}C-labelled equivalents. To load cells with β-

alanine, we replaced histidine, an essential amino acid, with carnosine, which forces myocytes to sequester β-alanine. Thus, four conditions were studied: medium with labelled BCAAs (A), medium with labelled BCAAs and histidine replaced with carnosine (B), medium with labelled propionate (C), medium with labelled propionate and histidine replaced with carnosine (D) (**Figure 3B**). We identified a significant rise in labelled isoleucine in conditions A and B, and a rise in labelled propionate in conditions C and D, as well as the emergence of carnosine and β-alanine in conditions B and D, indicating that the loading manoeuvre was successful (**Figure 3B**). Some carnosine was ^{13}C-labelled, indicating that propiogenic substrates or propionate are converted to this dipeptide. The increase in propionate caused a build-up of 2-methylcitrate and a decrease in [citrate], indicating Krebs cycle inhibition (**Figure 3C**). However, β-alanine restored citrate and halved the 2-methylcitrate/citrate ratio[37] (**Figure 3C**). For note, propionate also increased levels of labelled and unlabelled fumarate and malate, indicating recruitment into the Krebs cycle via succinyl-CoA, although this pathway would be inactive in PA.

Additional ^{13}C-tracing experiments confirmed the incorporation of propionate into propionyl-CoA (at carbon-1) and the metabolic processing of BCAA, as shown by the rise in labelled tiglyl-CoA (isoleucine metabolite) and (iso)butyryl-CoA (valine metabolite) and, eventually, propionyl-CoA (at all carbons) (**Figure 3D**). Loading cells with β-alanine reduced propionyl-CoA levels (B v A; D v C; **Figure 3E**). We found that propionate hinders leucine metabolism by raising isovaleryl-CoA and tiglyl-CoA levels, but this effect was lessened with raising β-alanine. These observations suggest that raising [β-alanine] facilitates metabolic flows related to propionyl-CoA (**Figure 3F**).

Disturbed propionyl-CoA metabolism affects contraction

The functional impact of the PA-linked metabolic disturbance was studied in terms of cardiac contraction. In particular, we investigated whether the sex-dependence in metabolic changes also produces a sex-dependent cardiac phenotype. At 8 weeks, body weight was significantly lower in female (but not male) amPA. There was no evidence for cardiac hypertrophy (heart weight/tibia length, cell size) or pulmonary congestion (lung wet:dry weight) (**Figure 4A/B**). Although PA is a form of systemic acidosis, intracellular pH (pH_i) in myocytes was unchanged (**Figure 4B**). We found no major changes in the electrocardiogram (**Extended Data Fig 1A** and **Supplementary Table 3**), but cine-MR imaging revealed that

end-systolic volume (ESV), controlled for body weight, was more profoundly increased in female PA hearts, indicative of a less complete ejection (**Figure 4C/Supplementary Table 4**). This was verified by echocardiography, which showed reduced cardiac output at 8 weeks (**Extended Data Fig 1B**, **Supplementary Table 5**), persisting at 14 and 20 weeks in a subset of animals selected for a longitudinal study (**Figure 4D**). Whilst an increase in E'/A' was detected on tissue Doppler imaging, this was not associated with a change in E/E', the clinical marker of diastolic function.

Less complete ejection is consistent with a higher ESV and lower stroke volume (SV), and one possible mechanism is dysregulated Ca^{2+} signalling. We imaged Ca^{2+} in isolated myocytes loaded with the ratiometric, red-shifted Ca^{2+}-indicator FuraRed. A ratiometric readout is critical for enabling comparisons between groups[38], and red-shifted fluorescence is less susceptible to bleed-through from mitochondrial autofluorescence that may be altered in metabolic disorders. A limitation of FuraRed is its low Ca^{2+} dissociation constant (K_d), which gives weaker resolving power at higher [Ca^{2+}]. However, the FuraRed calibration curve[39] indicates saturation for ratios >2.4, sufficient to provide good resolving power at the peak of Ca^{2+} events. Ca^{2+} handling was interrogated using a concatenated protocol[39] that consisted of a train of electrically-evoked calcium transients (CaT), followed by a caffeine-evoked Ca^{2+} release (CaffT) from the sarcoplasmic reticulum (SR) (**Figure 4E**). Recovery from the CaT and CaffT informed the SR Ca^{2+} ATPase (SERCA) activity (**Extended Data Fig 2A**) and sarcolemmal Na^{+}/Ca^{2+} exchange (NCX) activity (**Extended Data Fig 2B**), respectively. Given the lack of evidence for cellular hypertrophy, cytoplasmic Ca^{2+} buffering capacity was assumed to be no different in amPA. At 8 weeks, we observed a rise in diastolic [Ca^{2+}] in female amPA myocytes (**Figure 4E**). This occurred without a rise in systolic [Ca^{2+}], which is striking because, normally, higher diastolic [Ca^{2+}] leads to greater SR Ca^{2+} loading and larger CaTs[38]. Overall, CaT amplitude was not significantly affected, which argues against systolic dysfunction, as supported by measurements of cell-shortening in isolated myocytes (**Extended Data Fig 2C**). Higher diastolic [Ca^{2+}] implies a right-shift in the Ca^{2+}-activation curve of SERCA; for example, due to a reduction in apparent Ca^{2+} affinity. The steepness of SERCA's flux-Ca^{2+} relationship was, however, unaltered in PA (**Extended Data Fig 2A/B**). Thus, at matching [Ca^{2+}], SERCA flux was attenuated in female amPA myocytes, which explains why the higher diastolic [Ca^{2+}] did not evoke a larger CaT. Higher diastolic [Ca^{2+}] leads to less complete myofilament de-activation, particularly at the physiological heartrate of mice. Such diastolic dysfunction would explain lower SV and higher ESV. The evolution of

changes in CaTs was followed to 20 weeks, at which additional stress and compensatory responses may affect the heart. In older adults, female PA mice had more substantial remodelling, characterised by an increase in CaT amplitude, possibly reflecting compensation (**Extended Data Fig 2D**).

To test if the presence of propionate anions affects Ca^{2+} handling acutely, CaTs were measured in wild-type adult rat myocytes superfused with propionate-containing solution. Propionate did not affect Ca^{2+} signals (**Extended Data Fig 2E**). To test for slower-onset actions, wild-type NRVMs were cultured in the presence of 6 mM propionate, shown earlier to produce a saturating increase in [propionyl-CoA] (**Figure 3A**). We saw no hypertrophic effect (**Extended Data Fig 3A/B**) but a profound lengthening of the CaT, relative to its action potential (**Extended Data Fig 3C/D**). These findings indicate a possible transcriptional effect of propionate.

Transcriptional changes evoked by propionate/propionyl-CoA

We performed RNA-seq analysis on snap-frozen ventricular tissue from 8-week amWT and amPA mice to seek transcriptional responses. Lysates were prepared from ventricular tissue rather than isolated myocytes because of concerns that the relatively long digestion procedure may affect propionate-dependent epigenetic changes which can be short-lived (**Extended Data Fig 4**). Principal component analysis demonstrated a separation by genotype in female mice (**Extended Data Fig 5**). We identified >1,000 differentially expressed genes (DEGs) in PA mice (**Figure 5A/B**, p.adj<0.05), most of which were sex-specific (690 in females, 348 in males), with only 53 concordant responses. Female PA mice showed a more profound transcriptional response, including a significant upregulation of genes in the 'cardiac muscle contraction' pathway (p.adj=10^{-4}, **Figure 5C**, **Extended Data Fig 6A-C**).

To define the gene-set that responds directly to propionate/propionyl-CoA, we measured short-term (24-h) transcriptional responses to propionate in NRVMs that lack confounding systemic influences. To detect the widest scope of "propionate-sensitive" DEGs, we treated myocytes with 6 mM propionate to evoke a saturating rise in propionyl-CoA (**Figure 3A**). The *in vivo* propionate response is likely to be much milder, thus only a subset of *in vitro* DEGs is expected to overlap with DEGs identified in PA mice. *In vivo* DEGs that are not detected *in vitro* are unlikely to be a primary response to propionate/propionyl-CoA,

but possibly a stress or compensatory response. Propionate applied to NRVMs (nrPRO) resulted four times as many DEGs as in amPA mice (**Figure 5D/E**). KEGG pathway enrichment analyses identified several amino acid and toxin-handling pathways as upregulated in PA mice, of which "tyrosine metabolism" and "xenobiotic metabolism by P450" were also detected in nrPRO (**Extended Data Fig 6D**). To test how the *in vitro* responses relate to propionate chemistry, we treated NRVMs with 3-hydroxypropionate but found that selected genes were not induced (RT-qPCR; **Figure 5F**). Other polar derivatives detected by metabolomics (e.g. 3-acetylpropionate) are unlikely to evoke transcriptional responses.

Propionate treatment could increase histone acylation as a substrate for direct propionylation by acyl-transferases[9], by increasing net histone acetylation through HDAC inhibition[8,14,15], or by activating p300 acetyl-transferase[13]. To parse these effects, NRVMs were treated with butyrate, a 4-carbon acyl that also inhibits HDACs and activates p300. Both propionate and butyrate induced a significant increase in acetylation of H3K9ac (**Figure 5G**). Propionate, additionally, increased histone propionylation, detected with a pan-propionyllysine (Kpr) antibody (**Figure 5G**). Propionate's half-maximal effect on H3K9ac was at ~0.6 mM, and saturated at ~80% of the response to butyrate (**Figure 5H**). Interestingly, 2-fluoroacetate, which previous studies have shown to produce propionate-like toxicity[40] did not affect H3K9ac levels. Treatment with propionate increase in H3K27ac in nuclei, although neonatal myocytes showed a more peripheral effect compared to adult myocytes (**Figure 5I**, **Extended Data Fig 7**). Our data indicate that propionate/propionyl-CoA can act as acyltransferase substrate for propionylation, and also alter net histone acetylation in a manner similar to butyrate. To identify the genes in the latter group, the transcriptional response of nrPRO (4,361 DEGs) was compared to responses to *in vitro* butyrate treatment (nrBUT; 8,056 DEGs; **Figure 5J**). 82% of the propionate-sensitive DEGs also responded to butyrate and produced a strong correlation, presumably reflecting their common denominator of increased acetylation. The remaining propionate-sensitive DEGs (782, 18%) did not correlate positively with butyrate and are likely to reflect propionate-specific actions, including propionylation.

Finally, we compared nrPRO responses with DEGs in PA mice. 261 DEGs were identified as both PA-responsive *in vivo* and sensitive to propionate and butyrate *in vitro*. Of these, the majority (178) were identified in females, with only 18 in both sexes (**Figure 5K**). These DEGs can be attributed to a direct effect of propionate/propionyl-CoA in the amPA heart (**Extended Data Fig 6B/C**). Examples of prominently affected genes *in vivo* and *in*

vitro included *Pde9a*, *Mme*, *Gsta3*, and *Egr1*. *Pde9a* induction in NRVMs was concentration-dependent with propionate, having a half maximal effect near ~1 mM (**Extended Data Fig 8A**). Transcript levels (RT-qPCR) confirmed *Egr1* downregulation and *Gsta3* upregulation in both male and female PA mice, and that the upregulation of *Pde9a* and *Mme* was specific to females. Intriguingly, wild-type *Mme* and *Pde9a* transcript levels were higher in males (**Figure 5L**).

Changes in cyclic nucleotide signalling and phosphorylation

The most prominent propionate-related transcriptional response in amPA mice was a three-fold induction of *Pde9a* in females, the only major PDE gene affected in amPA hearts (**Extended Data Fig 8B**). This is relevant to contractile function because previous studies have implicated PDE9A in diastolic dysfunction through its role in degrading cGMP triggered by natriuretic signalling[41,42]. Furthermore, the signalling consequences of *Pde9a* induction may synergise with raised diastolic [Ca^{2+}] in reducing SV in female PA hearts. *Pde9a* induction occurred without changes in transcript levels of natriuretic peptide genes, indicating that the net effect on cGMP signalling in female PA hearts is likely to downward (**Extended Data Fig 8C**). To confirm that propionate-evoked *Pde9a* upregulation increases cGMP-degradative capacity, we cultured NRVMs with 3 mM propionate for 48-h and the catalytic activity of PDE9A was measured using an intracellular cGMP-sensitive FRET probe (cGI-500) from the response to a selective PDE9A inhibitor PF-9613 (**Figure 6A**). The PF-9613 sensitive component was three-fold higher in propionate-treated myocytes, confirming elevated PDE9A activity. To gain insight into the scope for cGMP signalling in amPA hearts, we assayed cGMP levels in cardiac lysates, which generates a snapshot of what is otherwise a dynamic signal (**Figure 6B**). The widest range in [cGMP] was noted in WT female hearts, which could be explained by lower PDE9A activity allowing greater signal variability. PA reduced [cGMP] variation in females only, consistent with the *Pde9a* response. Strikingly, this result was consistent with *Pde9a* transcript levels (**Figure 5L**).

In the heart, cGMP and cAMP signalling is intertwined[43]. A bellwether of cyclic nucleotide signalling is the activity of Na^+/H^+ exchange (NHE1), the gene for which (*Slc9a1*) was not differentially expressed in PA mice thus any changes in activity are likely post-translational[44]. NHE1 activity[44] was significantly faster in amPA myocytes from females, but not males (**Figure 6C**). Critically, the pH-dependence of NHE1 markedly changed shape, as

expected from post-translational modifications[45]. This finding is consistent with a previous study that showed NHE1 activation after ablating atrial natriuretic peptide signalling[46]. Since PDE9a is believed to selectively reduce cGMP from a natriuretic peptide trigger[41], *Pde9a* induction may explain accelerated NHE1 in female PA hearts.

Next, we undertook an unbiased phosphoproteomic approach on female hearts to seek evidence for changes in phosphopeptides that may be substrates for PKG and other kinases. 27 serine/threonine (S/T) sites and 3 tyrosine (Y) sites (26 proteins) were more phosphorylated in amWT, and 26 other S/T and one Y site (21 proteins) were more phosphorylated in amPA (**Figure 6D; Supplementary Tables 6/7**). Affected proteins included sarcomeric, cytoskeletal, kinases, and those involved in ionic signalling and metabolic processes. Several sites were identified as potential substrates of PKA/PKG; noteworthy is phospholamban (Pln) enriched in WT. In amPA, the reduction in phospholamban phosphorylation at S16 is predicted to reduce SERCA activity, which may explain why raised diastolic [Ca^{2+}] does not produce a rise in CaT amplitude in female amPA myocytes. Additionally, several CAMK-family kinase substrates were affected, which may relate to the raised diastolic [Ca^{2+}] in female amPA (**Figure 4E**). Net dephosphorylation at Myl2, Tpm1, Tns1, Ttn, Myh3, Myh6 and net phosphorylation at Myom2 and two additional sites at Myh6 may affect myocardial stiffness. Changes to Pdha1, Tpi1, Pgm5, Apoa1bp, Aldoa, and Ckm phosphorylation may related to metabolic changes in PA[52]. The lower abundance of Pdha1 and Pln phosphopeptides in PA mice is consistent with a study of PDE9A inhibition in mice[41]. Taken together, our data indicate important changes in protein phosphorylation, including sites that can link *Pde9a* induction with contractile dysfunction.

Histone acylation evoked by propionate/propionyl-CoA

We reasoned that the transcriptional changes in the PA mouse heart relate to increased histone acetylation and propionylation. Whereas the role of histone acetylation in the heart is well established, less is known about histone propionylation in cardiac cells. To test this, we performed *in vitro* ^{13}C tracing experiments in NRVMs using labelled valine and isoleucine (48-h treatment) or [1-^{13}C]propionate (24-h treatment), followed by proteomic analyses of acid-extracted histones (**Figure 7A** and **Supplementary Table 8**; exemplar MS spectra in **Extended Data Fig 9**). Propionylation of histone H3 was detected on multiple lysine residues, with the incorporation of ^{13}C-propionate. This indicates that propionyl-CoA

374 derived from either ^{13}C-BCAAs or ^{13}C-propionate can be used as a substrate for
375 propionylation. A stable putative (iso)butyrylation at H3K18 and K122 was also detected.
376 Intriguingly, histone propionylation displayed three distinct dynamic properties. Firstly,
377 unlabelled propionate was detected at H3K122, indicating a relatively stable modification,
378 which only weakly incorporates label even after 48-h treatment with heavy propionate.
379 Secondly, H3K9 propionylation was exclusively labelled with ^{13}C, suggesting turn-over within
380 the 24-h window. Finally, elevated propionate signalling resulted in ^{13}C-labelled
381 propionylation of H3K14 and H3K23, indicating that increased modification of these residues
382 may play a role in the nuclear response to elevated propionate.

383 To test for epigenetic changes triggered by histone acylation, we performed reference-
384 normalised chromatin immunoprecipitation-sequencing (ChIP-seq) on formaldehyde-fixed
385 ventricular tissue from female amPA and amWT mice, using antibodies recognising H3K27ac
386 and pan-propionyllysine (Kpr) (**Figure 7B**). A pan-propionyllysine antibody was preferred
387 over residue-specific alternatives because it captures the effect of PA on multiple residues.
388 Histone acetylation and propionylation co-localised at the promoters of many active genes,
389 including *Pde9a* and *Mme* (**Figure 7C**), and correlated strongly (**Figure 7D**), which is
390 consistent with both moieties being deposited at the same genomic loci by the same lysine
391 acyltransferases[41]. Consistent with this, genes that were upregulated in PA mice were more
392 likely to be marked with both H3K27ac and propionylation (**Extended Data Fig 10A**).
393 However, the overlap was not complete, with some genes showing a peak of H3K27ac but
394 not propionylation.

395 Globally elevated histone acetylation and propionylation was observed in the amPA
396 heart (**Figure 7E**), arguing that endogenously sourced propionate can induce direct
397 propionylation and net acetylation. While the level of modifications was increased, the
398 number of peaks observed was broadly similar (**Extended Data Fig 10B**), indicating that
399 elevated propionate does not result in the targeting of acylation to novel genomic loci. To
400 determine whether increased histone acylation could explain gene expression changes in
401 amPA mice, we studied changes in H3K27ac and Kpr levels at the promoters of DEGs.
402 Indeed, promoters showed an increase in both modifications irrespective of their
403 transcriptional response. Strikingly, the increase for H3K27ac was significantly greater at
404 upregulated DEGs, indicating a correlation between the extent of histone acetylation and
405 transcriptional response (**Figure 7F, Extended Data Fig 10C;** NB: there was not enough
406 statistical power in the analysis of DEGs with changed Kpr levels at their promoters to perform

the analogous analysis). ChIP-qPCR for the upregulated genes *Pde9a* and *Mme* confirmed significantly higher levels of H3K27ac and Kpr in female amPA mice (**Figure 7G**). We corroborated this using a site-specific propionylation antibody recognising H3K23pr (**Figure 7G**), a major propionylation site in cardiomyocytes. A second batch of ChIP-qPCR experiments compared histone modifications between male and female mice to seek a sex-dependence. In contrast to the significant PA-associated increase in H3K27ac in females, the level of H3K27ac at promoters of *Pde9a*, *Mme* and *Gsta3* was unaffected in male PA mice (**Figure 7H**). This finding suggests that the stronger transcriptional response in female PA mice is related to more profound changes in histones.

Finally, we tested whether the histone modifications in female PA mice could be evoked *in vitro*. In propionate-treated NRVMs, we found that histone acetylation at *Pde9a* and *Mme* promoters was [propionate]-dependent (**Extended Data Fig 10D**) and consistent with the effect of propionate on H3K9ac (**Figure 5H**; K_i~0.6 mM). ChIP-seq in NRVMs treated with 6 mM propionate for 24-h (i.e. saturating [propionyl-CoA]) revealed an increase in H3K27ac at active gene promoters, indicating that the chromatin changes observed in female amPA hearts could be attributed to elevated propionate (**Extended Data Fig 10E-G**). As with mice, *in vitro* propionate treatment evoked a stronger change in H3K27ac among promoters of upregulated genes, providing a basis for differential gene expression (**Extended Data Fig 10H**). ChIP-qPCR experiments confirmed that upregulated genes *Pde9a* and *Mme* showed a strong increase in H3K27ac and Kpr levels (**Extended Data Fig 10I**).

DISCUSSION

This study establishes a link between disrupted propionate metabolism and epigenetic changes in the heart. The concordance between metabolic disturbances, histone modifications, transcriptional responses, and cardiac derangements in female PA mice suggests an epigenetic basis for the cardiac actions of propionate. In human PA patients, multiple organs are affected but deaths are commonly cardiac[19]. An indication that perturbed propionate can disrupt cardiac function came from comparing PA with methylmalonic acidaemia (MMA), which affects the enzyme downstream of PCC and has a less definitive cardiac disease phenotype[19]. Here, we provide the first demonstration that an endogenous source of propionate can modify histones in the heart, and show how these modifications trigger transcriptional responses relevant to cardiac function. Our results describe a novel

signalling axis, relevant to metabolic diseases of the heart whenever a rise in propionyl-CoA is implicated. Given that propiogenic substrates and gut bacteria can yield substantial quantities of propionate, these responses may have broad impact not limited to PA.

Our study noted a greater excess of propionyl-CoA and acyl-CoA intermediates of propiogenic substrate catabolism in female PA hearts, compared to males, despite comparable plasma levels of propionate and propionyl-carnitine, a surrogate of systemic propionate-load. Sexual dimorphism in CoA handling had been noted previously[47] and likely relates to sexual maturity; if so, it will not manifest in PA patients who are typically paediatric, but the mechanistic causes may provide directions for therapy. The metabolic disturbance in PA mice was relatively limited (~130 metabolites) and included twenty-two metabolites showing a sex-dependence. The most prominent sex-dependent response was an increase in β-alanine and its dipeptides (carnosine and anserine) in male PA hearts. β-alanine, a downstream derivative of propionyl-CoA, is a rate-limiting precursor of carnosine[35]. Through the actions of testosterone, male mice accumulate more carnosine in skeletal muscle[48], and a similar mechanism is believe to operate in the heart[28]. We traced propionate to carnosine *in vitro*, and propose that this pathway is scaled-up in male PA hearts. Raised carnosine protects from oxidative stress[28], improves mitochondrial function and facilitates the clearance of propionate-related metabolites. Indeed, loading propionate-stressed myocytes *in vitro* with β-alanine reduced the 2-methylcitrate/citrate ratio (a PA marker) as well as propionyl-CoA, isovaleryl-CoA, (iso)butyryl-CoA, and tiglyl-CoA.

We found that PA hearts had increased histone propionylation and acetylation, typically deposited at common genomic loci. Isotope tracing demonstrated that propionate and propiogenic substrates convert to propionyl-CoA, which then modifies histone H3 at various lysine residues. Under baseline metabolic conditions, propionyl-CoA propionylates H3K9 and H3K122, whereas under circumstances of elevated propionyl-CoA, H3K23 and H3K14 are targeted. The increase in histone acetylation could be explained in terms of the inhibitory effect of propionate on HDACs[14,17,18] or an activatory effect of propionyl-CoA on p300 acetylase[13]. In support of net histone acetylation, many of the transcriptional responses to propionate *in vitro* were also evoked by treatment with butyrate, which raises acetylation but not propionylation. Propionate anions inhibit HDACs with an inhibitory constant in the in range of hundreds of micromolar[13], and if this was a relevant mechanism, the intracellular concentration of propionate *in vivo* would have to be substantially higher than in plasma. This

scenario would be expected if propionate was produced by cardiac metabolism. It is possible that propionyl-CoA/propionate levels are highly compartmentalised in cardiac nuclei[16].

Consistent with the sex-dependent metabolic disturbance, we described more profound histone modifications and stronger transcriptional responses in female PA hearts. Genes induced in female PA hearts only includes *Pde9a* and *Mme*, part of natriuretic peptide-triggered cGMP signalling pathway[49,50]. At least some of the changes in the cardiac phosphoproteome may be linked to a downscaling of cGMP signals arising from *Pde9a* induction. Among differentially abundant phosphopeptides were contractile elements, whose phosphorylation status may affect myocardial stiffness. It was noteworthy that female PA mice had a more pronounced contractile dysfunction, characterised by a raised ESV and reduced SV. We excluded systolic dysfunction because the amplitude of Ca^{2+} transients and cell-shortening were unaltered in PA. However, raised diastolic [Ca^{2+}] in female PA myocytes would lead to less complete myofilament de-activation during diastole. The observation that elevated diastolic [Ca^{2+}] did not produce the expected rise in CaT amplitude indicates that the SR takes Ca^{2+} less avidly in PA, which likely relates to the right-shift in the Ca^{2+}-activation curve of SERCA. A plausible explanation relates to changes in phospholamban phosphorylation, but further work is required to dissect this pathway. Overall, the remodelling in female PA hearts has features of diastolic dysfunction. Supporting this model, previous studies linked *Pde9a* induction to diastolic dysfunction[41] and low PKG activity with raised resting tension and impaired relaxation[42]. Notwithstanding the contractile phenotype in female PA mice, it is important to note that some important clinical signatures of diastolic dysfunction were not observed; for example, there was no increase in E/E' ratio or evidence for pulmonary oedema. It is possible that a more severe phenotype will develop with larger and longer propionyl-CoA disturbances.

Since PA is defined as an acidosis, it is intuitive to speculate about a role for reduced pH_i in the contractile dysfunction. Moreover, we observed an increase in NHE1 activity in female PA myocytes. However, measurements of resting pH_i revealed no effect of PA, arguing against a role of disturbed intracellular acid-base balance in PA cardiac dysfunction. Whereas NHE1 is the major pH regulator responsible for extruding large acid-loads from the cytoplasm, transporters of the Na^+-HCO_3^- family are critical in keeping resting pH_i near physiological levels. Nonetheless, higher NHE1 activity in female PA mice may increase susceptibility to Na^+ overloading during acid-stress, which would be arrhythmogenic. Further experiments in stressed hearts would provide insight into this additional disease mechanism.

Although chromatin immunoprecipitation analyses revealed a wide scope for propionate to modify histones, the coupling between histone marks and transcriptional activity is highly non-stoichiometric. An increase in histone acylation may produce a noticeable transcriptional change at only a small subset of genes. Indeed, we measured a robust response at the transcript level for a subset of genes. Whilst we observed an increase in H3K23pr at the promoter of *Pde9a* and *Mme* in female PA mice, further work is needed to link specific histone residues to transcriptional responses, and to determine whether their acetylation and propionylation cause moiety-specific responses. To that end, the generation of site-specific antibodies is essential.

Whilst *Pde9a* induction is a formidable candidate for cardiac dysfunction, there will be a myriad of coinciding transcriptional responses in PA, each contributing to the disease state. We speculate that a targeted approach of silencing any isolated transcriptional response may not necessarily reverse all PA-related changes. The therapeutic priority should, instead, focus on reducing the total propionyl-CoA load[51]. We postulate that raising β-alanine could be therapeutic, possibly as a dietary regime enriched in the free amino acid or its dipeptides.

We conclude that disruptions to metabolism that raise propionyl-CoA can have profound effects through epigenetic actions that impact contraction in a range of cardiometabolic diseases. Metabolic stress, such as that emerging in diabetes, or with abnormal gut microbiome activity, may amplify propionate-generating pathways and increase histone acylation in the heart. It will therefore be important to investigate these histone responses in the broader context of cardiac disease.

METHODS

Experimental models and sample collection

All protocols were conducted in accordance with the University of Oxford Animal Welfare and Ethical Review Body and authorised by the UK Animals (Scientific Procedures) Act 1986. Animals were sacrificed using an appropriate method of humane killing (Schedule 1) or anaesthetic overdose. Experimental protocols and data analysis were randomised, but blinding was not always possible, due to the majority of work being conducted by a single operator.

In vitro cardiomyocyte models: Supporting *in vitro* experiments were performed on neonatal or adult rat ventricular myocytes treated with exogenous propionate. For this purpose, rat hearts were used as a refinement measure because they yield a greater number of cells for culture than mouse hearts, yet both species have similar cardiac physiology and gene regulation[52]. Experiments were performed on ventricular myocytes either isolated from 275-300g adult or post-natal day 1-2 (P1/P2) neonatal Sprague-Dawley rats (Charles River Laboratories). The procedures for isolating ventricular myocytes are provided below.

In vivo model of disrupted propionate metabolism: The majority of experiments were performed on adult male and female mice that were 8 weeks of age, from the FVB *Pcca*$^{-/-}$ A138T line generated by Guenzel *et al.*[23]. A small selection of experiments was performed in 20-week-old mice and indicated accordingly. Mice were bred and housed in individually ventilated cages and all animals had *ad libitum* access to water and food (Teklad #2918 global 18% protein rodent diet). Mice used were either wild-types (*Pcca*$^{+/+}$ A138T) for control experiments, or homozygous (*Pcca*$^{-/-}$ A138T) animals, referred to as amWT and amPA respectively. Only heterozygous or wild-type dams were used for breeding and genotyping by PCR was performed as previously described[23].

Tissue harvesting and sample collection: The majority of experiments were conducted on ventricular myocytes freshly isolated in Langendorff mode or on cryoground tissues that were snap-frozen by liquid nitrogen, with the exception of chromatin immunoprecipitation, which was performed on formaldehyde-crosslinked hearts fixed in Langendorff mode. To harvest tissues, mice were killed humanely by intraperitoneal injection of an appropriate volume adjusted for body weight of sodium pentobarbitone (stock 200 mg/mL) pre-mixed at a 2:1 ratio with sodium heparin (stock 5,000 I.U./mL). Upon confirmation of anaesthesia, the beating heart was rapidly excised by incising the aorta and blood was allowed to pool in the thoracic cavity. The heart was promptly arrested in ice-cold 1x PBS, the atria dissected away and the total ventricle blotted dry before being snap-frozen in liquid nitrogen. Pooled whole blood in the thoracic cavity was immediately collected (within 30 seconds of excising the heart) by gentle aspiration with a 1 mL syringe and injection into lithium heparin tubes (BD Vacutainer, #368495). Blood was kept on ice and promptly centrifuged at 1,200 RCF at 4°C for 10 mins to collect plasma; the red cells and buffy coat were discarded. All samples were stored at -80°C until use. Further details are provided in subsequent sections.

Human plasma samples: Measurements and analyses were performed according to guidelines set by the Royal College of Pathologists and Great Ormond Street Hospital

(GOSH) NHS Foundation Trust. As part of ongoing clinical care, plasma samples are collected from PA patients for measurements of propionate and derivatives. Once these tests are completed, surplus acellular plasma is anonymised and used for diagnostic measurements, in line with GOSH departmental policy and approvals. Samples are non-identifiable and no additional information was obtained beyond the presented measurements herein.

Isolation of adult mouse ventricular myocytes

Isolation of primary ventricular myocytes was as previously described[53] through Langendorff-perfused hearts using a combination of enzymatic (~1 mg/mL Collagenase, Worthington Biochemical Corporation; 0.025 mg/mL Type XIV Protease, #P5147, Sigma-Aldrich/Merck) and mechanical dispersion. The isolation solution for adult mice contained in mmol/L: 130 NaCl, 5.6 KCl, 5 HEPES, 0.45 NaH_2PO_4, 10 glucose, 20 taurine, 3.5 $MgCl_2$; pH adjusted to 7.40 at 37°C with NaOH. The isolation solution for adult rats contained in mmol/L (unless stated otherwise): 120 NaCl, 4 KCl, 10 HEPES, 2 NaH_2PO_4, 11 glucose, 20 taurine, 1.2 $MgCl_2$, 0.0173% v/v pyruvic acid; pH adjusted to 7.40 at 37°C with NaOH. Following digestion of the heart, ventricular tissue was minced in isolation solution containing 200 µM $CaCl_2$ and 1% BSA (w/v) to quench enzymatic activity. Cells were filtered through a 400 µm nylon mesh and the remaining tissue was further dissociated through subsequent digestions for 5 mins per round at 37°C combined with gentle trituration. Cells were pelleted by centrifugation at 40 RCF for 1 min, washed once in isolation solution containing 500 µM $CaCl_2$, then finally in 1 mM $CaCl_2$ prior to use. Myocytes were allowed to rest for at least 30 mins prior to use and only quiescent rod-shaped myocytes were selected for experiments.

Isolation of neonatal rat ventricular myocytes

Neonatal rat ventricular myocytes (NRVMs) were isolated from P1/P2 SD rats as previously described[53]. Hearts were pooled from a litter of 12 pups for the isolation of myocytes. After Schedule 1, hearts were excised and washed ice-cold 1x ADS buffer, containing (in mmol/L): 106 NaCl, 5.3 KCl, 20 HEPES, 0.8 NaH_2PO_4, 0.4 $MgSO_4$, 5 glucose; pH adjusted to 7.40 at 37°C with NaOH. After removing the atria under a stereoscopic microscope, the ventricles were finely minced and digested with 0.45 mg/mL Type A Collagenase (Roche) and 1.25 mg/mL Pancreatin (Sigma-Aldrich/Merck) for 5 mins at 37°C with gentle stirring. The

supernatant from the first digestion was discarded. The remaining tissue was digested for 20 mins at 37°C with gentle stirring. The supernatant, containing myocytes and fibroblasts, was collected and enzymatic activity was quenched using newborn calf serum (NCS). The cells were then centrifuged at 250 RCF for 5 mins in a swing-out rotor centrifuge and the pellet was resuspended in fresh pre-equilibrated medium (see below) containing 10% horse serum (HS) and 5% NCS and stored in a humidified 5% CO_2 incubator. The digestion/collection process was repeated until all ventricular tissue was digested. The final supernatant was 'pre-plated' on untreated 10 cm petri-dishes for 2 hrs at 37°C to promote the attachment of fibroblasts, after which, the myocyte-enriched supernatant was collected and seeded on the appropriate cell culture platform pre-coated with fibronectin. Cells were maintained in a humidified 5% CO_2 incubator at 37°C and cultivated in media as described below.

Media for standard cell culture

Stock media was based on 20% (v/v) M199 (Sigma-Aldrich/Merck, M4530) and 80% (v/v) $NaHCO_3$-free DMEM (Sigma-Aldrich/Merck, D7777) supplemented with 24 mM $NaHCO_3$ and 20 mM NaCl (to adjust osmolality to physiological levels). 1% (v/v) penicillin-streptomycin was included in media (100 U/mL penicillin, 100 µg/mL streptomycin; Sigma-Aldrich/Merck, P4333). All media was prepared using ultra-pure water, sterile-filtered (0.22 µm), and stored at 4°C. Before use, media was pre-equilibrated in a humidified 5% CO_2 incubator for a minimum period of 1 hour to achieve equilibration of pH and temperature[54]. NRVMs were isolated in stock media containing 10% horse serum (HS) and 5% NCS. On day-1 post-isolation, serum was reduced 10-fold (1% HS and 0.5% NCS) and on day-2, cells were serum-starved. NRVMs were treated on day-3 for 24-48 h under serum-free conditions in treatment media prepared using $NaHCO_3$-free DMEM (D7777) supplemented with 24 mM $NaHCO_3$, and where appropriate, sodium propionate or sodium butyrate, with various concentrations of NaCl to balance osmolality between treatment medias. Dulbecco's PBS containing calcium and magnesium (Gibco, 14040-133) was used for washing cells between media changes.

Custom media for ^{13}C tracing

All media were prepared using ultra-pure water, sterile-filtered (0.22 µm), and stored at 4°C. Custom media were prepared from commercially available DMEM powder that does not

contain glucose, amino acids, sodium bicarbonate, sodium pyruvate and Phenol Red (US Biologicals, D9800-20A). The final concentration of amino acids was based on classical DMEM formulations. 'Stock tracer media' was prepared from DMEM powder and supplemented with (in mmol/L): 21.1 glucose, 0.399 L-arginine•HCl, 0.2 L-cysteine•2HCl, 0.399 glycine, 0.219 L-Histidine•HCl•H_2O, 0.8 L-isoleucine, 0.8 L-leucine, 0.8 L-lysine•H_2O, 0.201 L-methionine, 0.4 L-phenylalanine, 0.4 L-serine, 0.798 L-threonine, 0.078 L-tryptophan, 0.397 L-tyrosine•2Na•2H_2O, 0.802 L-valine, 24.4 $NaHCO_3$, 0.042 Phenol Red•Na, 1 sodium pyruvate, 19.9 NaCl. 1% (v/v) penicillin-streptomycin (final concentration 100 U/mL penicillin and 100 µg/mL streptomycin; Sigma-Aldrich/Merck, P4333) and 1% (v/v) L-glutamine (final concentration 2 mM L-glutamine; GlutaMAX, Thermo Scientific, 35050-038) was added to all freshly prepared media, in serum-free conditions. This custom media was used to prepare different tracer medias containing either alone or in combination, where indicated, 0.8 mM $U^{13}C_6$ L-isoleucine (Cambridge Isotope Laboratories, CLM-2248-H), 0.8 mM $U^{13}C_5$ L-valine (Sigma-Aldrich, 758159), and/or 1 mM 1-^{13}C sodium propionate (Cambridge Isotope Laboratories, CLM-771-PK). Where appropriate, custom media was prepared without L-histidine and supplemented with 5 mM carnosine.

Plasma propionate and plasma acylcarnitine mass spectrometry measurements

Analysis of plasma propionate and plasma acylcarnitine derivatives were performed by tandem mass spectrometry at Great Ormond Street Hospital, London.

Plasma propionate: Plasma specimens were prepared by adding to 50 µL of plasma 10 µL of saturated analar sodium bicarbonate and 10 µL of 0.5 mM sodium propionate 1-^{13}C as the heavy isotope internal standard. Following protein precipitation with 400 µL of absolute ethanol the separated liquid extract was blow-dried with nitrogen gas at 38ºC and reconstituted in 200 µL of 1:1 methanol:water mixture. 20 µL of reconstituted extract, equivalent to 4 µL of plasma, was injected into the mobile phase stream of 50% methanol in water with 0.02% NH_3. The mobile flow rate was 5 µL/min over a period of 2.0 min rising to 300 µL/min by 2.2 min and maintained at that a flow rate of 300 µL/min until 3.0 minutes. For the analysis by tandem mass spectrometry, electrospray negative ionization was employed in the multiple reaction monitoring mode with the following mass transitions to identify and quantify propionate $CH_3CH_2C00^-$ m/z 73>73 and $CH_3CH_2{}^{13}C00^-$ m/z 74>74.

Plasma acylcarnitines: The acylcarnitine method employed was based upon a published method[55]. Acylcarnitines were analysed on 5 µL of plasma as their butyl-ester derivatives. A combined mixture of heavy isotope internal standards was added to the plasma specimens prior to butylation with HCl butanol. The final concentration of the free carnitine internal standard was 100 µmol and the propionylcarnitine internal standard was 5 µmole in the plasma specimen. For this study, the free carnitine and propionylcarnitine were analysed in positive ion mode using precursor-ion (parent-ion) scan. As all acylcarnitines species have a common product (m/z 85) hence the precursor-ion mode allows analysis of a wide complete range of different butylated acylcarnitine derivatives. The butylated precursor free carnitine ion (m/z 218) was quantified against a 9 deuterium-labelled heavy isotope free carnitine with a butylated precursor ion (m/z 227), and the butylated precursor propionate ion (m/z 274) against a 3 labelled heavy isotope propionate a butylated precursor ion (m/z 277). The processed liquid sample is introduced into the ion source using positive mode electrospray ionization at atmospheric pressure. The mobile phase was 80% methanol in water with a flow rate of 5 µL/min over a period of 2.0 minutes rising to 300 µL/min by 2.2 min and maintained at that a flow rate of 300 µL/min until 3.0 min.

Unlabelled metabolomic analyses

Analyses were performed in the Department of Chemistry, University of Oxford.

Tissue preparation: Tissue metabolites were extracted from cryoground heart or liver tissue by adding 500 µL of 80% (v/v) MS-grade MeOH to 50 mg of tissue. The tissue underwent 2-3 rounds of brief homogenisation (~10 secs) then centrifuged at 21,000 RCF for 20 mins at 4°C. Pelleted insoluble material was discarded and the supernatant was processed with 10 kDa cut-off ultracentrifugation filter columns (Amicon Ultra-0.5 Centrifugal Filter Units, Merck/Sigma-Aldrich, UFC501096) at 21,000 RCF for 20 mins at 4°C. The infranatant was transferred to Protein LoBind 1.5 mL tubes (Eppendorf) and kept on ice. Nucleic acid concentration was estimated with a spectrophotometer (NanoDrop, Thermo Fisher) and all tissue samples were diluted to the sample with the lowest concentration using 80% MeOH, before being processed downstream.

Plasma preparation: Plasma metabolomics samples were prepared by adding 230 µL of MS-grade 1-butanol:methanol (1:4 v/v) to every 100 µL of plasma. The sample was vortexed well

and processed with 10 kDa cut-off ultracentrifugation filter columns at 21,000 RCF for 30 mins at 4°C. The infranatant was then processed downstream.

Ion-exchange chromatography and mass spectrometry: Ion-exchange chromatography[56] was performed using an ICS-5000+ HPLC system incorporating an electrolytic anion generator (KOH based) which was programmed to produce a OH^- gradient over 37 min. An inline electrolytic suppressor removed OH^- ions and cations from the post-column eluent stream prior to MS analysis (Thermo Scientific Dionex AERS 500). A 10 µL partial loop injection was used for all analyses and the chromatographic separation was performed using a Thermo Scientific Dionex IonPac AS11-HC 2 × 250 mm, 4 µm particle size column with a Dionex Ionpac AG11-HC 4 µm 2x50 guard column inline. The IC flow rate was 0.250 mL/min. The total run time was 37 mins and the hydroxide ion gradient comprised as follows: 0mins, 0mM; 1min, 0mM; 15mins, 60mM; 25mins, 100mM; 30mins, 100mM; 30.1mins, 0mM; 37mins, 0mM. Analysis was performed in negative ion mode using a scan-range from *m/z* 60-900 and resolution set to 70,000. The tune file source parameters were set as follows: Sheath gas flow 60 mL/min; Aux gas flow 20 mL/min; Spray voltage 3.6v; Capillary temperature 320°C; S-lens RF value 70; Heater temperature 350°C. AGC target was set to 1e6v ions and the Max IT value was 250ms. The column temperature was kept at 30°C throughout the experiment. Full scan data were acquired in continuum mode. The derivatisation of samples was based on a modified version of the Waters AccQ-Tag method[57]. Thermo Ultimate 3000 UHPLC system coupled directly to a Q-Exactive Hybrid Quadrupole-Orbitrap mass spectrometer. A 5 µL partial loop injection was used for all analyses with pre and post injection wash program. A Waters AccQ-Tag column (2.1x100mm) was used with a flow rate of 0.5mL/min. The total run time was 9.5 mins. Mobile phase A and B comprised commercially available AccQ-Tag reagents prepared as recommended by Waters (Waters PLC, Elstree, UK). The gradient elution program was modified from the published AccQ-Tag method as follows: 0mins, 0.1%B; 0.54min, 9.1%B; 5.74min, 21.2%B; 7.74mins, 59.6%B; 8.04min, 90%B; 8.05min, 90%B; 8.64min, 0%B; 9.5min, 0.1%B. The column temperature was kept at 40°C throughout the experiment. Mass spectrometry analysis was performed in positive ion mode separately using a scan-range from *m/z* 70-1050 and resolution set to 70,000. The tune file source parameters were set as follows: Sheath gas flow 60 mL/min; Aux gas flow 20 mL/min; Spray voltage 3.6v; Capillary temperature 320 °C; S-lens RF value 70; Heater temperature 350°C. Full MS setting were AGC target 3e6 ions and the Max IT value was 200ms. Full scan data were acquired in continuum mode.

Data processing and statistics: Raw data files were processed using ProgenesisQI (Waters, Elstree, UK) and included alignment of retention times, peak picking, characterising multiple adduct forms and metabolite identification using authentic standards. Matching of retention times (1 min window), accurate mass values (<5ppm), relative isotope abundances (>90%) and fragmentation patterns were used for metabolite identifications. Where measured, fragmentation patterns were matched to at least the base peak and two additional peak matches in the MS/MS spectrum to within 12ppm (the top 10 data-directed fragmentation method could not provide fragment ions for all ions in the MS 1 spectrum). Metaboanalyst[58] (https://www.metaboanalyst.ca/) was used for further data processing and statistical analysis of the data. p-values were FDR-corrected (Benjamini-Hochberg).

^{13}C tracing metabolomic analyses

Analyses were performed in the Department of Chemistry, University of Oxford.

Sample preparation: Samples for ^{13}C tracing metabolomics was performed in cultured NRVMs with custom media as described above (*'isolation of neonatal ventricular myocytes'* and *'^{13}C tracing custom media'*). Between 2-2.5 M NRVMs were seeded per 60 mm Petri dish for each condition. On day-3 post-isolation, NRVMs were treated with culture media for 48 h. A total of 400 µL of ice-cold MS-grade methanol was for each Petri dish for cell lysis. The lysate was scraped and collected into 1.5 mL tubes, and centrifuged at 21,000 RCF for 30 mins at 4°C. The supernatant was collected and metabolites prepared following 10 kDa cut-off ultracentrifugation as described above under section *'Metabolomics'*.

Anion-exchange chromatography mass spectrometry (IC-MS): Ion exchange chromatography was performed using an ICS-5000+ HPLC system coupled to a high-resolution Q-exactive orbitrap mass spectrometer (Walsby-Tickle et al., 2020). The IC-5000+ system incorporated an electrolytic anion generator (KOH based) programmed to produce an OH^- gradient over 37 min. An inline electrolytic suppressor removed OH^- ions and cations from the post-column eluent stream before MS analysis (Thermo Scientific Dionex AERS 500). A 10 µL partial loop injection was used for all analyses, and the chromatographic separation was performed using a Thermo Scientific Dionex IonPac AS11-HC 2 × 250 mm, 4 µm particle size column with a Dionex Ionpac AG11-HC 4 µm 2x50 guard column inline. The IC flow rate was 0.250 mL/min. The total run time was 37 mins, and the hydroxide ion gradient comprised as follows: 0mins, 0mM; 1min, 0mM; 15mins, 60mM; 25mins, 100mM;

30mins, 100mM; 30.1mins, 0mM; 37mins, 0mM. Mass spectrometry analysis was performed in negative ion mode using a scan range from *m/z* 60-900 and a resolution set to 70,000. The tune file source parameters were assessed: Sheath gas flow 60 mL/min; Aux gas flow 20 mL/min; Spray voltage 3.6kV; Capillary temperature 320 ^{o}C; S-lens RF value 70; Heater temperature 350^{o}C. AGC target was set to 1e6v ions, and the Max IT value was 120ms. The column temperature was kept at 30°C throughout the experiment. Full scan data were acquired in continuum mode.

Reversed-phase chromatography mass spectrometry of derivatised samples (RPLC-MS): Samples were derivatised using a modified version of the Waters AccQ-Tag method (Salazar et al., 2011). RPLC-MS analysis of derivatised samples was also performed using the Acquity UPLC system liquid chromatograph (Waters, Elstree, UK) coupled directly to a Xevo G2-XS QTOF high-resolution tandem mass spectrometer. A 5 µL partial loop injection was used for all analyses with pre and post-injection wash programs. A Waters AccQ-Tag column (2.1x100mm) was used with a flow rate of 0.6mL/min. The total run time was 9.5 mins. Mobile phases A and B comprised commercially available AccQ-Tag reagents prepared as Waters (Waters, Elstree, UK) recommended. The gradient elution program was modified from the published AccQ-Tag method as follows: 0mins, 0.1%B; 0.54min, 9.1%B; 5.74min, 21.2%B; 7.74mins, 59.6%B; 8.04min, 90%B; 8.05min, 90%B; 8.64min, 0%B; 9.5min, 0.1%B. The column temperature was kept at 50°C throughout the experiment. Mass spectrometry analysis was performed in positive ion mode using a scan range from *m/z* 150-1200. The centroid data were collected in MSE mode and the time was set to 0.2 s, t. The tune file source parameters were set as follows: Source temperature 140 C; Cone gas flow 50 L/h; Desolvation gas flow 800 L/h; Cone voltage and Capillary voltage were set to 40.0 V and 2.0 kV in negative ion mode, respectively; Full scan data were acquired in continuum mode.

Data processing and analysis of the mass spectrometry data: Raw data files were converted into mzML format using ProteoWizard MSConvert (Chambers et al., 2012) prior to data processing and isotopologue extraction using El Maven (Clasquin et al., 2010). Selected metabolites were identified using an in-house database of authentic metabolite standards by matching accurate mass values and chromatographic retention times from the experimental samples with database values. Peaks were aligned across samples in El Maven using standard settings and a 5ppm *m/z* window was used for extracted ion chromatograms for each isotopologue. Summed peak area abundances and individual isotopologue abundances for each identified metabolite were extracted and compared across each sample.

Acyl-CoA and ^{13}C tracing metabolomic analyses

Analyses were performed in the Babraham Institute, Cambridge.

Sample preparation: Samples for acyl-CoA analysis were performed in cultured NRVMs with custom media as described above (*'isolation of neonatal ventricular myocytes'* and *'^{13}C tracing custom media'*). Between 2-2.5 million NRVMs were seeded per 60 mm Petri dish for each condition. On day-2 post-isolation, NRVMs were serum-starved and on day-4 treated with custom media for 24 h. A total of 1 mL of ice-cold MS-grade 10% TCA (v/v) was used for each Petri dish for cell lysis. The lysate was scraped and collected into 1.5 mL tubes and snap-frozen on dry ice. Samples were subsequently processed as described below.

Generation of internal standards: $^{15}N_1{}^{13}C_3$-labeled acyl-CoA internal standards were generated in yeast and extracted for use in quantitation experiments as described[59]. Briefly, Pan6Δ *S. cerevisiae* were cultured at 30 ˚C 200 rpm in synthetic defined media composed of Yeast Nitrogen Base without Amino Acids and Calcium Pantothenate (Formedium, CYN3301) and Drop-out Mix Complete w/o Yeast Nitrogen Base (Formedium, DC50149) with the addition of $^{15}N_1{}^{13}C_3$-calcium pantothenate 50 mM (CK Isotopes, CNLM-7694-0.01) for 72 h. 1 mM of sodium propionate (Sigma-Aldrich, P5436-100G) was added for the final 3 hours to boost $^{15}N_1{}^{13}C_3$-labeled propionyl-CoA generation. Cells were pelleted by centrifugation at 500 RCF at 4 ˚C for 10 minutes and extracted in ice cold 10% (w/v) trichloroacetic acid (TCA). Cells were disrupted by sonication with a probe tip sonicator (60 x 0.5 s pulses at medium intensity). Protein was removed by centrifugation 16,000 x g at 4 ˚C and clarified supernatant containing internal standards was stored at -80 ˚C until use. Labeling efficiency was confirmed > 99% by MS analysis.

Short chain acyl-CoA extraction: Cells and pre-weighed tissue samples were stored at -80 ˚C in 1.5 mL tubes prior to extraction. Samples were thawed on ice and kept on ice throughout processing. For quantitation experiments, an equal volume of internal standard was added to each sample across each experiment. The volume of internal standard used was adjusted to match the experimental sample type (e.g. higher volume was used for tissue than for cell experiments in order to scale signal intensities of internal standards to unlabeled acyl-CoA in the sample). Standard curves were generated in parallel by addition of an equal volume of internal standard to serial dilutions of acyl-CoA standard mixture. The acyl-CoA standard mixture stock contained succinyl-CoA and acetyl-CoA at 50 mM and other CoAs at 5mM, as

indicated in the table below. Internal standard was not added to isotope tracing samples. The samples were then sonicated for 10 × 0.5s low power pulses for cells but 20 x 1 s high power pulses for heart tissues. Protein was pelleted by centrifugation at 16,000 × g from 10 min at 4°C. The supernatant was purified by solid-phase extraction using Oasis HLB 1cc (30 mg) SPE columns (Waters). Columns were washed with 1 mL methanol, equilibrated with 1 mL water, loaded with supernatant of 10% TCA, desalted with 1 mL water, and eluted with 1 mL methanol containing 25 mM ammonium acetate. The purified extracts were evaporated to dryness under nitrogen then resuspended in 55 µL 5% (w/v) 5-sulfosalicylic acid in water.

Liquid chromatography: Analytes were separated by liquid chromatography (LC) on a Vanquish Duo UHPLC (Thermo) on a Waters XSelect Premier HSST3 2.5 µm particle size 2.1 × 100 mm column. A 5 µL sample aliquot was injected with the column temperature set at 25 °C, and the flow rate set at 0.2 mL/min. Two mobile phases were used for elution, including water with 5 mM ammonium acetate as phase A, 95:5 acetonitrile: water with 5 mM ammonium acetate as phase B. A third phase was used for column washing: 80:20 acetonitrile:water with 0.1% formic acid as phase C. The elution gradient (A,B) started with 0% phase B, was held for 2 min, then increased to 25% phase B at 5.5 min, and then to 100% phase B at 6 min held to 14.5 min. At minute 14.5, flow was switched to 100% phase C and held until 19.5 min. Lastly, the gradient was switched to 2% B at 19.5 min and held until 25 min for re-equilibration. The sample manager temperature was set as 4 °C.

Mass spectrometry: The MS data acquisition was performed by using an Orbitrap IQ-X Tribrid Mass Spectrometer (Thermo). A heated ESI source was used at positive ion mode. The spray voltage was set as 3.5 kV. The capillary temperature and aux gas heater temperature were set as 320 and 350 °C, respectively. Sheath gas and aux gas flow rate were set at 35 and 7 (in arbitrary units), respectively. The S-lens rf level was 60%. For MS1 full scan, the orbitrap scan resolution was set at 120,000 (defined at 200 m/z), while data-dependent-MS2 ion trap scan resolution were default at normal mode. The MS full scan range was 600-1100 m/z, while the automatic gain control (AGC) target and maximum injection time were 400,000 and 50 ms respectively. Meanwhile, the MS2 scan range was 100-500 m/z; the automatic gain control (AGC) target and maximum injection time were 10,000 and 35 ms. For data dependent MS2 (ddMS2) mode, a targeted mass list was used as mass trigger for MS2 with a mass tolerance of 10 ppm for targeted molecules (indicated in **Supplementary Table 10**) and the isolation width of the precursor ion was set at 0.7 m/z. Other ddMS2 parameters were scan Higher energy Collision Dissociation (HCD) energy of 40%. Additionally, a dynamic

exclusion filter is used to prevent ddMS2 of same precursor ion whereby ddMS2 is excluded for 5 seconds if the same ions are detected 3 times in a row. Additionally, an intensity filter of 1000 (arbitrary units) was used for filtering background ions, alongside a precursor sort filter to prioritise the lower intensity precursor ions.

Data analysis: Full scan MS1 data were quantified by peak integration using Tracefinder v5.1 (Thermo Scientific) software. ddMS2 fragmentation was used to validate characteristic neutral loss for CoA molecules using FreeStyle 1.8 SP2 (Thermo Scientific)[60]. Molecules were quantified as monoisotopic mass H^+ (see **Supplementary Table 10** for complete mass list). Retention times were matched to analytical standards in standard curves for further validation. For quantitation, relative AUC was calculated by dividing AUC of analyte by the matching internal standard. If signal was insufficient for matching internal standard a high abundance internal standard at closest retention time was used instead. For absolute quantitation, standard curves were generated by plotting relative AUC against the known quantity of acyl-CoA analytical standards. Quantity in samples was interpolated within the linear range of the curve using PRISM software (Version 9.4.0). Isotopic enrichment was calculated in tracing experiments by normalisation to unlabeled control samples using the FluxFix calculator[61]. See **Supplementary Table 11** for mass list for acyl-CoA analysis used in standard curves.

Electrocardiography (ECG)

Surface ECGs were acquired from unconscious mice during the diurnal period using a non-invasive surgical monitoring platform (Indus Instruments MouseMonitor+; courtesy of Dr Carolyn Carr, University of Oxford). Anaesthesia was induced in an anaesthetic chamber by 2.5% isoflurane in oxygen and nitrous oxide (O_2:N_2O 4:1, total of 2 L/min). Anaesthesia was maintained at 1.8-2% for the duration of the experiment (O_2:N_2O 4:1, total of 2 L/min). Conductive electrode cream (Indus Instruments ECG Electrode Crème, #600-0001-01-S) was applied to the paws of the forelimb and hindlimb and secured onto the contact electrodes with hypoallergenic tape. Signals were grounded to the chassis and filtered as follows: high-pass filter 1 Hz, low-pass filter OFF, notch filter 50 Hz. Data were acquired using the manufacturer's software in their native format (.iird) and exported as .csv files. Downstream data analysis was performed in MATLAB. ECGs were recorded for 45 secs and an average over 30 secs was analysed to extract wave amplitudes (P, Q, R, S, J, T) relative to the

isoelectric line, and the duration between waves (RR, PR, QT). Recordings in animals with a core temperature <35°C during the recording or traces without a clear R wave were excluded.

Magnetic resonance (MR) imaging

Cine-MRI was performed in 8-week-old mice in the diurnal period as described previously[62,63]. Anaesthesia was induced in an anaesthetic chamber by 2.5% isoflurane in oxygen and nitrous oxide (O_2:N_2O 4:1, total of 2 L/min). After induction, the mouse was transferred to the cradle positioned in the horizontal supine position, and anaesthesia was maintained at 1.8-2% for the experiment (O_2:N_2O 4:1, total of 2 L/min). The temperature of the cradle was maintained at 35°C via warm airflow through an integrated heat exchanger to maintain core temperature at 37°C. A bespoke ECG and respiratory gating device was used to monitor heart and respiration signals. ECG signals were obtained from electrodes inserted subcutaneously into the chest and respiratory signals were obtained from a wire loop positioned loosely at the level of the sternum. A custom-made $^{1}H/^{13}C$ butterfly surface coil (loop diameter, 20 mm) was also placed over the mouse chest to localise the signal from the heart. The cradle was inserted into a horizontal-bore 7 tesla MR scanner interfaced to a direct-drive console, with the animal's heart positioned at the isocentre of the scanner. Correct positioning of the mouse was confirming by acquiring cardiac-triggered and respiration-gated axial FLASH (proton fast low-angle shot) images. Long-axis scans were taken to orientate the scanning angle and to set up true short-axis views. High-resolution cine-MR short-axis images were then acquired in 9-10 contiguous slices (1 mm thick) covering the entire heart. Functional parameters of contractile function were derived from short-axis images. Each *in vivo* scanning protocol lasted ~45-50 mins. Animals were allowed to recover fully from anaesthesia. For each 1 mm slice, end-diastolic and end-systolic frames were selected according to the size of the left-ventricular (LV) lumen. For each frame, the epicardial and endocardial border (drawing around any papillary muscles) were outlined using the free-hand tool in Fiji ImageJ. The epicardial and endocardial area for each frame were summed across the Z-stack to cover the entire heart to render LV end-diastolic and end-systolic volumes (EDV and ESV, respectively).

Echocardiography

LV size and function were assessed *in vivo* by 2D echocardiography in isoflurane-anaesthetised mice using a high-resolution VisualSonics ultrasound system (Vevo 3100) with a 40 MHz transducer (MX400). Mice were maintained on 1-1.5% isoflurane in oxygen (1 L/min), placed on a homeothermic table, and parasternal short-axis B-mode views were obtained at the level of the papillary muscles. LV wall thickness and chamber dimensions were determined in the parasternal short-axis view (M-mode), from which LV structural and functional parameters were derived. 2D images of the heart were obtained from the apical 4-chamber view to assess mitral blood flow (E and A) and tissue (e' and a') Doppler velocities. Body temperature, heart rate and respiratory rate were controlled during imaging and all experiments were performed under physiological conditions. Data analysis was performed by a single operator blinded to genotype using VevoLAB (version 5.5.1). Measurements were made directly from the 2-D images and are therefore expressed as areas.

Fluorescence imaging of ventricular myocytes

To record Ca^{2+} transients (CaTs), adult ventricular myocytes were AM-loaded for 10 mins at room temperature with FuraRed (Invitrogen; F3021) at a concentration of 9.2 μM with 0.1% (w/v) Pluronic-F127. Ratiometric Ca^{2+} imaging was executed in dual-excitation mode (excitation alternating between 490 nm and 435 nm/emission 645 ± 37.5 nm). FuraRed ratios were calibrated to [Ca^{2+}] as described previously[53]. To measure cell size, adult ventricular myocytes were AM-loaded for 6 mins at room temperature with cSNARF-1 (Invitrogen, C1272) at a concentration of 17.6 μM (excitation 555 nm/emission 580 nm and 640 nm). In neonatal ventricular myocytes, action potentials were imaged in cells loaded for 30 mins at room temperature with FluoVolt (Invitrogen, F10488; 1:1,000 v/v; supplemented with PowerLoad at 1:100 v/v) in single-excitation mode (excitation 488 nm/emission >510 nm). CaTs were imaged in neonatal ventricular myocytes AM-loaded for 10 mins at room temperature with Fluo-3 (Invitrogen, F1242) at a concentration of 35.4 μM with 0.07% (w/v) Pluronic-F127 in single-excitation mode (excitation 488 nm/emission >510 nm).

Images were analysed to remove background and calculate the fluorescence ratio of the two wavelengths. An algorithm identified the CaT and caffeine responses, the starting point of the response, and obtained an averaged CaTs of a train. This provided measurements of diastolic, systolic, resting and peak-caffeine Ca^{2+} responses, as well as time-courses of recovery required to calculate SERCA and NCX, as described previously[53]. Fluorescence

images were also used to calculate cell shortening. This was obtained by thresholding the fluorescence map to identify the myocyte, and measuring its area during the experimental protocol, followed by normalisation to diastolic area.

Dual-excitation FuraRed imaging and single-excitation FluoVolt/Fluo-3 imaging was performed on an Olympus IX73 inverted microscope with an sCMOS camera (optiMOS, QImaging) and LED light source (CoolLED pE-4000), synchronised to the camera using a multichannel streaming device (MultiStream Pro, Cairn Research) and operated by MicroManager (version 1.4.23). cSNARF-1 imaging was performed in xy mode on a Zeiss LSM 700 inverted confocal microscope. Adult ventricular myocytes were superfused at 37°C with solution containing (in mmol/L): 125 NaCl, 22 $NaHCO_3$, 4.5 KCl, 1 $MgCl_2$, 1 $CaCl_2$, 11 glucose, 1 probenecid (5% CO_2/air). Selected solutions contained 10 mM caffeine or 6 mM sodium propionate (osmolality balanced by adjusting [NaCl]). Neonatal ventricular myocytes were superfused at 37°C with solution containing (in mmol/L): 135 NaCl, 20 HEPES, 4.5 KCl, 1 $MgCl_2$, 1 $CaCl_2$, 11 glucose, 1 probenecid; pH adjusted to 7.40 at 37°C with NaOH.

Sulforhodamine B assay for cellular biomass

Cardiomyocyte hypertrophy was assessed for using a quantitative *in vitro* assay utilising sulforhodamine B (SRB)[64]. Isolated NRVMs were plated on specialised 96-well microplates (Ibidi µ-Plate 96-Well Black, #89626) at 60,000 cells per 200 µL well and treated for 48 hrs under serum-free conditions. After treatment, cells were rinsed in ice-cold PBS and fixed in 4% (w/v) paraformaldehyde/PBS (pH 7.4) for 10 mins at 4°C. The remaining steps were performed at room temperature. After fixation, cells were permeabilised in 0.5% (v/v) Triton-X 100 for 10 mins. Myocytes were then stained with the nuclear dye Hoechst-33342 (Invitrogen, #H3570) for 5 mins (0.1% v/v in PBS), before staining with 0.004% (w/v) SRB dissolved in 1% (v/v) acetic acid for 10 mins. Wells were then rinsed four times with 1% acetic acid and dried. Plates were then imaged on a BioTek Cytation 5 plate-reader system with a dry 4x objective and sequential excitation at 377 nm and 531 nm. Fluorescence was then measured at 417-477 nm and 630-650 nm, respectively. The Hoechst and SRB images were analysed in MATLAB to quantify nuclear and extra-nuclear regions (nSRB and eSRB, respectively) and data were presented as the eSRB/nSRB ratio.

Immunoblotting of histone extracts

Histones were extracted from cultured NRVMs using the EpiQuik Total Histone Extraction Kit (Epigentek, #OP-0006). Extracted histones were quantified using BCA assay (Pierce BCA Protein Assay Kit; Thermo Scientific, #23227) and stored in -80°C until use. Samples were prepared in 4x Laemmli sample buffer (Bio-Rad) under reducing conditions (β-mercaptoethanol) and boiled at 100°C for 5 mins. SDS-PAGE was performed using pre-cast 4-20% gradient gels (Bio-Rad, Mini-PROTEAN TGX Precast Protein Gels, #4561096). Separated proteins were blotted onto PVDF membranes (Bio-Rad) for 90 mins at 90 V. The PVDF membrane was blocked in 5% milk in 0.1% TBS-T (20 mM Tris-base, 137 mM NaCl, 0.1% v/v Tween 20, pH 7.40) for 1 hr at room temperature. Primary antibodies were prepared in TBS-T with 1% BSA and membranes probed overnight at 4°C. Primary antibodies used were against H3K9ac (#C5B11, Cell Signalling Technology; 1:2000), pan-propionyllysine (#PTM201, PTM Biolabs; 1:2000), total H3 (#1B1B2, Cell Signalling Technology; 1:2000), total H4 (#D2X4V, Cell Signalling Technology; 1:1000). Blots were washed 5 times with TBS-T for 5 mins and probed with HRP-conjugated secondary antibodies (Novus Biologicals) for 1 hr at room temperature. After incubation with the secondaries, the TBS-T washes were repeated and blots were developed, using enhanced chemiluminescence (ECL) substrate and a ChemiDoc system (Bio-Rad).

Immunofluorescence

Immunofluorescence was performed for histone modifications in the nuclei of ARVMs and NRVMs. Myocytes were plated on 12-well chamber glass slides (Ibidi, #81201). Myocytes were fixed with ice-cold methanol for 10 mins at 4°C and the remaining steps were performed at room temperature. After methanol-fixation and prior to blocking, ARVMs were pre-treated with TrueBlack lipofuscin autofluorescence quencher (Biotium, #23007) for 5 mins at room temperature. Cells were blocked in PBS containing 3% BSA for 1 hr. Primary antibodies were loaded in PBS/3% BSA for 90 mins. Primary antibodies used were against H3K27ac (#D5E4, Cell Signalling Technology; 1:100), total H3 (#1B1B2, Cell Signalling Technology; 1:300), vimentin (#ab24525, Abcam; 1:300). Vimentin was used to identify any contaminant fibroblasts in NRVM preps. Cells were washed three times with PBS-0.05% Tween 20 then incubated with the secondary antibodies in PBS/3% BSA for 1 hr. After secondary antibody incubation, the wash step was repeated and the slide was covered, following application of anti-fade reagent (ProLong Gold antifade, Invitrogen, #P36934), with a cover glass (Ibidi, #10811; 170 μm thickness). Secondary antibodies used were Alexa Fluor Plus 488

conjugated anti-rabbit IgG (#A32731, Invitrogen; 1:1000), Alexa Fluor Plus 555 conjugated anti-mouse IgG (#A32727, Invitrogen; 1:1000), Alexa Fluor 405 conjugated anti-chicken IgY (#ab175675, Abcam; 1:500). Selected coverslips were stained with Hoechst-33342 (0.1% v/v in PBS), a DNA stain that emits blue fluorescence when excited at 405 nm (Invitrogen, H3570). Immunofluorescence was performed on a Zeiss LSM 700 confocal microscope with a 40x oil-immersion objective in *xy* mode, with sequential excitation of wavelengths 405, 488 and 555 nm.

Whole-cell ELISA

Quantitative indirect ELISA was performed on fixed myocytes. NRVMs were seeded onto clear 96-well microplates at a density of 45,000 cells per well in culture media. At day-2 post-isolation, myocytes were serum-starved and on day-3 treated for 24 h under serum-free conditions. After 24 hrs, cells were rinsed twice with cold 1x PBS, fixed with ice-cold methanol for 10 mins at 4°C, followed by a preliminary blocking stage with 0.3% H_2O_2 in PBS for 10 mins at room temperature. Cells were blocked in blocking buffer containing 10% FCS in PBS-T (0.05% Tween-20) for 1 hr at room temperature. Primary antibody was applied for 2 hrs at room temperature in blocking buffer. Primary antibodies were against H3K9ac (#C5B11, Cell Signalling Technology; 1:300) and total H3 (#1B1B2, Cell Signalling Technology; 1:300). Cells were then washed four times with PBS-T (0.05% Tween-20) then incubated for 1 hour at room temperature with HRP-conjugated secondary antibody in blocking buffer. Secondary antibodies were polymeric HRP goat α-rabbit IgG (#ab214880, Abcam; 1:4) and polymeric HRP goat α-mouse IgG (#ab214879, Abcam; 1:4). The PBS-T washing steps were repeated and the ELISA was performed immediately. Development of the ELISA was based on McIlwain's solution, containing 280 mM Na_2HPO_4 and 100 mM citric acid (pH 5.0 at room temperature). Immediately prior to use, H_2O_2 and o-phenylenediamine dihydrochloride (OPD) was added to McIlwain's solution (10 mg OPD and 10 µL of 30% H_2O_2 in 10 mL McIlwain's). 50 µL of McIlwain's development solution was added to each well and the reaction was stopped by 100 µL of 2.0 M H_2SO_4. Absorbance was read immediately at 490 nm using a plate-reader platform (Cytation 5, BioTek).

RNA extraction

All procedures for RNA extraction were performed in DNase/RNase-free conditions. For NRVMs, the media was rinsed away with ice-cold PBS and RNA extracted by TRIzol reagent, according to the manufacturer's protocol. Ventricular tissue from 8-week mice was snap-frozen and cryoground. Bulk RNA was extracted using the Zymo Quick-RNA Miniprep Plus Kit (R1057), following the manufacturer's protocol with some modifications in the tissue digestion stage. All centrifugation steps were performed at 16,000 RCF at 4°C. 20 mg of cryoground tissue was mechanically homogenised on ice with disposable probes (Qiagen TissueRuptor II) in 350 µL of DNA/RNA Shield. 45 µL of Proteinase K mix was added to 300 µL of sample, incubated for 30 mins at 55°C, and centrifuged for 2 mins after incubation. The supernatant was transferred to new microcentrifuge tubes and 300 µL RNA Lysis Buffer was added at 1:1 to the supernatant. Thereafter, the RNA purification procedure followed the manufacturer's protocol, with some differences: half volume ethanol (300 µL) was added, in order to isolate RNAs ≥ 200 nt for poly(A) enrichment; DNase I treatment was performed in-column; RNA was eluted in non-DEPC-treated nuclease-free water.

RNA-sequencing

Library preparation and RNA-sequencing (RNA-seq) was performed by the Oxford Genomics Centre, Wellcome Centre for Human Genetics, University of Oxford. The assessment of RNA integrity was performed using the Agilent RNA 6000 Nano Kit with an Agilent 2100 Bioanalyzer. Samples were loaded onto a microplate (LVis Plate, BMG Labtech) and absorbance (A_{260}/A_{280}) read using a SECTROstar Nano plate-reader (BMG Labtech). For library preparation, RNA was fractionated by enrichment for poly(A). Poly(A)+ RNA was converted to a library of cDNA fragments and adapter-ligated. Samples were sequenced on an Illumina NovaSeq 6000 System across 2 x 10-plex units, to achieve an approximate sequencing depth of 25 million reads per sample. Raw reads were 150 bp in length. The following analysis was performed on a UNIX platform. Spliced Transcripts Alignment to a Reference (STAR) was used to align raw reads to the UCSC mouse reference genome *mm10* or *rn6*[65]. PCR duplicates were removed. featureCounts was used to generate the list of differentially expressed genes (DEGs) and their abundance in the samples, expressed as counts per million (cpm)[66]. DEG analysis was performed using DESeq2[67]. The Wilkinson formula for analysing mouse data was genotype + sex + genotype:sex. NRVM data were analysed at three treatment levels (control, propionate, butyrate). After identifying the DEGs, the mouse and NRVM datasets were analysed and compared accordingly.

Reverse transcription quantitative real-time PCR (RT-qPCR)

RT-qPCR was performed in accordance with the MIQE guidelines[68] and were performed in DNase/RNase-free conditions. First-strand cDNA was synthesised using the High-Capacity cDNA Reverse Transcription Kit (Applied Biosystems, #4368814). RT-qPCR was performed on a ViiA 7 System (Life Technologies) using Fast SYBR Green (Fast SYBR Green 2X Master Mix; Applied Biosystems, #4385612). Each reaction used 4 ng of cDNA and the concentration of primers was 200 nM. Fold-changes were determined by the $2^{-\Delta\Delta Ct}$ method[69]. For mouse RT-qPCR experiments, genes of interest were normalised to the geometric mean of four reference genes (*Gusb*, *Pol2a*, *Tbp* and *Ywhaz*) previously described as stable in the heart[70]. For rat RT-qPCR experiments, genes of interest were normalised to *Hprt1*. Primers used are listed in **Supplementary Table 12**.

^{13}C tracing histone MS-MS

Analyses were performed at the Target Discovery Institute, University of Oxford.

Sample preparation: Samples for ^{13}C tracing metabolomics was performed in cultured NRVMs with custom media as described above (*'isolation of neonatal ventricular myocytes'* and *'^{13}C tracing custom media'*). Between 2-2.5 M NRVMs were seeded per 60 mm Petri dish for each condition. For tracer experiments using U^{13}C amino acids, NRVMs were treated for 48 hrs on day-3 post-isolation, whilst NRVMs were treated for 24 hrs on day-4 post-isolation for tracer experiments using 1-^{13}C propionate. For harvesting the NRVMs and isolation of intact histones, cells were trypsinised with 1x trypsin-EDTA and resuspended in ice-cold 1x PBS containing 10 mM sodium butyrate and protease inhibitor cocktails. The cell suspension was transferred to 1.5 mL tubes and centrifuged at 1,000 RCF for 2 mins at 4°C. The supernatant was discarded and the pellet resuspended in 150 µL ice-cold hypotonic lysis buffer, containing (in mmol/L): 10 Tris-HCl pH 8.0, 1 KCl, 1.5 $MgCl_2$, 1 DTT, 10 sodium butyrate and protease inhibitor cocktail. The samples were incubated on a rotator for 30 mins at 4°C, then centrifuged at 10,000 RCF for 10 mins at 4°C. The supernatant was discarded. The pellet containing intact nuclei was resuspended in 100 µL of ice-cold 0.4 M HCl and incubated on a rotator for 1 hr at 4°C. Samples were then centrifuged at 16,000 RCF for 10 mins at 4°C and the supernatant containing histones were transferred to 1.5 mL tubes. Histones were precipitated by adding 1 mL of ice-cold acetone to each sample, thoroughly

mixing, then incubating overnight at -20°C. The next day, histones were pelleted by centrifuging at 16,000 RCF for 10 mins at 4°C and the pellet washed with 1 mL ice-cold acetone. Centrifugation was repeated at 16,000 RCF for 5 mins at 4 °C, the supernatant was carefully removed and the pellet allowed to air-dry at room temperature for 20 mins. Dried histone pellets were reconstituted in 25 µL ultra-pure water and stored at -80°C until further processing.

Propionic anhydride derivatisation and in-solution trypsin digestion: Histone protein concentration was quantified by BCA assay and 20 µg of histone protein was used for sample preparation. D10-propionic anhydride derivatisation of histones was performed based on the H 42x hydroxylamine (HA) method from Meert, *et al.*[71] to cap unmodified lysines at the protein level. Propionic anhydride reagent for pre-trypsinisation propionylation was freshly prepared immediately before use by mixing D10-propionic anhydride (Eurisotop, DLM-3305-0.5) with isopropylalcohol at a 1:79 (v/v) ratio. 20 µg of vacuum-dried histones (SpeedVac) were resuspended in 20 µL 1M TEAB (Merck, 18597) and an equal volume of propionic anhydride reagent was immediately added. After incubating at room temperature for 30 min, 20 µL of ultra-pure water was added and the sample incubated at 37°C for 30 min. The sample was vacuum-dried and resuspended in 100 µL of buffer containing 50 mM TEAB, 1 mM $CaCl_2$ and 5% ACN. 100 µg Trypsin Gold (Promega V5280) was reconstituted in 200 µL 50 mM ammonium bicarbonate and trypsin was added to each sample at a histone:enzyme ratio of 20:1 and incubated overnight (16 hrs) at 37˚C. Samples were vacuum-dried and resuspended in 200 µL 0.5 M hydroxylamine (Merck, 438227) to reverse overacylation. 60 µL ammonium hydroxide (Merck, 338818) was added to increase pH to 12 (assessed with pH paper), the sample incubated at room temperature for 20 min then vacuum-dried until the total sample volume was <100 µL. 25 µL 20% TFA was added to lower pH to ≤3 and proceeded to sample clean-up. C18 desalting and clean-up was performed using Pierce C18 100 µL tips (Thermo Fisher, 87784). Tips were washed with 50% ACN and equilibrated with 0.1% TFA. Equilibrated tips were used to dispense and aspirate the sample ~10 times, before rinsing tips with 0.1% TFA/5% ACN and eluting the peptides in 0.1% TFA/50% ACN into Protein LoBind tubes (Eppendorf). Samples were dried down and vacuum-dried peptides were stored in -20°C until analysis.

LC-MS/MS: The Orbitrap Fusion Lumos Tribid mass spectrometer (Thermo Fisher Scientific) coupled to an Ultimate 3000 UHPLC (Thermo Fisher Scientific) was used to analyse the purified tryptic peptides. Six per cent of tryptic peptides were loaded onto a trap column

(PepMapC18; 300µm x 5mm, 5µm particle size, Thermo Fisher) and separated on a 50cm-long EasySpray column (ES803, Thermo Fischer) using a-60 minute linear gradient from 2 % to 35% buffer B (A: 5% DMSO, 0.1% formic acid; B: 5% DMSO, 0.1% formic acid in acetonitrile) at 250 nl/min flow rate. Eluted peptides were then analysed on an Orbitrap Fusion Lumos Tribrid (instrument control software v3.3). Data were acquired in data-dependent mode, with the advance peak detection (APD) enabled. Survey scans were acquired in the Orbitrap at 120 k resolution over a m/z range 400 -1500, AGC target of 4e5 ions and S-lens RF of 30. MS/MS spectra were obtained in the Orbitrap at 30k resolution with a Quad isolation window of 1.6, AGC target of 5e4 ions, maximum injection time of 54 ms, with HCD activation and a fixed collision energy set at 30%.

Data analysis: Data were analysed using FragPipe v19.1. Initially the data were analysed using the FragPipe open search workflow to determine the amino-acid mass shift induced by growing cells in presence of heavy Isoleucine and heavy valine; or $1C^{13}$ propionic acid, as well as the mass shift induced by *the in vitro* derivatisation at protein level of non-modified lysines with D10-propionic acid in the histone enriched fractions (pre-trypsin digestion). The data were searched against the reviewed SwissProt-uniprot Rattus norvegicus proteome (downloaded 20230203_10102 sequences) and analysed using the default open search parameters. The open searched identified mass shifts of +5.01677 in Val, 6.02129 in Leu as a result of the incorporation of heavy Val and Ile into proteins, respectively; +57.02956 in K corresponding to a K propionylation with $1C^{13}$; +61.0574 in K and n-term corresponding to D10-propionylation and +59.03627 in K corresponding to propionylation with three C^{13} (3-Pro; probably coming from heavy Val or Ile). These mass shifts were used for a second FragPipe analysis. In this second FragPipe analysis we used the Label Free Quantitation with Match Between Runs workflow (LFQ-MBR) with the minor changes on the default settings. Briefly, data were searched against the Rat proteome, selecting trypsin as proteolytic enzyme (maximum 2 missed cleavages) and oxidation (M; +15.9949), acetylation (K, N-terminal; +42.0106), heavy Val (+5.01677), heavy Ile (+6.02129), propionyl anhydride (K; 56.0262; Pro), propionyl:13C1(K, +57.02956; 1-Pro), D10-propionic anhydride (k, n-terminus; +61.0574), propionyl mono-methyl (K, +70.0422; Pro-me) and heavy propionylation (k; +59.03627; 3-Pro) as variable modifications. MBR (match between runs) ion FDR of 1% was applied. Intensities and MaxLFQ intensities were reported in the data outputs. FragPipe modified-combined_peptides output was used to look at changes on Histone propionylation induced by the experimental treatment. The mass spectrometry raw related to histone post-

translational modifications had been deposited to the Proteome eXchange Consortium via the PRIDE partner repository[72] with the dataset identifier PXD043513.

Chromatin immunoprecipitation (ChIP)

For mouse ChIP, 8-week-old mouse hearts were fixed for 10 min at room temperature with 1 % formaldehyde in modified AMVM isolation solution containing 0.5 mM EGTA (solution pH 7.4 at room temperature) in Langendorff mode. Fixed ventricles were minced and rinsed twice in PBS, then lysed in ChIP lysis buffer (1 % SDS, 10 mM Tris-HCl pH 8.0, 1 mM EDTA) by homogenisation (Qiagen TissueRuptor II). For NRVM ChIP, NRVMs were fixed for 10 min with 1 % formaldehyde in PBS, then lysed in ChIP lysis buffer. Samples were sonicated using a Covaris (Woburn, MA) to achieve 200-300 bp fragments, according to the manufacturer's protocol. For reference-normalised ChIP-sequencing, fixed, sonicated, *Drosophila* S2 cells were added to the sonicated samples at a ratio of 4:1 mouse/rat:*Drosophila*. Insoluble material was pelleted, and soluble sonicated chromatin was incubated overnight with antibodies against H3K27ac (Diagenode C15410196), pan-propionyllysine (PTM-Bio PTM-201), or H3K23pr (Abcam ab241466). Protein-A/G Plus Agarose beads (ThermoFisher Scientific) were used to isolate antibody-chromatin complexes, then washed three times with RIPA buffer (50 mM HEPES-KOH pH 7.6, 500 mM LiCl, 1 mM EDTA, 1% NP-40, 0.7% Na deoxycholate) and once with TE-NaCl (10 mM Tris-HCl pH 8.0, 1 mM EDTA, 50 mM NaCl). Samples were treated with RNase A and proteinase K, and crosslinks were reversed at 65˚C overnight, then DNA was purified by phenol/chloroform extraction. For ChIP-qPCR, DNA was quantified with SYBR Green MasterMix (ThermoFisher Scientific) relative to input chromatin. Primers used are listed in the table at the end of this section. Sequencing libraries for ChIP-seq were prepared using the NEBNext Ultra II DNA Library Preparation Kit (NEB), and 40 bp paired-end sequencing was conducted using a NextSeq 500 (Illumina). Bioinformatic analysis was conducted as previously described[73]. Sequencing quality was assessed with fastQC (http://www.bioinformatics.babraham.ac.uk/projects/fastqc/), then reads were trimmed with trim_galore (https://www.bioinformatics.babraham.ac.uk/projects/trim_galore/) and mapped against rat, mouse or *Drosophila* genome assembly mm10, rn6 or dm6, respectively, using Bowtie2[74]. PCR duplicates were removed with Picard MarkDuplicates (http://broadinstitute.github.io/picard/). Sequence tag directories were generated using the Homer tool makeTagDirectory, then makeBigWig.pl was used to generate bigwig files for visualisation in UCSC[75]. Peaks were called using findPeaks -style histone, with the input track

providing background correction, and metagene profiles were generated using annotatePeaks.pl. Reference normalisation was achieved by calculating the ratio of dm6:mm10 or dm6:rn6 reads in input and IP samples, and used to scale bigwigs and metaplots. See **Supplementary Table 13** for list of primers.

Förster resonance energy transfer (FRET)

FRET imaging was performed as previously described[76]. NRVMs were transduced with second-generation adenoviral vectors encoding for the cGi500 FRET-based cGMP sensor[77] on day-2 post-isolation. FRET imaging was performed on an inverted microscope (Olympus IX71) using a PlanApoN, 40×, NA 1.42 oil immersion objective, 0.17/FN 26.5 (Olympus). The microscope was equipped with a CoolSNAP HQ2 monochrome camera (Photometrics, USA) and an optical beam-splitter device to simultaneously record YFP and CFP emissions (Dual-view simultaneous-imaging system, DV2 MAG Biosystems). FRET filter settings used throughout were: CFP excitation filter ET436/20x, dichroic mirror 455DCLP (Chroma Technology) in the microscope filter cube; dichroic mirror 505DCLP, YFP emission filter 545 nm, and CFP emission filter 480 nm (Chroma Technology) in the beam splitter. Images were acquired and processed using Meta imaging series 7.1, MetaFluor (Molecular Devices). Fluorescence emission images were acquired every 5 sec. Basal FRET was measured as the background-subtracted 480 nm/545 nm fluorescence emission intensity on excitation at 436 nm. FRET changes were measured as changes in the background-subtracted 480 nm/545 nm fluorescence emission intensity on excitation at 430 nm, where R is the 480 nm/545 nm value at time t. Cells were cultured on sterilised laminin-coated borosilicate glass coverslips, which allowed the transfer to a perfusion chamber. The solution for the measurements contained (in mmol/L): 125 NaCl, 5 KCl, 1 Na_2PO_4, 1 $MgSO_4$, 20 HEPES, 5.5 Glucose and 1 $CaCl_2$ (pH 7.4 at room temperature). Reagents used on experiments: PF04449613 (‘PF9613’, BioTechne Tocris), IBMX (Sigma-Aldrich/Merck), SNAP (Cayman Chemicals), BAY41-2272 (Sigma-Aldrich/Merck).

cGMP ELISA

cGMP concentration in mouse heart tissue was measured using a commercially available ELISA kit (Amersham cGMP Enzyme immunoassay EIA Biotrak System, Cytiva, RPN226). The manufacturer protocol was used following ‘Protocol 2 – Acetylation EIA Procedure’ with

some minor modifications. 30 mg of snap-frozen ventricular tissue was homogenised on ice with 270 µL of cold 6% (w/v) trichloroacetic acid to give a 10% (w/v) homogenate. Samples were centrifuged at 2,000 RCF for 15 mins at 4°C. The pellet was kept for protein quantification (see below) and the supernatant washed 4 times with 1 mL of water-saturated diethyl ether (prepared by mixing diethyl ether and ultra-pure water at 1:1 ratio and vigorously mixing). The upper ether layer was discarded after each wash and the remaining aqueous extract vacuum-dried overnight (SpeedVac). The dried extract was resuspended in 1 mL of diluted assay buffer by mixing at 1,500 RPM (ThermoMixer, Eppendorf) for 5 mins at room temperature. The resuspended mix was centrifuged briefly at 16,000 RCF for 30 secs to clear insoluble debris and the manufacturer protocol was followed for the remainder of the assay. A two-sample F-test for equal variance was used to test for statistical significance. To normalise measured cGMP concentrations to protein concentration, insoluble pellets were lysed in 130 µL of urea buffer (8M urea, 1M thiourea, 0.5% CHAPS, 50 mM DTT, 24 mM spermine) for 15 minutes at room temperature by mixing at 1,500 RPM (ThermoMixer). Total protein concentration was determined by Bradford assay.

Phosphoproteomics

Analyses were performed in the Department of Biochemistry, University of Oxford.

Sample preparation: Snap-frozen ventricular tissue was resuspended in 1 mL of lysis buffer (100 mM TEAB, 150 mM NaCl, 0.5% NP-40, protease and phosphatase inhibitors). The heart was thawed for 2-3 minutes before homogenising (Qiagen TissueRuptor II). Homogenised sample was incubated on ice for 15 mins then centrifuged at 16,000 RCF for 30 mins at 4°C. Supernatant was collected containing whole cell protein lysate and protein concentration determined using a spectrophotometer to measure absorbance at 280 nm (NanoDrop, Thermo Fisher). 400 µg of protein was taken forward and all samples normalised to a total volume of 80 µL using lysis buffer. Detergent was removed using commercially available resin according to the manufacturer's protocol (HiPPR Detergent Removal Resin, Thermo Fisher, 88305). Proteins were denatured by adding to the samples freshly prepared solution of 8M urea in 100 mM ammonium bicarbonate (pH 7.8) at a 1:1 ratio. Samples were incubated for 10 mins at room temperature with gentle shaking at 650 RPM (ThermoMixer, Eppendorf). Cysteines were reduced with 10 mM TCEP ((tris(2-carboxyethyl)phosphine)) and incubated for 30 mins at room temperature. ClAM (2-chloroacetamide) was freshly prepared in 8M

urea/100 mM ammonium bicarbonate solution and protected from light. Cysteines were then alkylated by adding 50 mM ClAM (2-chloroacetamide) and incubating in the dark for 30 mins at room temperature. Samples were pre-digested using LysC at a ratio of 1 µg LysC to 100 µg of protein by incubating for 2 hrs at 37°C with shaking at 800 RPM. The urea concentration was reduced to 2 M by diluting the sample with 100 mM ammonium bicarbonate solution and $CaCl_2$ was added to a final concentration of 2 mM. 1 µg of trypsin was added for 100 µg of protein and samples were digested overnight (16 hrs) at 37˚C with shaking at 800 RPM. Trypsin digestion was ceased by adding formic acid to a final concentration of 5% and the samples centrifuged at 16,000 RCF for 30 mins at 4°C to remove aggregates. The supernatant was collected and proceeded with desalting and sample clean-up using bespoke C18 columns produced using C18 resin and sterile 200 µL pipette tips. C18 resin was activated using 100% ACN and the columns equilibrated using 0.1% TFA. Peptides were eluted in 2 rounds of centrifugation using 100 µL of 50% ACN/0.1% TFA solution. Samples were transferred to Protein LoBind tubes and vacuum-dried overnight (SpeedVac). Phosphopeptide enrichment was performed using titanium dioxide (TiO_2) microspin columns (TopTip, Glygen, TT2TIO) as described previously[78,79].

LC-MS/MS: Peptides were separated by nano liquid chromatography (Thermo Scientific Ultimate RSLC 3000 or Easy-nLC) coupled in line with a Q Exactive mass spectrometer equipped with an Easy-Spray source (Thermo Fisher Scientific). Peptides were trapped onto a C18 PepMac100 precolumn (300µm i.d.x5mm, 100Å, Thermo Fisher Scientific) using Solvent A (0.1% Formic acid, HPLC grade water). The peptides were further separated onto an Easy-Spray RSLC C18 column (75µm i.d., 50cm length, Thermo Fisher Scientific) using a 60 minutes linear gradient (15% to 35% solvent B (0.1% formic acid in acetonitrile)) at a flow rate 200 nL/min. The raw data were acquired on the mass spectrometer in a data-dependent acquisition mode (DDA). Full-scan MS spectra were acquired in the Orbitrap (Scan range 350-1500m/z, resolution 70,000; AGC target, 3e6, maximum injection time, 50ms). The 10 most intense peaks were selected for higher-energy collision dissociation (HCD) fragmentation at 30% of normalized collision energy. HCD spectra were acquired in the Orbitrap at resolution 17,500, AGC target 5e4, maximum injection time 60ms with fixed mass at 180m/z. Charge exclusion was selected for unassigned and 1+ ions. The dynamic exclusion was set to 40 s.

Data processing: Tandem mass (MS/MS) spectra were searched using Sequest HT in Proteome discoverer software version 1.4 as follows: MS/MS data from TiO2 enriched

samples were searched against a protein sequence database containing 17,962 protein entries, including 17,679 Mus musculus proteins (Uniprot release from 2023-03-28) and 283 common contaminants. During database searching cysteines (C) were considered to be fully carbamidomethylated (+57,0215, statically added), methionine (M) to be fully oxidised (+15,9949, dynamically added), all N-terminal residues to be acetylated (+42,0106, dynamically added) and Serine (S), Threonine (T) and Threonine (Y) to be phosphorylated (+79,966, dynamically added). Two missed cleavages were permitted. Peptide mass tolerance was set at 20ppm on the precursor and 0.6 Da on the fragment ions. Data was filtered at FDR below 1% at PSM level. Significant phosphorylated sequences were identified at 0.05 FDR and processed for kinase consensus site search (Phosphosite Plus v6.7). Intensity data for identified phospho-peptides was logged to base 2 prior to statistical analysis using a two-sample t-test used to assess the difference in means between the two conditions. The data is displayed as a volcano plot with negative log10 of the p-value on the y-axis and difference between the means on the x-axis. Thresholds of FDR <0.05 with a log2(fold change) of >2 were used to determine significance of each phospho-site. Kinase substrates were annotated with putative kinases with log2(scores) better than 3. The mass spectrometry raw related to phosphoproteomics had been deposited to the Proteome eXchange Consortium via the PRIDE partner repository[72] with the dataset identifier PXD043384.

Statistics and data analysis

Statistical comparisons were made using paired or unpaired Student's t-tests, repeated measures or two-way ANOVA with Tukey's post hoc tests, regression analyses, or Pearson's correlation analyses, as appropriate. Hierarchical statistical analysis was performed for cardiomyocyte studies using in R using previously published methods[80] to avoid pseudoreplication error. P<0.05 or P.adj<0.05 was considered significant. Presented data represent mean ± SEM, unless stated otherwise.

DATA AVAILABILITY

All data supporting the findings of this study are available in the Supplement or from the corresponding authors on reasonable request. High-throughput sequencing data have been deposited in the Gene Expression Omnibus (GEO) under accession number GSE205838.

Mass spectrometry data have been deposited to the ProteomeXchange Consortium via the PRIDE partner repository with the dataset identifier PXD043384 for phosphoproteomics data and PXD043513 for histone proteomics data.

ACKNOWLEDGEMENTS

In memory of Holger Kramer. We thank Lourdes Desviat (Universidad Autonoma de Madrid) and Michael A. Barry (Mayo Clinic) for providing the mouse model. We gratefully acknowledge Nicola Smart, Carolyn Carr, Mark Richards, Aminah Loonat, Stefania Monterisi, Johanna Michl, Chela Alonso and Elizabeth Slee (University of Oxford) and Michael Shattock and Yujin Chung (King's College London) for providing training and research materials. Supported by a British Heart Foundation (BHF) 4-Year Non-Clinical PhD Studentship FS/16/59/32735 to K.C.P. Research reported in this article was funded by grant PAF112/115 from the Propionic Acidemia Foundation to P.S., British Heart Foundation Programme Grant RG/15/9/31534 to P.S., European Research Council Consolidator Award SURVIVE #723997 to P.S., Metabolic Support UK Initial Grant to P.S., funding support from the Organic Acidemia Association to P.S, Oxford BHF Centre of Research Excellence RE/18/3/34214 to P.S., Oxford Medical Sciences Internal Fund Pump-Priming grant 0011976 to K.C.P, Medical Research Council Molecular Haematology Unit grant MC_UU_00016/6 to N.T.C and T.A.M, Kay Kendall Leukaemia Fund Intermediate Fellowship KKL1443 to N.T.C., and a Biotechnology and Biological Sciences Research Council grant BB/P013406/1 to S.T.

AUTHOR CONTRIBUTIONS

P.S. conceived and directed the study; K.C.P. performed the majority of experiments; K.C.P. and N.T.C. contributed to the direction of the study; K.C.P., N.T.C., N.L., S.K., Y.J.C., I.V., D.H., M.F., E.P., L.W., G.R., A.H. performed measurements and analyses; E.K.G., M.G.R., K.L.F. provided biological materials; J.H. analysed the data; A.K., R.C., M.K.C., A.H. and H.K. provided training and/or expertise; M.F., M.Z., R.F. and J.M. provided resources; K.C.P, N.T.C. and P.S., analysed and interpreted the data; P.S. wrote the first draft of the manuscript; K.C.P., N.T.C., S.T., J.H. contributed to manuscript revisions; S.T., T.A.M. and P.S provided supervision and funding; all authors reviewed and approved the manuscript.

COMPETING INTERESTS

N.T.C and T.A.M are shareholders in and consultants for Dark Blue Therapeutics Ltd. The remaining authors declare no competing interests.

FIGURE LEGENDS

Figure 1. Metabolic consequences of disrupted propionyl-CoA carboxylase activity. (A) Selected metabolic pathways processing propionate. Propiogenic substrates (e.g. branched-chain amino acids, odd-numbered fatty acids, methionine, cholesterol) yield propionyl-CoA in the mitochondrial (MITO) matrix. Under restricted recruitment into the Krebs cycle by genetically-ablated PCC (red cross), propionyl-CoA is converted to 2-methylcitrate, propionyl-glycine, propionyl-carnitine or other derivatives. Some derivatives interconvert to free propionate that readily crosses membranes in its protonated form. (B) GC-MS/MS of plasma samples from 8-week female and male mice of WT or PA genotype: free propionate, propionylcarnitine (C3-carnitine), free carnitine, acetylcarnitine (C2-carnitine) (two-way ANOVA; significant effect of genotype at **/*** $P<0.01$/$P<0.001$; (N=6 biologically independent samples). Also shown are data from 8 patients with a managed form of PA and two control, non-PA patient samples for reference. Mean±SEM. (C) Correlations between plasma parameters. Also shown is the relationship ($P<0.05$, Pearson's test) between mouse body weight and propionylcarnitine, with additional mouse samples included that had substantial weight loss. (D) Ion exchange mass spectrometry of sex-balanced plasma samples (N=6 amWT and 8 amPA biologically independent samples), (E) liver lysates (N=8 amWT and 8 amPA biologically independent samples) and (F) cardiac lysates (N=8 amWT and 8 amPA biologically independent samples). Heat-maps show differentially abundant metabolites. Symbol size is proportional to the square-root of mean signal intensity. [1] 2-methylcitrate, [2] cis-2-methylaconitate, [3] 3-acetylpropionate, [4] N-propionylglycine, [5] methionine sulfone. Analysis by one factor ANOVA (Metaboanalyst) corrected for multiple comparisons. (G) Ion-exchange mass spectrometry signal for selected substances detected in plasma, liver and cardiac lysates. Y-axis: intensity. Mean±SEM.

Figure 2. Metabolic consequences of disrupted propionyl-CoA metabolism in the heart. (A) Analysis of ACQ-derivatised amino acids and of underivatised carnitines in plasma (N=8 amWT and 8 amPA biologically independent samples) and (B) matching cardiac lysates. Heatmaps show metabolites that are significantly affected by genotype or an interaction between genotype and sex (two-way ANOVA with Tukey's multiple comparisons test, significance for $P.adj<0.05$). (C) Differentially abundant ($P.adj<0.05$ for genotype) carnitines and amino acids in plasma and (D) cardiac lysates. Diagonal pattern indicates

significant effect of sex (P.adj<0.05); hatched pattern indicates significant interaction between sex and genotype (P.adj<0.05). Mean±SEM. (E) Analysis of cardiac acyl-CoA by LC-MS. Heatmap summarises abundance (absolute quantity in pmol/mg heart tissue) grouped by genotype and sex. Histograms quantify changes, indicating significant (P<0.05) effect of genotype (GEN) or interaction between sex and genotype (SEXxGEN). N=8 amWT male hearts, 7 amPA male hearts, 8 amWT female hearts and 8 amPA female hearts; biologically independent samples. Statistical testing by two-way ANOVA with Tukey's multiple comparisons test. Mean±SEM. Abbreviations: Methylmalonyl-CoA (MM-CoA), BH(I)B-CoA (β -hydroxy(iso)butyryl-CoA). */**/*** P<0.05/<0.01/<0.001 for effect of genotype. ^{s}/^{ss}/^{sss} P<0.05/<0.01/<0.001 for effect of sex. $^{\#}$/$^{\#\#}$ P<0.05/<0.01 for effect of interaction between genotype and sex.

Figure 3. Raising and lessening propionyl-CoA *in vitro* with medium interventions. (A) Calibration experiment to titrate the amount of exogenous propionate needed produce a rise in propionyl-CoA in the range found in PA hearts. 48-h treatment of NRVMs with up to 6 mM sodium propionate. Measurements of acyl-CoAs in NRVM lysates (N=6 biologically independent samples from 6 isolations; left axis) were compared to measurements in PA and wild-type mice (right axis). Mathematical minimisation procedure best-fitted calibration constants to indicate that ~1 mM propionate produces rise in propionyl-CoA within the range of PA mice (red dots). Mean±SEM. (B) ^{13}C tracing experiment in NRVMs with raised propionyl-CoA (exogenous propionate treatment) and for raised β-alanine (histidine in medium replaced with carnosine; yellow banding). Table shows the four treatment conditions (A/B/C/D). For conditions A/B, Ile and Val were uniformly labelled (^{13}C on all carbons). For conditions C/D, 1 mM labelled propionate (^{13}C at carbon-1) was added to the medium. Condition C/D produced a rise in propionate. N=7 biologically independent samples per condition from 7 isolations. Mean±SEM. */** P<0.05/<0.01. (C) Ion-exchange mass spectrometry identifies Krebs cycle intermediates. MeCit/Cit: 2-methylcitrate/citrate ratio. */** P<0.05/<0.01. Mean±SEM. (D) ^{13}C tracing of Ile/Val carbons (conditions A/B) or propionate carbon-1 (conditions C/D), expressed as percent molar enrichment. N=7/condition from 7 isolations. Key shows number of ^{13}C labelled atoms. (E) Acyl-CoA measurements expressed as either absolute quantification calibrated against standard curves, or as relative AUC (without standards). N=7 biologically independent samples per condition from 7 isolations. */** P<0.05/<0.01 for effect of propionate treatment. $^{\#}$/$^{\#\#}$ P<0.05/<0.01 for effect of raising β-

alanine. Statistical testing by repeated measures two-way ANOVA. Mean±SEM. (F). Summary of findings. Brown-filled symbols indicate carbons of acetyl-CoA or propionyl-CoA competing for entry into the Krebs cycle as citrate or 2-methylcitrate. Raising β-alanine favours the former. Propionate also enters the Krebs cycle as succinyl-CoA but this pathway is not normally available in PA due to PCC inactivation. Abbreviations: Methylmalonyl-CoA (MM-CoA), BH(I)B-CoA (β-hydroxy(iso)butyryl-CoA), 2M3HB-CoA (2-Methyl-3-hydroxybutyryl-CoA), 2M2PE-CoA (*trans*-2-methyl-pentenoyl-CoA).

Figure 4. Mice with disrupted propionyl-CoA handling develop cardiac contractile dysfunction. (A) Body weight, heart weight-to-tibia length ratio and wet:dry lung weight ratio (N=10, 14, 16, 19 animals). *GEN denotes significant (P<0.05) effect of genotype. Two-way ANOVA followed by multiple comparisons test. (B) Cell dimensions and intracellular pH measured in cSNARF1-loaded myocytes. Hierarchical analyses from a total of 93-113 cells/genotype from 4-5 isolations. (C) Cine-MR imaging of 8-week mouse hearts showing rendered heart mass, LV end-diastolic (ED) end-systolic (SV) volumes, LV ED and LV ES after normalising to body weight, i.e. indexed (N=8, 10, 10, 9 animals). *GEN denotes significant (P<0.05) effect of genotype. *GENxSEX denotes significant (P<0.05) interaction between sex and genotype (ordinary two-way ANOVA with Tukey's multiple comparisons test). (D). Echocardiography of female mice scanned at three time-points (8, 14, 20 weeks), and their body weight. E/E' and E'/A' measured from pulsed-wave and tissue Doppler in apical four-chamber view; stroke volume and cardiac output measured in parasternal short-axis view (N=4, 4 animals; repeated measurements ANOVA). *GEN denotes significant (P<0.05) effect of genotype. Mean±SEM. (E) Calcium signalling measured by fluorescence imaging of myocytes freshly isolated from 8-week-old amPA or amWT hearts. Protocol measured electrically-evoked calcium transients (CaTs) to obtain diastolic and systolic [Ca^{2+}], and CaT amplitude (amp). After a train of CaTs, a caffeine-evoked transient (CaffT) was produced to interrogate resting [Ca^{2+}], SR [Ca^{2+}] load, and fractional release. Hierarchical analysis of 226-240 myocytes from N=7, 7, 8, 9 isolations. * P<0.05. Mean±SEM.

Figure 5. Cardiac gene expression changes in response to propionate. (A) RNA-seq analysis of cardiac lysates from sex-balanced amPA and amWT hearts (N=5 biologically independent samples each). Heatmap shows all genes significantly affected by genotype

(adjusted P<0.05), grouped by sex. DESeq2 analysis using design ~genotype+sex+sex:genotype. (B) Volcano plot showing DEGs identified in male and female amPA, relative to amWT. Selected genes are labelled. Corrected for multiple comparisons. (C) Violin plot of the log_2-fold change in expression of genes of the cardiac muscle contraction KEGG pathway in male and female PA mice, relative to wild-type. Midline shows median, with upper and lower hinges showing 25th and 75th percentile, respectively. Upper and lower whiskers extend to the largest and smallest datapoints within 1.5 times the interquartile range of either hinge. (D) RNA-seq analysis of lysates obtained from cultured neonatal rat ventricular myocytes treated with 6 mM propionate (nrPRO) or 6 mM butyrate (nrBUT) for 24-h. Heatmap shows responses, relative to untreated controls (nrCON). Experiments were grouped from 3 biologically independent isolations. (E) Volcano plot shows transcriptional responses to propionate treatment, highlighting four genes of 'cardiac muscle contraction' pathway. Corrected for multiple comparisons. (F) RT-qPCR validation of selected genes confirms effect of propionate, but not of 3-hydroxy derivative (N=6 per condition from 4 isolations). Paired two-tailed T-test. Mean±SEM. (G) Western blot of histone extracts from cultured neonatal myocytes treated with 3 mM propionate (P), 3 mM butyrate (B) or control (C) probed using antibodies against pan-propionylation (Kpr), H3K9ac and total histone H3. Includes repeats from independently collected lysates (N=4 C, 4 P and 2 B from 4 isolations). (H) Whole-cell ELISA measurements of H3K9ac to H3 ratio in fixed neonatal myocytes treated for 24-h, normalised to untreated control. Best-fit (non-cooperative Hill curve) indicates half-maximal concentration (N=6 biologically independent measurements from 6 isolations, with each measurement determined from technical triplicates). Mean±SEM. But: 3mM butyrate; F-Ace: 3 mM 2-fluoroacetate. (I) Immunofluorescence imaging of adult and neonatal myocyte nuclei following treatment (4-h or 24-h respectively) with propionate, showing H3K27ac response. Further quantification in **Extended Data Fig 7**. (J) Comparison of DEGs sensitive to propionate and butyrate *in vitro*. Red symbols denote DEGs that respond to both propionate and butyrate (Pearson's R=0.9198); orange symbols denote DEGs that respond to propionate only (Pearson's R=-0.1456). (K) Venn diagrams showing number of DEGs according to response *in vivo* (mouse heart) and *in vitro* (cultured myocytes) grouped by sex. (L) RT-qPCR of selected propionate-sensitive DEGs in mouse hearts (N=5, 5, 5, 5 biologically independent samples). Ordinary two-way ANOVA with Tukey's multiple comparisons test. */*** P<0.05/<0.001. Mean±SEM.

Figure 6. Disrupted propionyl-CoA handling evokes changes in protein phosphorylation. (A) Representative cGMP FRET trace in NRVMs treated for 48-h with 3 mM propionate (PRO) to induce *Pde9a* expression, showing effect of PDE9A-specific inhibitor (PF-9613; 100 µM), IBMX (100 µM) and SNAP/BAY-41 (50 µM and 5 µM, respectively). Double-normalised FRET signal in response to PF-9613 treatment at steady-state, showing significant increase in propionate-treated (PRO) myocytes. Bar chart shows quantification of effect of PF-9613 relative to untreated (CON) NRVMs. Hierarchical analysis of 88-117 myocytes from N=4 isolations. Unpaired two-tailed T-test. **** P<0.0001. Mean±SEM. (B) cGMP assay in murine cardiac lysates, normalised to protein content (N=8 biologically independent samples per sex and genotype). Violin plots show distribution of measurements as a proxy of the scope for cGMP signalling. F-test was performed to compare variance in WT versus PA hearts (* P<0.05). (C) Transmembrane H^+ fluxes generated by Na^+/H^+ exchange activity in myocytes isolated from mouse hearts. Female PA myocytes have higher NHE1 activity, which is consistent with a higher engagement of cGMP signalling triggered by natriuretic peptide signalling. Two-way ANOVA analysis of data from 20-35 myocytes from 6 isolations per category. Mean±SEM. (D) Phosphoproteomics of lysates prepared from female PA and WT hearts (N=6 biologically independent samples per sex and genotype). Differentially abundant peptides (p.adj<0.05), colour coded by type of protein. Shape of symbol indicates the most likely kinase (phosphosite functional score>3) for the given peptide substrate. Two-sample T-test, corrected for multiple comparisons.

Figure 7. Chromatin immunoprecipitation (ChIP) reveals increased histone acetylation and propionylation at propionate-responsive genes. (A) ^{13}C tracing of propionyl-CoA from propiogenic substrates (isoleucine/valine) or from exogenous propionate, to identify propionylation sites on histone H3 under baseline and elevated propionate signalling, respectively. Lysine propionylation identified by LC-MS/MS. Heatmap shows label-free quantification intensity for the various lysines (x axis). The modifications include stable (unlabelled) propionylation (Pro) ['unlab C3'] or (iso)butyration ['unlab C4'], or propionylation with one labelled carbon from 1-^{13}C propionate (1-Pro) or three labelled carbons from ^{13}C Ile/Val (3-Pro). Grey indicates no signal. Intensity expressed as $\log_{10}$. Brackets indicate residues present on the same peptide. (B) Reference-normalised ChIP-seq in female amWT and amPA mouse hearts, using antibodies against histone H3K27ac and pan-propionylation (Kpr). ChIP-seq tracks are shown at the *Pde9a* and *Mme* promoter loci. (C) Overlap of

H3K27ac and Kpr peaks in female amWT mice. (D) Correlation of H3K27ac and Kpr levels at H3K27ac peaks in female amPA mice. (E) Metaplots showing the mean level of H3K27ac or Kpr at active gene promoters in female amWT or amPA mice, relative to the transcriptional start site (TSS). (F) Median log_2-fold change (FC) (amPA to amWT) in H3K27ac or Kpr levels for genes that are up-regulated, down-regulated or unaffected in PA. Error bars show 95% confidence intervals. ****P<0.0001. (G) ChIP-qPCR at the *Pde9a* and *Mme* promoters using antibodies against H3K27ac (N=8 biologically independent samples per genotype), pan-Kpr (N=3 amWT and 5 amPA biologically independent samples) and H3K23pr (N=3 biologically independent samples per genotype). Locations of primer pairs are shown in panel B. Unpaired two-tailed T-tests. */** P<0.05/<0.01. Mean±SEM. (H) ChIP-qPCR at the promoters of *Pde9a*, *Mme*, and *Gsta3* for H3K27ac, in male or female amWT and amPA mice. PA was associated with a significant increase in H3K27ac only in females. N=4 biologically independent samples. Ordinary two-way ANOVA with Tukey's multiple comparisons test. */*** P<0.05/<0.001. Mean±SEM.

REFERENCES

1 Shvedunova, M. & Akhtar, A. Modulation of cellular processes by histone and non-histone protein acetylation. *Nat Rev Mol Cell Biol* **23**, 329-349 (2022).

2 Sabari, B. R., Zhang, D., Allis, C. D. & Zhao, Y. Metabolic regulation of gene expression through histone acylations. *Nat Rev Mol Cell Biol* **18**, 90-101 (2017).

3 Backs, J. & Olson, E. N. Control of cardiac growth by histone acetylation/deacetylation. *Circ Res* **98**, 15-24 (2006).

4 Hulikova, A. *et al.* Alkaline nucleoplasm facilitates contractile gene expression in the mammalian heart. *Basic Res Cardiol* **117**, 17 (2022).

5 Gillette, T. G. & Hill, J. A. Readers, writers, and erasers: chromatin as the whiteboard of heart disease. *Circ Res* **116**, 1245-1253 (2015).

6 Papait, R., Serio, S. & Condorelli, G. Role of the Epigenome in Heart Failure. *Physiol Rev* **100**, 1753-1777 (2020).

7 Wongkittichote, P., Ah Mew, N. & Chapman, K. A. Propionyl-CoA carboxylase - A review. *Molecular genetics and metabolism* **122**, 145-152 (2017).

8 Koh, A., De Vadder, F., Kovatcheva-Datchary, P. & Backhed, F. From Dietary Fiber to Host Physiology: Short-Chain Fatty Acids as Key Bacterial Metabolites. *Cell* **165**, 1332-1345 (2016).

9 Chen, Y. *et al.* Lysine propionylation and butyrylation are novel post-translational modifications in histones. *Mol Cell Proteomics* **6**, 812-819 (2007).

10 Simithy, J. *et al.* Characterization of histone acylations links chromatin modifications with metabolism. *Nat Commun* **8**, 1141 (2017).

11 Kebede, A. F. *et al.* Histone propionylation is a mark of active chromatin. *Nat Struct Mol Biol* **24**, 1048-1056 (2017).

12 Yan, K. *et al.* Deficient histone H3 propionylation by BRPF1-KAT6 complexes in neurodevelopmental disorders and cancer. *Sci Adv* **6**, eaax0021 (2020).

13 Thomas, S. P. & Denu, J. M. Short-chain fatty acids activate acetyltransferase p300. *Elife* **10** (2021).

14 Waldecker, M., Kautenburger, T., Daumann, H., Busch, C. & Schrenk, D. Inhibition of histone-deacetylase activity by short-chain fatty acids and some polyphenol metabolites formed in the colon. *J Nutr Biochem* **19**, 587-593 (2008).

15 Kruh, J. Effects of sodium butyrate, a new pharmacological agent, on cells in culture. *Mol Cell Biochem* **42**, 65-82 (1982).

16 Trefely, S. *et al.* Quantitative subcellular acyl-CoA analysis reveals distinct nuclear metabolism and isoleucine-dependent histone propionylation. *Mol Cell* **82**, 447-462 e446 (2022).

17 Zou, F. *et al.* Effects of short-chain fatty acids in inhibiting HDAC and activating p38 MAPK are critical for promoting B10 cell generation and function. *Cell Death Dis* **12**, 582 (2021).

18 Andresen, L. *et al.* Propionic acid secreted from propionibacteria induces NKG2D ligand expression on human-activated T lymphocytes and cancer cells. *J Immunol* **183**, 897-906 (2009).

19 Park, K. C., Krywawych, S., Richard, E., Desviat, L. R. & Swietach, P. Cardiac Complications of Propionic and Other Inherited Organic Acidemias. *Front Cardiovasc Med* **7**, 617451 (2020).

20 Richard, E., Pérez, B., Pérez-Cerdá, C. & Desviat, L. R. Understanding molecular mechanisms in propionic acidemia and investigated therapeutic strategies. *Expert Opin Orphan Drugs* **3**, 1427-1438 (2015).

21 Pougovkina, O., Te Brinke, H., Wanders, R. J., Houten, S. M. & de Boer, V. C. Aberrant protein acylation is a common observation in inborn errors of acyl-CoA metabolism. *J Inherit Metab Dis* **37**, 709-714 (2014).
22 Mihalik, S. J. *et al.* Increased levels of plasma acylcarnitines in obesity and type 2 diabetes and identification of a marker of glucolipotoxicity. *Obesity (Silver Spring)* **18**, 1695-1700 (2010).
23 Guenzel, A. J. *et al.* Generation of a hypomorphic model of propionic acidemia amenable to gene therapy testing. *Mol Ther* **21**, 1316-1323 (2013).
24 Miyazaki, T. *et al.* Fatal propionic acidemia in mice lacking propionyl-CoA carboxylase and its rescue by postnatal, liver-specific supplementation via a transgene. *J Biol Chem* **276**, 35995-35999 (2001).
25 Fulgencio-Covian, A. *et al.* Pathogenic implications of dysregulated miRNAs in propionic acidemia related cardiomyopathy. *Transl Res* **218**, 43-56 (2020).
26 Baumgartner, M. R. *et al.* Proposed guidelines for the diagnosis and management of methylmalonic and propionic acidemia. *Orphanet J Rare Dis* **9**, 130 (2014).
27 Kujoth, G. C. *et al.* Mitochondrial DNA mutations, oxidative stress, and apoptosis in mammalian aging. *Science (New York, N.Y.)* **309**, 481-484 (2005).
28 Boldyrev, A. A., Aldini, G. & Derave, W. Physiology and pathophysiology of carnosine. *Physiol Rev* **93**, 1803-1845 (2013).
29 Coude, F. X. *et al.* Correlation between blood ammonia concentration and organic acid accumulation in isovaleric and propionic acidemia. *Pediatrics* **69**, 115-117 (1982).
30 Merinero, B. *et al.* Late onset type of propionic acidaemia: case report and biochemical studies. *J Inherit Metab Dis* **4**, 71-72 (1981).
31 Rasmussen, K. *et al.* Excretion of propionylglycine in propionic acidaemia. *Clinical science* **42**, 665-671 (1972).
32 Guenzel, A. J., Collard, R., Kraus, J. P., Matern, D. & Barry, M. A. Long-term sex-biased correction of circulating propionic acidemia disease markers by adeno-associated virus vectors. *Hum Gene Ther* **26**, 153-160 (2015).
33 Salazar, C., Armenta, J. M., Cortes, D. F. & Shulaev, V. Combination of an AccQ.Tag-ultra performance liquid chromatographic method with tandem mass spectrometry for the analysis of amino acids. *Methods Mol Biol* **828**, 13-28 (2012).
34 Cheema-Dhadli, S., Leznoff, C. C. & Halperin, M. L. Effect of 2-methylcitrate on citrate metabolism: implications for the management of patients with propionic acidemia and methylmalonic aciduria. *Pediatr Res* **9**, 905-908 (1975).
35 Yan, K. *et al.* Integrated Multilayer Omics Reveals the Genomic, Proteomic, and Metabolic Influences of Histidyl Dipeptides on the Heart. *J Am Heart Assoc* **11**, e023868 (2022).
36 Swietach, P. *et al.* Coupled Ca2+/H+ transport by cytoplasmic buffers regulates local Ca2+ and H+ ion signaling. *Proc Natl Acad Sci U S A* **110**, E2064-2073 (2013).
37 Al-Dirbashi, O. Y. *et al.* Assessment of methylcitrate and methylcitrate to citrate ratio in dried blood spots as biomarkers for inborn errors of propionate metabolism. *Sci Rep* **9**, 12366 (2019).
38 Eisner, D. A., Caldwell, J. L., Trafford, A. W. & Hutchings, D. C. The Control of Diastolic Calcium in the Heart: Basic Mechanisms and Functional Implications. *Circ Res* **126**, 395-412 (2020).
39 Chung, Y. J. *et al.* Iron-deficiency anemia reduces cardiac contraction by downregulating RyR2 channels and suppressing SERCA pump activity. *JCI Insight* **4** (2019).
40 Proudfoot, A. T., Bradberry, S. M. & Vale, J. A. Sodium fluoroacetate poisoning. *Toxicol Rev* **25**, 213-219 (2006).

41 Lee, D. I. *et al.* Phosphodiesterase 9A controls nitric-oxide-independent cGMP and hypertrophic heart disease. *Nature* **519**, 472-476 (2015).
42 Methawasin, M. *et al.* Phosphodiesterase 9a Inhibition in Mouse Models of Diastolic Dysfunction. *Circ Heart Fail* **13**, e006609 (2020).
43 Stangherlin, A. *et al.* cGMP signals modulate cAMP levels in a compartment-specific manner to regulate catecholamine-dependent signaling in cardiac myocytes. *Circ Res* **108**, 929-939 (2011).
44 Richards, M. A. *et al.* Nitric oxide modulates cardiomyocyte pH control through a biphasic effect on sodium/hydrogen exchanger-1. *Cardiovascular research* **116**, 1958-1971 (2020).
45 Vaughan-Jones, R. D., Spitzer, K. W. & Swietach, P. Intracellular pH regulation in heart. *J Mol Cell Cardiol* **46**, 318-331 (2009).
46 Kilic, A. *et al.* Enhanced activity of the myocardial Na+/H+ exchanger NHE-1 contributes to cardiac remodeling in atrial natriuretic peptide receptor-deficient mice. *Circulation* **112**, 2307-2317 (2005).
47 Subramanian, C. *et al.* Pantothenate kinase activation relieves coenzyme A sequestration and improves mitochondrial function in mice with propionic acidemia. *Sci Transl Med* **13**, eabf5965 (2021).
48 Penafiel, R., Ruzafa, C., Monserrat, F. & Cremades, A. Gender-related differences in carnosine, anserine and lysine content of murine skeletal muscle. *Amino Acids* **26**, 53-58 (2004).
49 Gallego-Villar, L. *et al.* In vivo evidence of mitochondrial dysfunction and altered redox homeostasis in a genetic mouse model of propionic acidemia: Implications for the pathophysiology of this disorder. *Free Radic Biol Med* **96**, 1-12 (2016).
50 Mishra, S. *et al.* Inhibition of phosphodiesterase type 9 reduces obesity and cardiometabolic syndrome in mice. *J Clin Invest* **131** (2021).
51 Armstrong, A. J. *et al.* A novel small molecule approach for the treatment of propionic and methylmalonic acidemias. *Molecular genetics and metabolism* **133**, 71-82 (2021).
52 Gibbs, R. A. *et al.* Genome sequence of the Brown Norway rat yields insights into mammalian evolution. *Nature* **428**, 493-521 (2004).
53 Chung, Y. J. *et al.* Iron-deficiency anemia reduces cardiac contraction by downregulating RyR2 channels and suppressing SERCA pump activity. *JCI Insight* **4**, e125618 (2019).
54 Michl, J., Park, K. C. & Swietach, P. Evidence-based guidelines for controlling pH in mammalian live-cell culture systems. *Commun Biol* **2**, 144 (2019).
55 Millington, D. S., Kodo, N., Norwood, D. L. & Roe, C. R. Tandem mass spectrometry: a new method for acylcarnitine profiling with potential for neonatal screening for inborn errors of metabolism. *J Inherit Metab Dis* **13**, 321-324 (1990).
56 Walsby-Tickle, J. *et al.* Anion-exchange chromatography mass spectrometry provides extensive coverage of primary metabolic pathways revealing altered metabolism in IDH1 mutant cells. *Commun Biol* **3**, 247 (2020).
57 Salazar, C., Armenta, J. M., Cortés, D. F. & Shulaev, V. Combination of an AccQ•Tag-Ultra-Performance Liquid Chromatographic Method with Tandem Mass Spectrometry for the Analysis of Amino Acids. *Methods Mol Biol* **2030**, 191-206 (2019).
58 Chong, J. *et al.* MetaboAnalyst 4.0: towards more transparent and integrative metabolomics analysis. *Nucleic Acids Res* **46**, W486-W494 (2018).
59 Snyder, N. W. *et al.* Production of stable isotope-labeled acyl-coenzyme A thioesters by yeast stable isotope labeling by essential nutrients in cell culture. *Anal Biochem* **474**, 59-65 (2015).

60 Snyder, N. W., Basu, S. S., Zhou, Z., Worth, A. J. & Blair, I. A. Stable isotope dilution liquid chromatography/mass spectrometry analysis of cellular and tissue medium- and long-chain acyl-coenzyme A thioesters. *Rapid Commun Mass Spectrom* **28**, 1840-1848 (2014).
61 Trefely, S., Ashwell, P. & Snyder, N. W. FluxFix: automatic isotopologue normalization for metabolic tracer analysis. *BMC Bioinformatics* **17**, 485 (2016).
62 Seymour, A. M. *et al.* In vivo assessment of cardiac metabolism and function in the abdominal aortic banding model of compensated cardiac hypertrophy. *Cardiovascular research* **106**, 249-260 (2015).
63 Tyler, D. J. *et al.* CINE-MR imaging of the normal and infarcted rat heart using an 11.7 T vertical bore MR system. *J Cardiovasc Magn Reson* **8**, 327-333 (2006).
64 Loonat, A. A. *et al.* A high-throughput ratiometric method for imaging hypertrophic growth in cultured primary cardiac myocytes. *J Mol Cell Cardiol* **130**, 184-196 (2019).
65 Dobin, A. *et al.* STAR: ultrafast universal RNA-seq aligner. *Bioinformatics* **29**, 15-21 (2013).
66 Liao, Y., Smyth, G. K. & Shi, W. featureCounts: an efficient general purpose program for assigning sequence reads to genomic features. *Bioinformatics* **30**, 923-930 (2014).
67 Love, M. I., Huber, W. & Anders, S. Moderated estimation of fold change and dispersion for RNA-seq data with DESeq2. *Genome Biol* **15**, 550 (2014).
68 Bustin, S. A. *et al.* The MIQE guidelines: minimum information for publication of quantitative real-time PCR experiments. *Clin Chem* **55**, 611-622 (2009).
69 Livak, K. J. & Schmittgen, T. D. Analysis of relative gene expression data using real-time quantitative PCR and the 2(-Delta Delta C(T)) Method. *Methods* **25**, 402-408 (2001).
70 Molina, C. E. *et al.* Identification of optimal reference genes for transcriptomic analyses in normal and diseased human heart. *Cardiovascular research* **114**, 247-258 (2018).
71 Meert, P. *et al.* Tackling aspecific side reactions during histone propionylation: The promise of reversing overpropionylation. *Proteomics* **16**, 1970-1974 (2016).
72 Perez-Riverol, Y. *et al.* The PRIDE database and related tools and resources in 2019: improving support for quantification data. *Nucleic Acids Res* **47**, D442-D450 (2019).
73 Crump, N. T. *et al.* BET inhibition disrupts transcription but retains enhancer-promoter contact. *Nat Commun* **12**, 223 (2021).
74 Langmead, B. & Salzberg, S. L. Fast gapped-read alignment with Bowtie 2. *Nat Methods* **9**, 357-359 (2012).
75 Kent, W. J. *et al.* The human genome browser at UCSC. *Genome Res* **12**, 996-1006 (2002).
76 Brescia, M., Chao, Y.-C., Koschinski, A., Tomek, J. & Zaccolo, M. Multi-Compartment, Early Disruption of cGMP and cAMP Signalling in Cardiac Myocytes from the mdx Model of Duchenne Muscular Dystrophy. *Int J Mol Sci* **21**, 7056 (2020).
77 Russwurm, M. *et al.* Design of fluorescence resonance energy transfer (FRET)-based cGMP indicators: a systematic approach. *Biochem J* **407**, 69-77 (2007).
78 Cundell, M. J. *et al.* A PP2A-B55 recognition signal controls substrate dephosphorylation kinetics during mitotic exit. *J Cell Biol* **214**, 539-554 (2016).
79 Holder, J., Mohammed, S. & Barr, F. A. Ordered dephosphorylation initiated by the selective proteolysis of cyclin B drives mitotic exit. *Elife* **9** (2020).
80 Sikkel, M. B. *et al.* Hierarchical statistical techniques are necessary to draw reliable conclusions from analysis of isolated cardiomyocyte studies. *Cardiovascular research* **113**, 1743-1752 (2017).

FIGURE 1

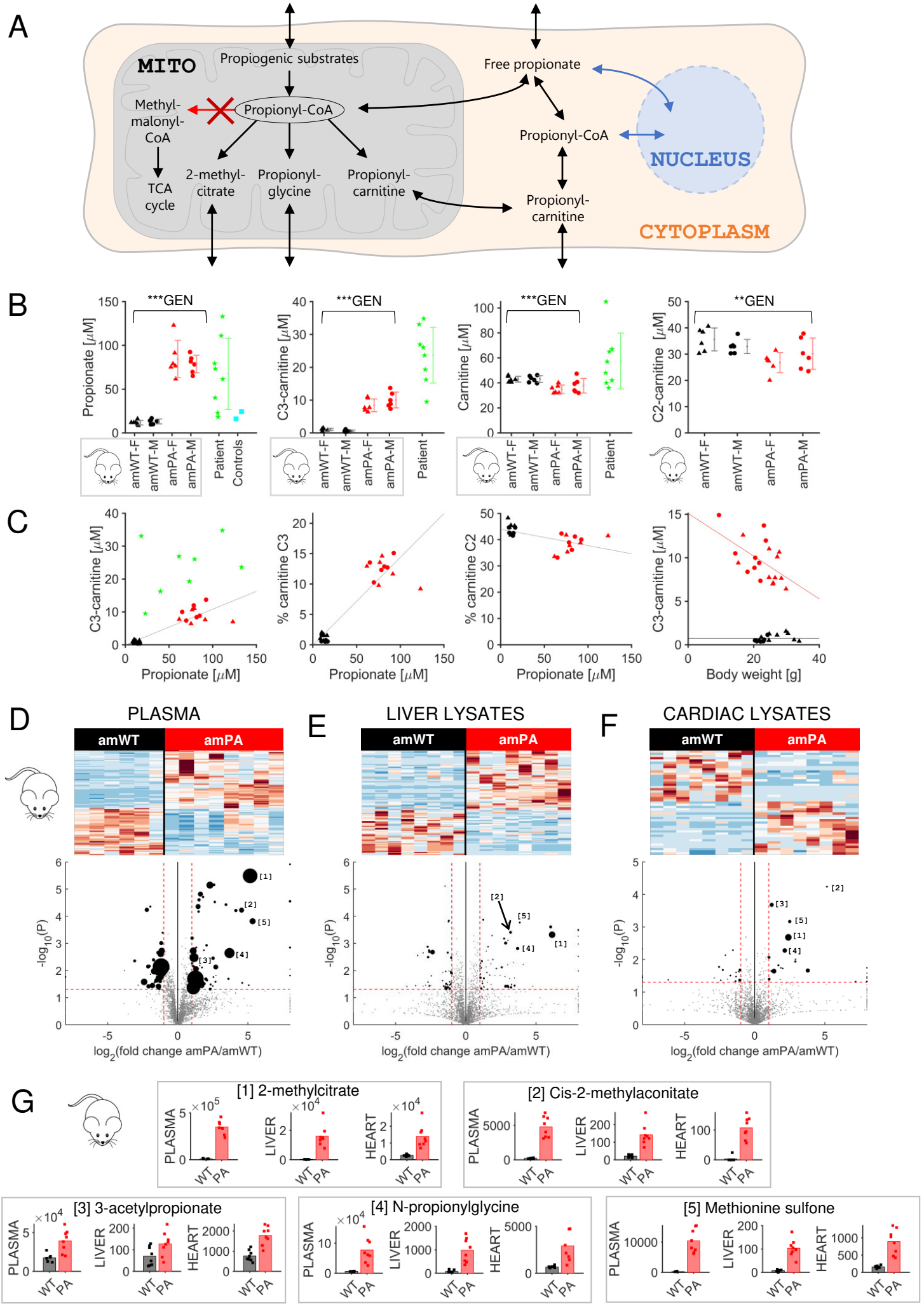
A
MITO
Propiogenic substrates
Methyl-malonyl-CoA
Propionyl-CoA
TCA cycle
2-methyl-citrate
Propionyl-glycine
Propionyl-carnitine
Free propionate
Propionyl-CoA
NUCLEUS
Propionyl-carnitine
CYTOPLASM
B
***GEN
Propionate [μM]
C3-carnitine [μM]
Carnitine [μM]
**GEN
C2-carnitine [μM]
amWT-F
amWT-M
ampA-F
ampA-M
Patient
Controls
C
C3-carnitine [μM]
Propionate [μM]
% carnitine C3
% carnitine C2
Body weight [g]
D
PLASMA
E
LIVER LYSATES
F
CARDIAC LYSATES
amWT
amPA
-log10(P)
log2(fold change ampA/amWT)
G
[1] 2-methylcitrate
[2] Cis-2-methylaconitate
[3] 3-acetylpropionate
[4] N-propionylglycine
[5] Methionine sulfone
PLASMA
LIVER
HEART
WT
PA

FIGURE 2

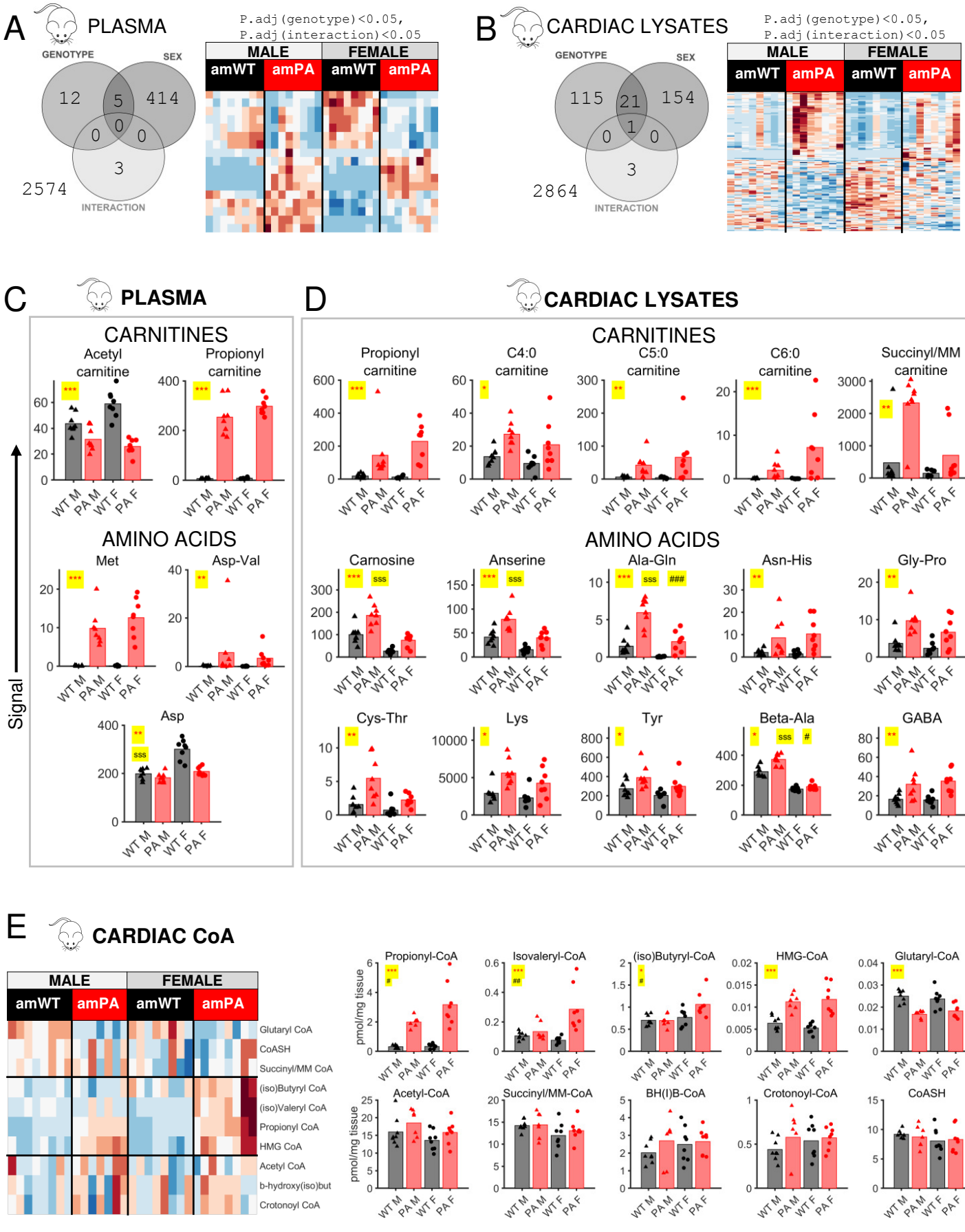
A
PLASMA
GENOTYPE
SEX
12
5
414
0
0
0
3
2574
INTERACTION
P.adj(genotype)<0.05,
P.adj(interaction)<0.05
MALE
FEMALE
amWT
amPA
amWT
amPA
B
CARDIAC LYSATES
GENOTYPE
SEX
115
21
154
0
1
0
3
2864
INTERACTION
P.adj(genotype)<0.05,
P.adj(interaction)<0.05
MALE
FEMALE
amWT
amPA
amWT
amPA
C
PLASMA
CARNITINES
Acetyl carnitine
Propionyl carnitine
AMINO ACIDS
Met
Asp-Val
Asp
Signal
D
CARDIAC LYSATES
CARNITINES
Propionyl carnitine
C4:0 carnitine
C5:0 carnitine
C6:0 carnitine
Succinyl/MM carnitine
AMINO ACIDS
Carnosine
Anserine
Ala-Gln
Asn-His
Gly-Pro
Cys-Thr
Lys
Tyr
Beta-Ala
GABA
WT M
PA M
WT F
PA F
E
CARDIAC CoA
MALE
FEMALE
amWT
amPA
amWT
amPA
Glutaryl CoA
CoASH
Succinyl/MM CoA
(iso)Butyryl CoA
(iso)Valeryl CoA
Propionyl CoA
HMG CoA
Acetyl CoA
b-hydroxy(iso)but
Crotonoyl CoA
Propionyl-CoA
Isovaleryl-CoA
(iso)Butyryl-CoA
HMG-CoA
Glutaryl-CoA
Acetyl-CoA
Succinyl/MM-CoA
BH(I)B-CoA
Crotonoyl-CoA
CoASH
pmol/mg tissue
WT M
PA M
WT F
PA F

FIGURE 3

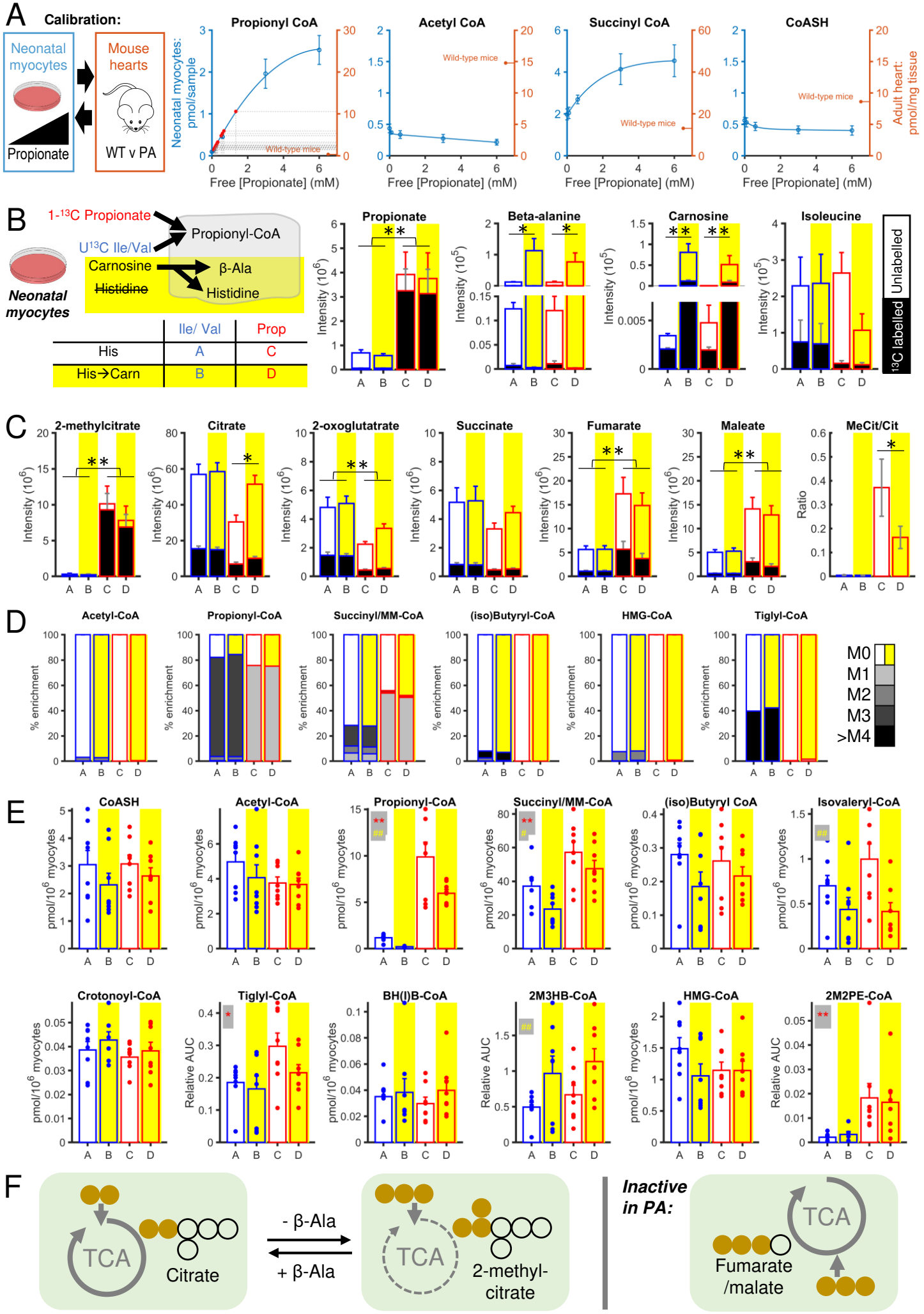
A
Calibration:
Neonatal myocytes
Mouse hearts
Propionate
WT v PA
Propionyl CoA
Acetyl CoA
Succinyl CoA
CoASH
Neonatal myocytes: pmol/sample
Adult heart: pmol/mg tissue
Wild-type mice
Free [Propionate] (mM)
B
1-13C Propionate
U13C Ile/Val
Carnosine
Histidine
β-Ala
Propionyl-CoA
Neonatal myocytes
Ile/ Val
Prop
His
His→Carn
A
B
C
D
Propionate
Beta-alanine
Carnosine
Isoleucine
Intensity (10^6)
Intensity (10^5)
Unlabelled
13C labelled
C
2-methylcitrate
Citrate
2-oxoglutatrate
Succinate
Fumarate
Maleate
MeCit/Cit
Ratio
D
Acetyl-CoA
Propionyl-CoA
Succinyl/MM-CoA
(iso)Butyryl-CoA
HMG-CoA
Tiglyl-CoA
% enrichment
M0
M1
M2
M3
>M4
E
CoASH
Acetyl-CoA
Propionyl-CoA
Succinyl/MM-CoA
(iso)Butyryl CoA
Isovaleryl-CoA
Crotonoyl-CoA
Tiglyl-CoA
BH(I)B-CoA
2M3HB-CoA
HMG-CoA
2M2PE-CoA
pmol/10^6 myocytes
Relative AUC
F
TCA
Citrate
- β-Ala
+ β-Ala
2-methyl-citrate
Inactive in PA:
Fumarate /malate

FIGURE 4

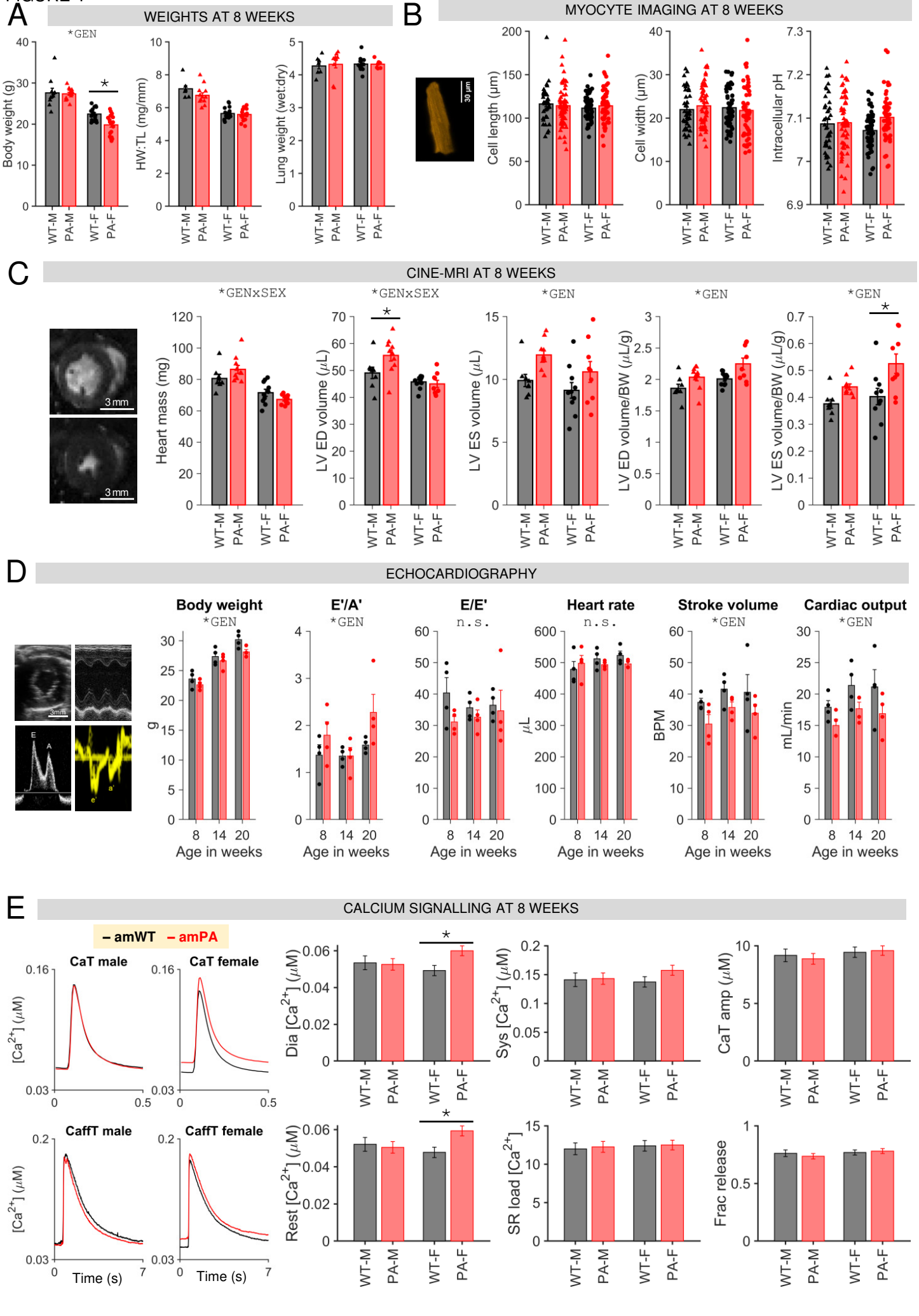
A
WEIGHTS AT 8 WEEKS
*GEN
Body weight (g)
HW:TL (mg/mm)
Lung weight (wet:dry)
WT-M
PA-M
WT-F
PA-F
B
MYOCYTE IMAGING AT 8 WEEKS
30 µm
Cell length (µm)
Cell width (µm)
Intracellular pH
C
CINE-MRI AT 8 WEEKS
*GENxSEX
*GEN
3 mm
Heart mass (mg)
LV ED volume (µL)
LV ES volume (µL)
LV ED volume/BW (µL/g)
LV ES volume/BW (µL/g)
D
ECHOCARDIOGRAPHY
3mm
E
A
e'
a'
Body weight
E'/A'
E/E'
Heart rate
Stroke volume
Cardiac output
n.s.
g
µL
BPM
mL/min
Age in weeks
E
CALCIUM SIGNALLING AT 8 WEEKS
– amWT – amPA
CaT male
CaT female
CaffT male
CaffT female
[Ca2+] (µM)
Time (s)
Dia [Ca2+] (µM)
Sys [Ca2+] (µM)
CaT amp (µM)
Rest [Ca2+] (µM)
SR load [Ca2+]
Frac release

FIGURE 5

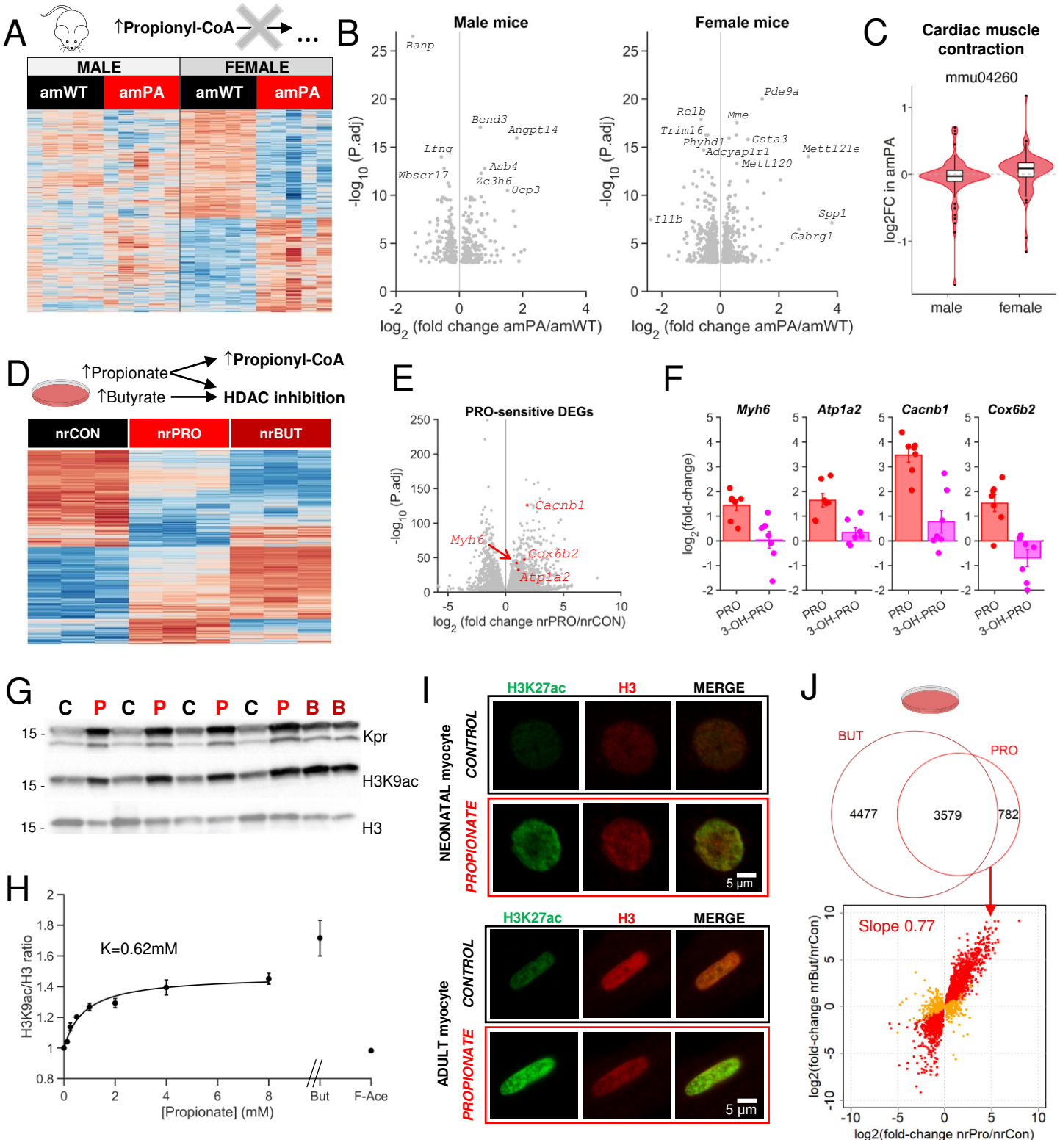
A
↑Propionyl-CoA
MALE
FEMALE
amWT
amPA
amWT
amPA
B
Male mice
Female mice
-log10 (P.adj)
log2 (fold change amPA/amWT)
Banp
Bend3
Angpt14
Lfng
Asb4
Wbscr17
Zc3h6
Ucp3
Pde9a
Relb
Mme
Trim16
Gsta3
Phyhd1
Adcyap1r1
Mett121e
Mett120
Il1b
Spp1
Gabrg1
C
Cardiac muscle contraction
mmu04260
log2FC in ampA
male
female
D
↑Propionate
↑Butyrate
↑Propionyl-CoA
HDAC inhibition
nrCON
nrPRO
nrBUT
E
PRO-sensitive DEGs
-log10 (P.adj)
log2 (fold change nrPRO/nrCON)
Cacnb1
Myh6
Cox6b2
Atp1a2
F
Myh6
Atp1a2
Cacnb1
Cox6b2
log2(fold-change)
PRO
3-OH-PRO
G
C P C P C P C P B B
Kpr
H3K9ac
H3
H
K=0.62mM
H3K9ac/H3 ratio
[Propionate] (mM)
But
F-Ace
I
H3K27ac
H3
MERGE
NEONATAL myocyte
CONTROL
PROPIONATE
ADULT myocyte
CONTROL
PROPIONATE
5 µm
J
BUT
PRO
4477
3579
782
Slope 0.77
log2(fold-change nrBut/nrCon)
log2(fold-change nrPro/nrCon)
K
In vivo
amPA female
amPA male
530
35
265
18
160
83
3318
Propionate and butyrate sensitive in vitro
In vivo
amPA female
amPA male
652
49
337
4
38
11
729
Propionate but not butyrate sensitive in vitro
L
Mme
Gsta3
Pde9a
Egr1
2ΔΔCT normalized to amWTF
amWT-M
ampA-M
amWT-F
ampA-F

FIGURE 6

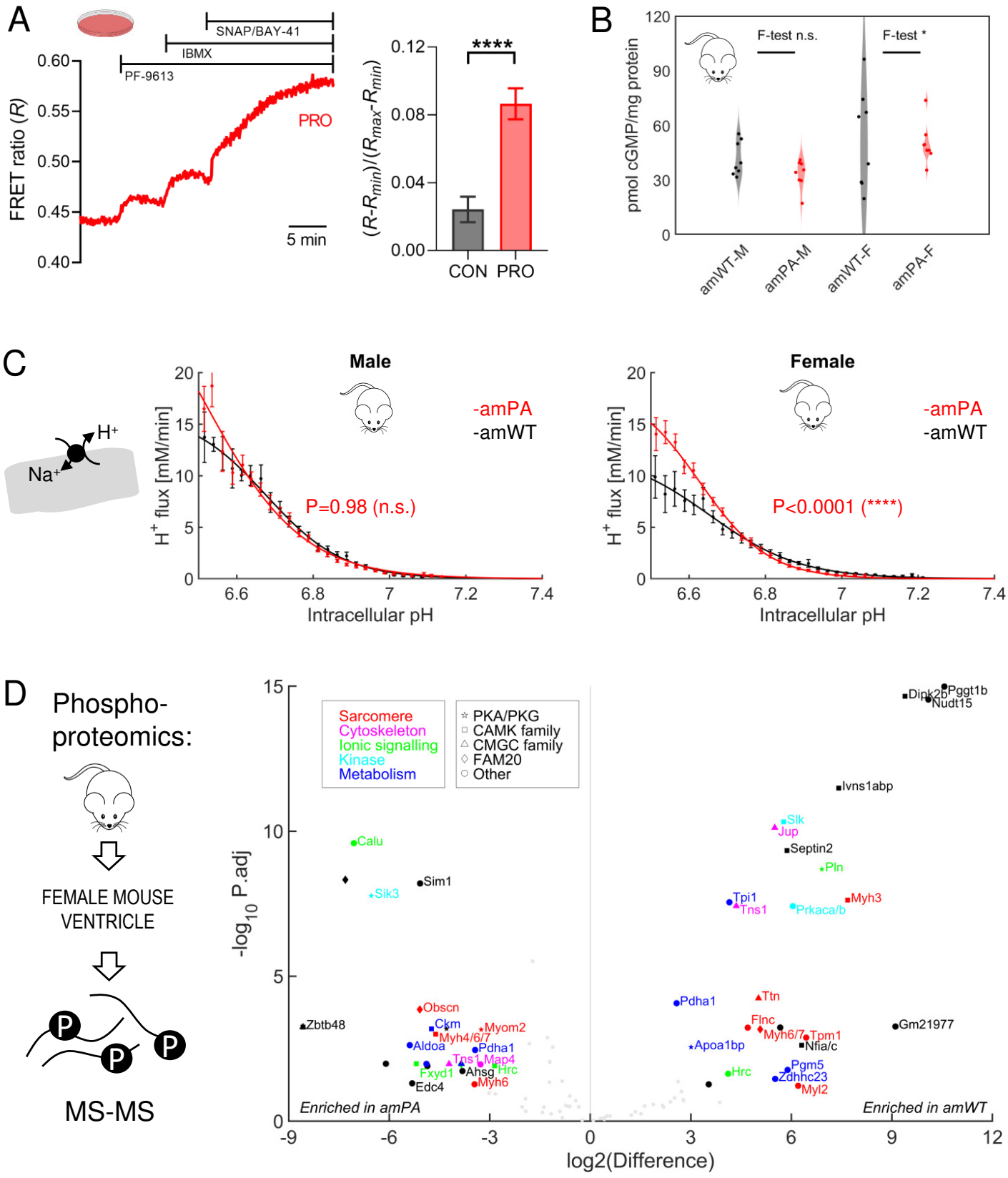
A
SNAP/BAY-41
IBMX
PF-9613
PRO
FRET ratio (R)
5 min
(R-Rmin)/(Rmax-Rmin)
****
CON PRO
B
pmol cGMP/mg protein
F-test n.s.
F-test *
amWT-M
amPA-M
amWT-F
amPA-F
C
Male
Female
-amPA
-amWT
H+ flux [mM/min]
Intracellular pH
P=0.98 (n.s.)
P<0.0001 (****)
Na+
H+
D
Phospho-proteomics:
FEMALE MOUSE VENTRICLE
MS-MS
Sarcomere
Cytoskeleton
Ionic signalling
Kinase
Metabolism
PKA/PKG
CAMK family
CMGC family
FAM20
Other
-log10 P.adj
log2(Difference)
Enriched in amPA
Enriched in amWT
Dipk2b
Pggt1b
Nudt15
Ivns1abp
Slk
Jup
Septin2
Pln
Tpi1
Tns1
Prkaca/b
Myh3
Calu
Sim1
Sik3
Pdha1
Ttn
Flnc
Myh6/7
Tpm1
Nfia/c
Gm21977
Apoa1bp
Pgm5
Zdhhc23
Myl2
Hrc
Obscn
Ckm
Myom2
Myh4/6/7
Aldoa
Pdha1
Tns1
Map4
Fxyd1
Ahsg
Hrc
Edc4
Myh6
Zbtb48

FIGURE 7

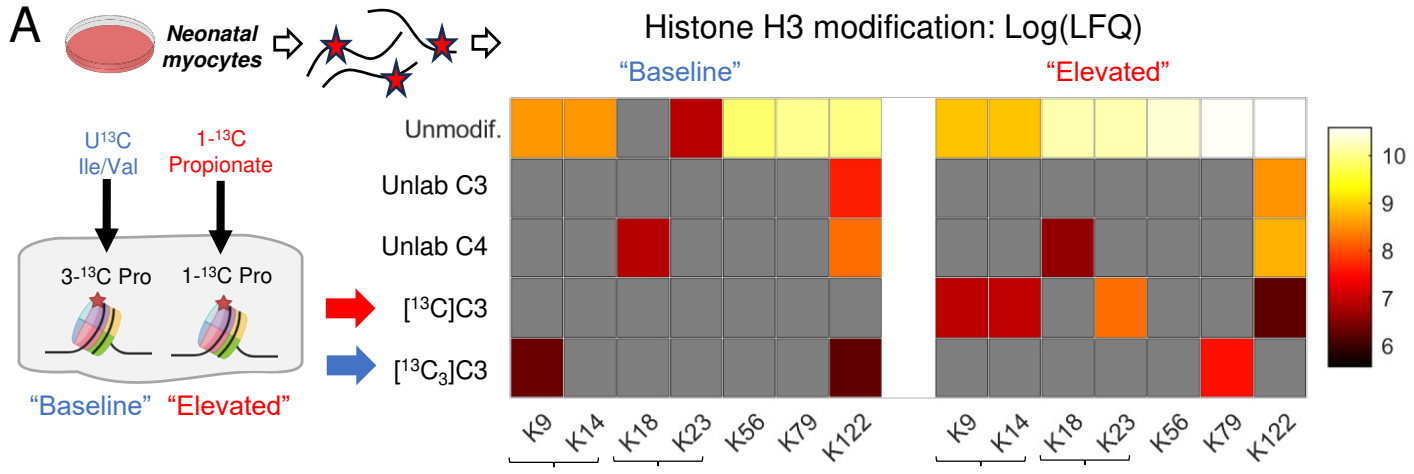
A
Neonatal myocytes
U13C Ile/Val
1-13C Propionate
3-13C Pro
1-13C Pro
"Baseline"
"Elevated"
Histone H3 modification: Log(LFQ)
"Baseline"
"Elevated"
Unmodif.
Unlab C3
Unlab C4
[13C]C3
[13C3]C3
K9
K14
K18
K23
K56
K79
K122
10
9
8
7
6

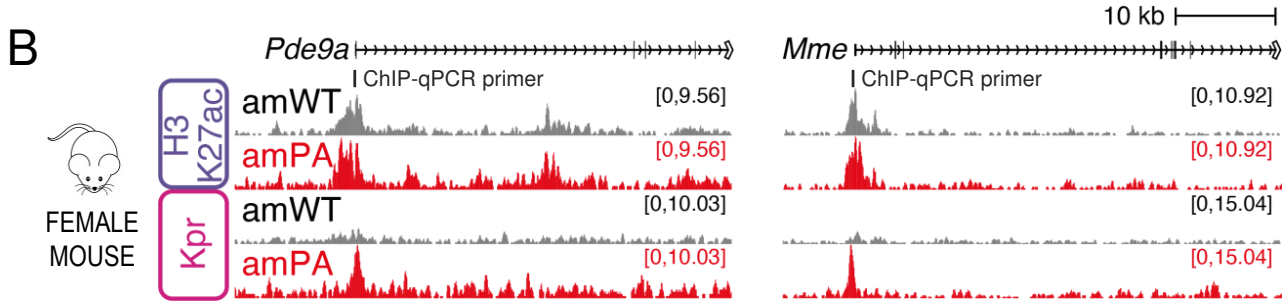
B
10 kb
Pde9a
Mme
ChIP-qPCR primer
H3 K27ac
Kpr
amWT
amPA
[0,9.56]
[0,10.03]
[0,10.92]
[0,15.04]
FEMALE MOUSE

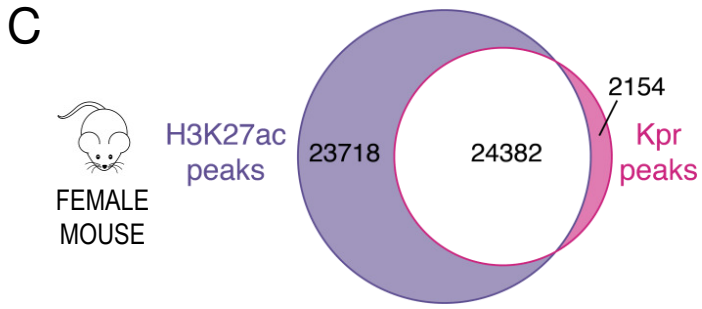
C
FEMALE MOUSE
H3K27ac peaks
23718
24382
2154
Kpr peaks

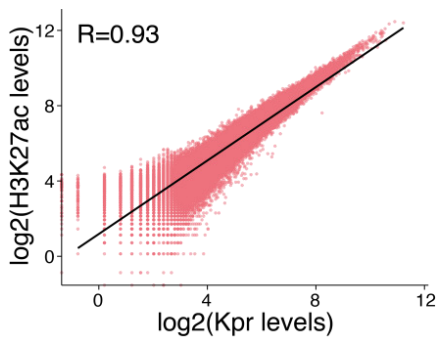
D
R=0.93
log2(H3K27ac levels)
log2(Kpr levels)

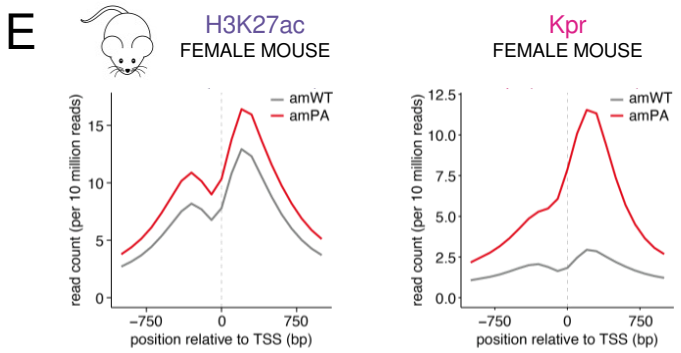
E
H3K27ac
FEMALE MOUSE
Kpr
FEMALE MOUSE
amWT
amPA
read count (per 10 million reads)
position relative to TSS (bp)

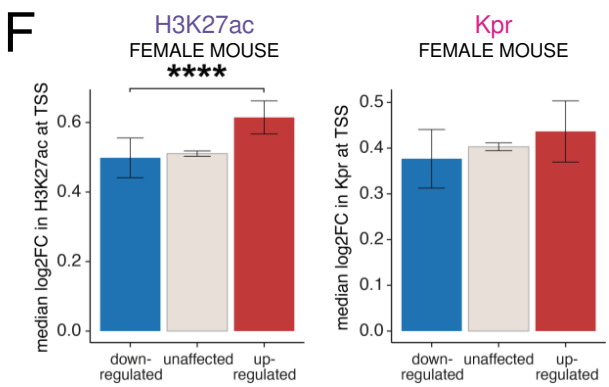
F
H3K27ac
FEMALE MOUSE
Kpr
FEMALE MOUSE
****
median log2FC in H3K27ac at TSS
median log2FC in Kpr at TSS
down-regulated
unaffected
up-regulated

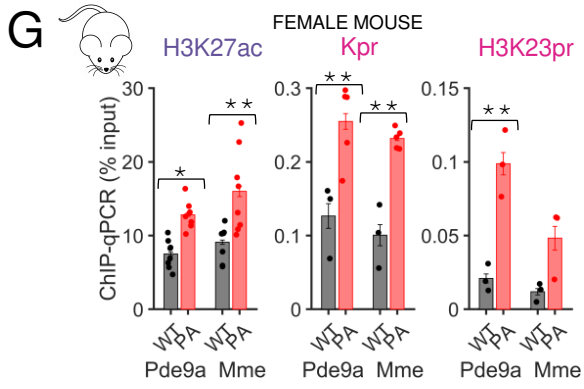
G
FEMALE MOUSE
H3K27ac
Kpr
H3K23pr
ChIP-qPCR (% input)
WT
PA
Pde9a
Mme

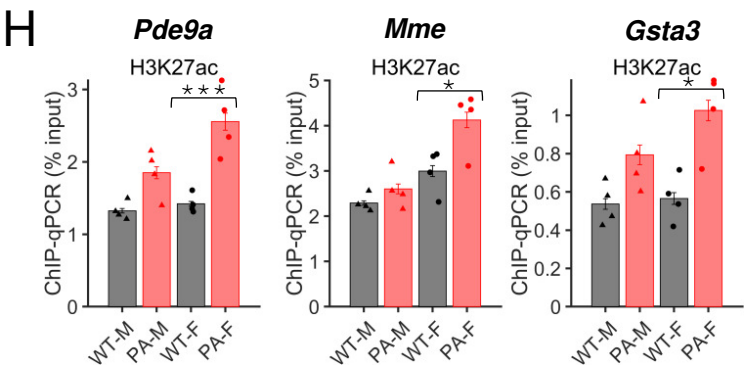
H
Pde9a
Mme
Gsta3
H3K27ac
ChIP-qPCR (% input)
WT-M
PA-M
WT-F
PA-F

A

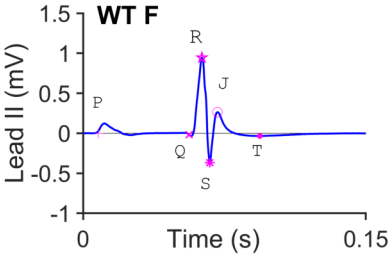
WT F
Lead II (mV)
Time (s)
P
Q
R
S
J
T

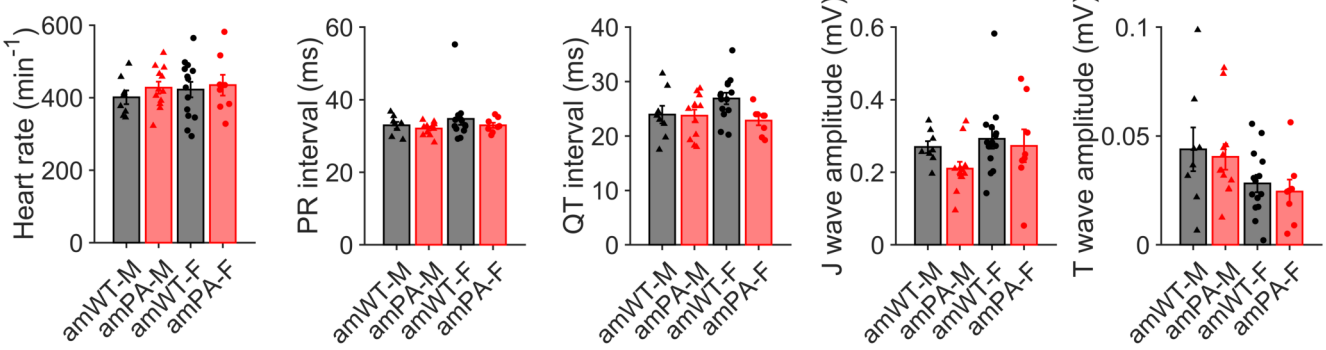
Heart rate (min-1)
PR interval (ms)
QT interval (ms)
J wave amplitude (mV)
T wave amplitude (mV)
amWT-M
amPA-M
amWT-F
amPA-F

B

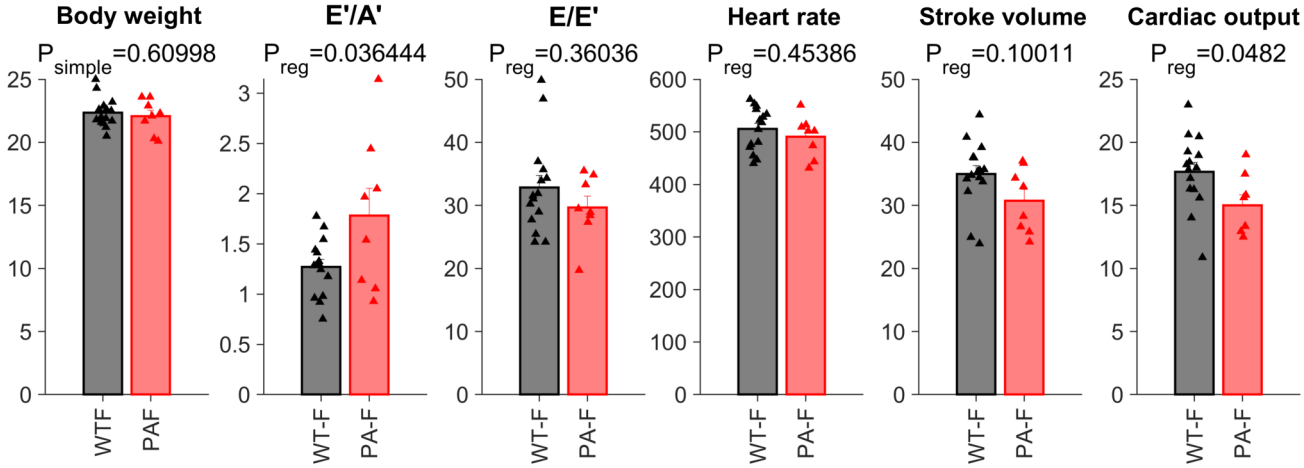
Body weight
P simple=0.60998
E'/A'
P reg=0.036444
E/E'
P reg=0.36036
Heart rate
P reg=0.45386
Stroke volume
P reg=0.10011
Cardiac output
P reg=0.0482
WTF
PAF
WT-F
PA-F

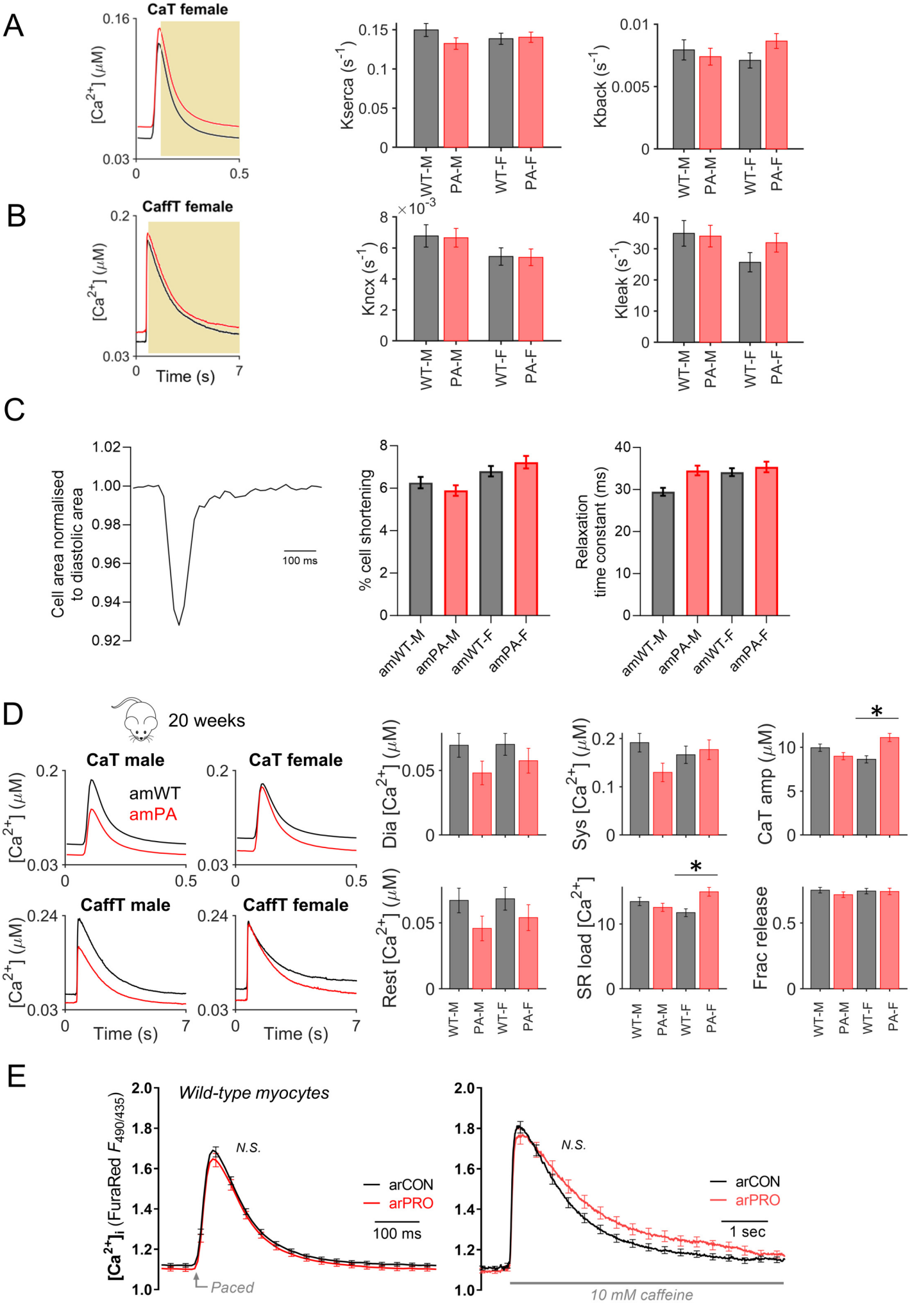
A
CaT female
[Ca2+] (μM)
0.16
0.03
0
0.5
Kserca (s-1)
0.15
0.1
0.05
0
Kback (s-1)
0.01
0.005
0
WT-M
PA-M
WT-F
PA-F
B
CaffT female
0.2
0.03
Time (s)
7
×10-3
Kncx (s-1)
8
6
4
2
Kleak (s-1)
40
30
20
10
C
Cell area normalised to diastolic area
1.02
1.00
0.98
0.96
0.94
0.92
100 ms
% cell shortening
Relaxation time constant (ms)
amWT-M
amPA-M
amWT-F
amPA-F
D
20 weeks
CaT male
CaT female
amWT
amPA
CaffT male
CaffT female
Dia [Ca2+] (μM)
Sys [Ca2+] (μM)
CaT amp (μM)
Rest [Ca2+] (μM)
SR load [Ca2+]
Frac release
*
E
Wild-type myocytes
[Ca2+]i (FuraRed F490/435)
2.0
1.8
1.6
1.4
1.2
1.0
N.S.
arCON
arPRO
100 ms
Paced
1 sec
10 mM caffeine

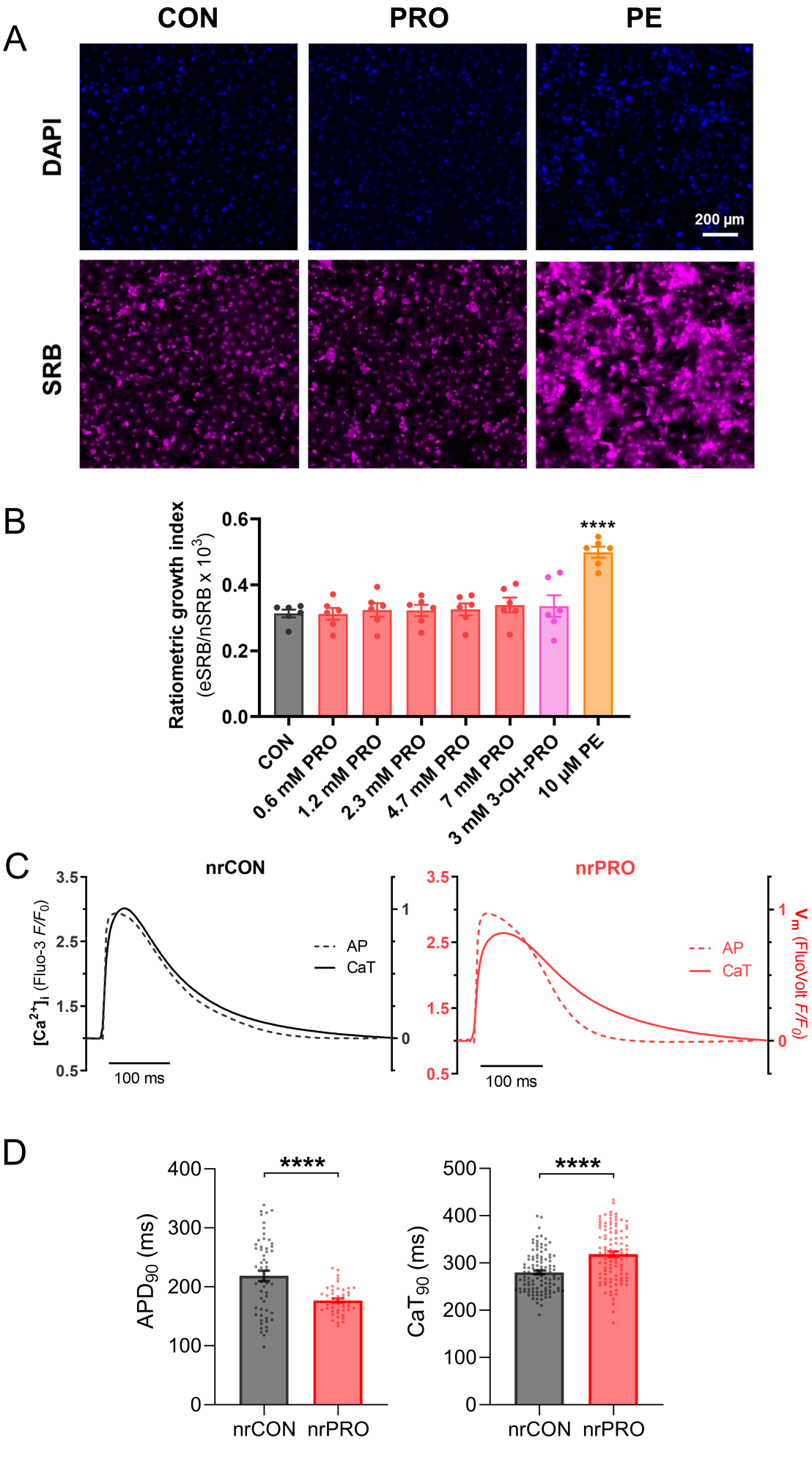
A
CON
PRO
PE
DAPI
SRB
200 µm
B
Ratiometric growth index
(eSRB/nSRB x 10^3)
0.6
0.4
0.2
0.0
****
CON
0.6 mM PRO
1.2 mM PRO
2.3 mM PRO
4.7 mM PRO
7 mM PRO
3 mM 3-OH-PRO
10 µM PE
C
nrCON
nrPRO
[Ca2+]i (Fluo-3 F/F0)
3.5
2.5
1.5
0.5
1
0
AP
CaT
100 ms
Vm (FluoVolt F/F0)
D
APD90 (ms)
CaT90 (ms)
400
300
200
100
0
500
****
nrCON
nrPRO

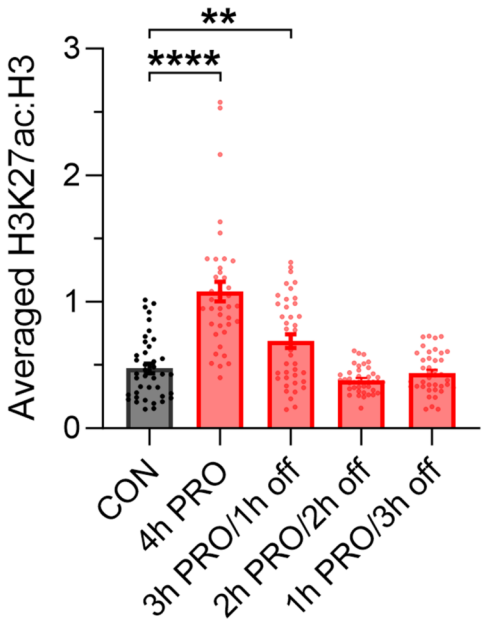
**
****
Averaged H3K27ac:H3
3
2
1
0
CON
4h PRO
3h PRO/1h off
2h PRO/2h off
1h PRO/3h off

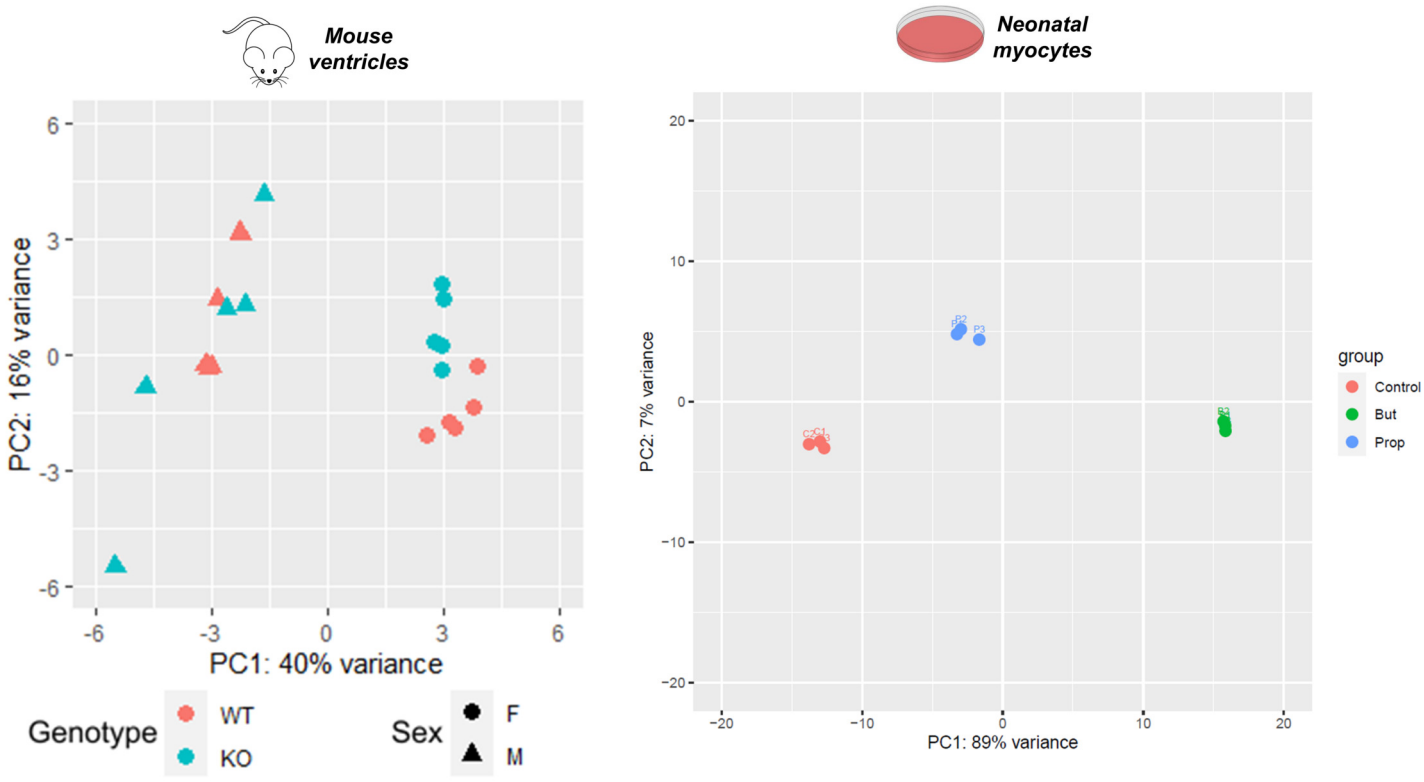
Mouse ventricles
PC2: 16% variance
PC1: 40% variance
Genotype
WT
KO
Sex
F
M
Neonatal myocytes
PC2: 7% variance
PC1: 89% variance
group
Control
But
Prop

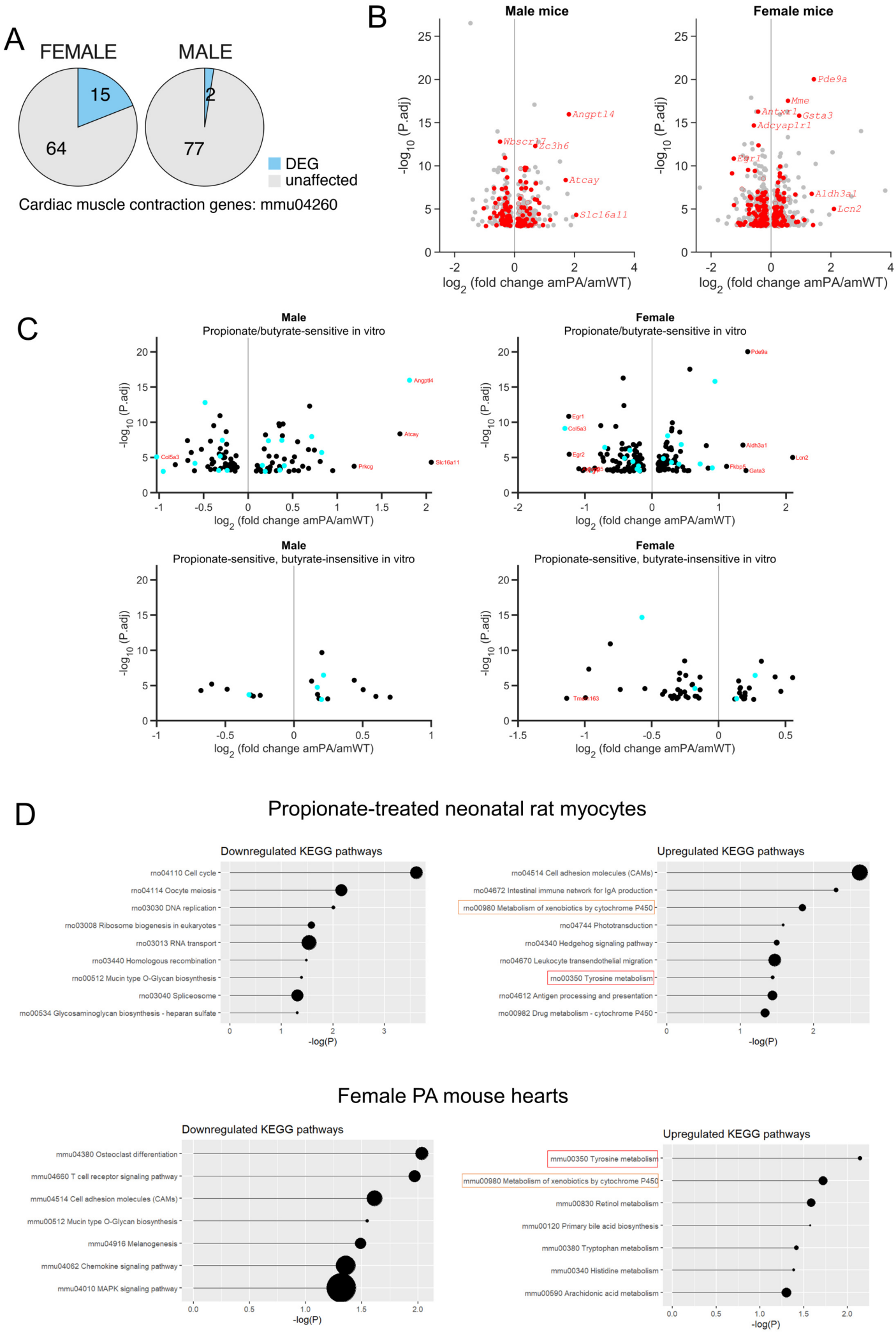
A
FEMALE
MALE
15
64
2
77
DEG
unaffected
Cardiac muscle contraction genes: mmu04260
B
Male mice
Female mice
-log10 (P.adj)
log2 (fold change amPA/amWT)
Angptl4
Wbscr17
Zc3h6
Atcay
Slc16a11
Pde9a
Mme
Antxr1
Gsta3
Adcyap1r1
Egr1
Aldh3a1
Lcn2
C
Male
Propionate/butyrate-sensitive in vitro
Female
Propionate/butyrate-sensitive in vitro
Male
Propionate-sensitive, butyrate-insensitive in vitro
Female
Propionate-sensitive, butyrate-insensitive in vitro
Angptl4
Atcay
Col5a3
Prkcg
Slc16a11
Pde9a
Egr1
Col5a3
Egr2
Aldh3a1
Lcn2
Fkbp5
Gata3
D
Propionate-treated neonatal rat myocytes
Downregulated KEGG pathways
rno04110 Cell cycle
rno04114 Oocyte meiosis
rno03030 DNA replication
rno03008 Ribosome biogenesis in eukaryotes
rno03013 RNA transport
rno03440 Homologous recombination
rno00512 Mucin type O-Glycan biosynthesis
rno03040 Spliceosome
rno00534 Glycosaminoglycan biosynthesis - heparan sulfate
-log(P)
Upregulated KEGG pathways
rno04514 Cell adhesion molecules (CAMs)
rno04672 Intestinal immune network for IgA production
rno00980 Metabolism of xenobiotics by cytochrome P450
rno04744 Phototransduction
rno04340 Hedgehog signaling pathway
rno04670 Leukocyte transendothelial migration
rno00350 Tyrosine metabolism
rno04612 Antigen processing and presentation
rno00982 Drug metabolism - cytochrome P450
-log(P)
Female PA mouse hearts
Downregulated KEGG pathways
mmu04380 Osteoclast differentiation
mmu04660 T cell receptor signaling pathway
mmu04514 Cell adhesion molecules (CAMs)
mmu00512 Mucin type O-Glycan biosynthesis
mmu04916 Melanogenesis
mmu04062 Chemokine signaling pathway
mmu04010 MAPK signaling pathway
-log(P)
Upregulated KEGG pathways
mmu00350 Tyrosine metabolism
mmu00980 Metabolism of xenobiotics by cytochrome P450
mmu00830 Retinol metabolism
mmu00120 Primary bile acid biosynthesis
mmu00380 Tryptophan metabolism
mmu00340 Histidine metabolism
mmu00590 Arachidonic acid metabolism
-log(P)

A

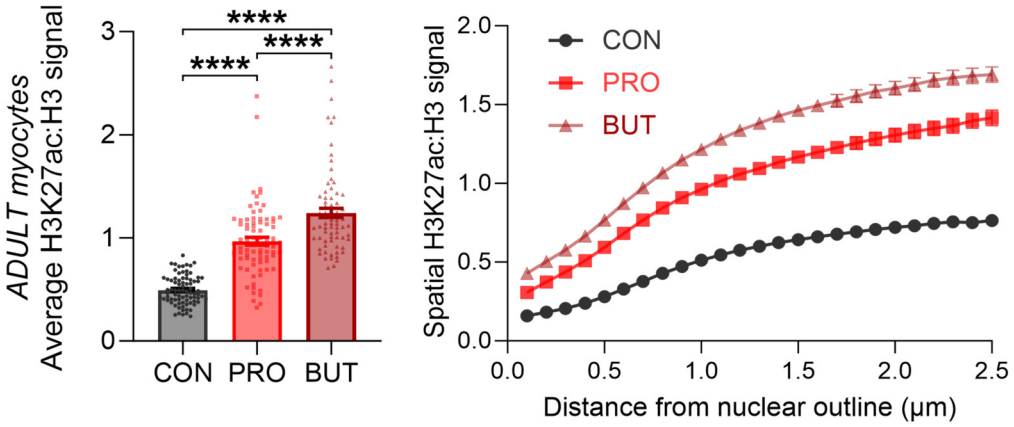
ADULT myocytes
Average H3K27ac:H3 signal
****
****
****
3
2
1
0
CON
PRO
BUT
Spatial H3K27ac:H3 signal
2.0
1.5
1.0
0.5
0.0
CON
PRO
BUT
0.0
0.5
1.0
1.5
2.0
2.5
Distance from nuclear outline (µm)

B

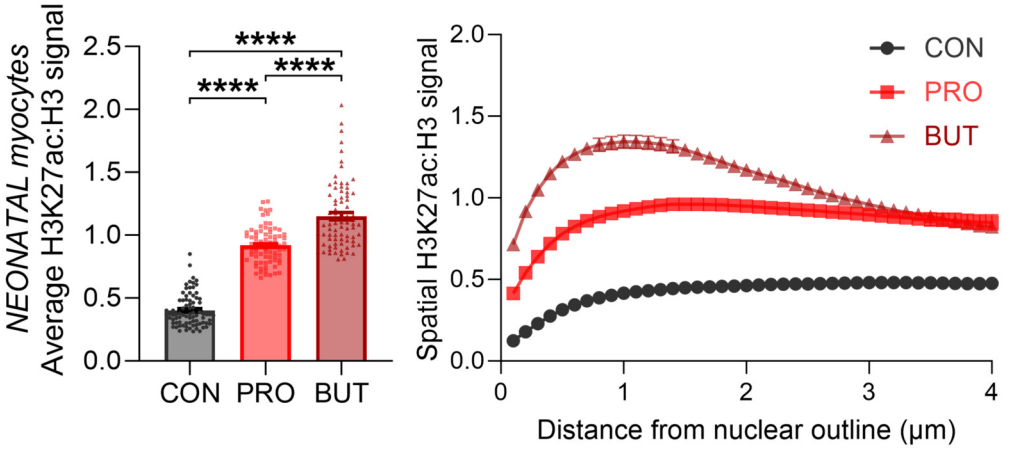
NEONATAL myocytes
Average H3K27ac:H3 signal
****
****
****
2.5
2.0
1.5
1.0
0.5
0.0
CON
PRO
BUT
Spatial H3K27ac:H3 signal
2.0
1.5
1.0
0.5
0.0
CON
PRO
BUT
0
1
2
3
4
Distance from nuclear outline (µm)

A

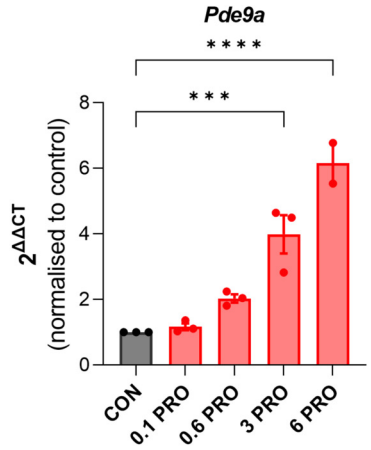
Pde9a
****
***
$2^{\Delta\Delta CT}$ (normalised to control)
0
2
4
6
8
CON
0.1 PRO
0.6 PRO
3 PRO
6 PRO

B

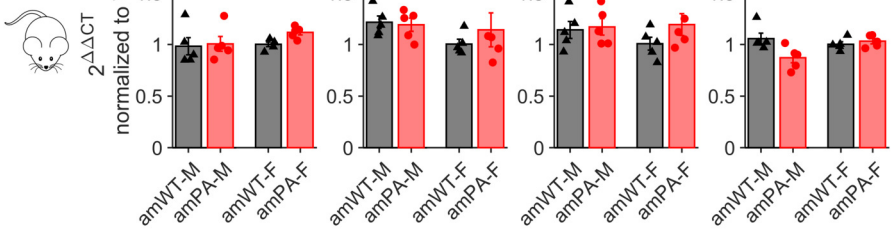
Pde1a
Pde1c
Pde2a
Pde5a
$2^{\Delta\Delta CT}$ normalized to WTF
0
0.5
1
1.5
2
amWT-M
amPA-M
amWT-F
amPA-F

C

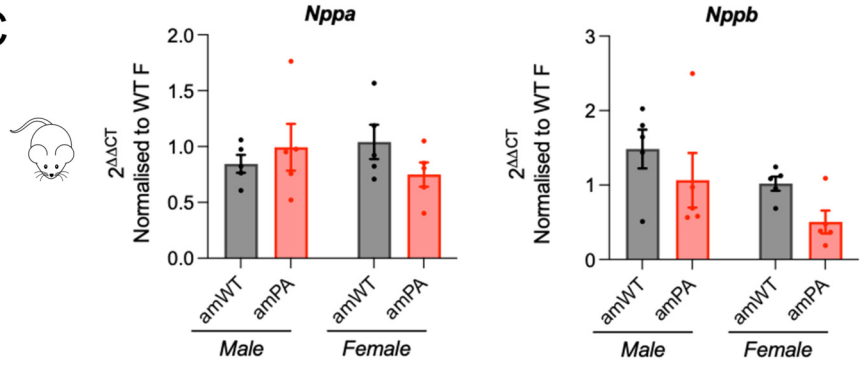
Nppa
Nppb
$2^{\Delta\Delta CT}$ Normalised to WT F
0.0
0.5
1.0
1.5
2.0
0
1
2
3
amWT
amPA
Male
Female

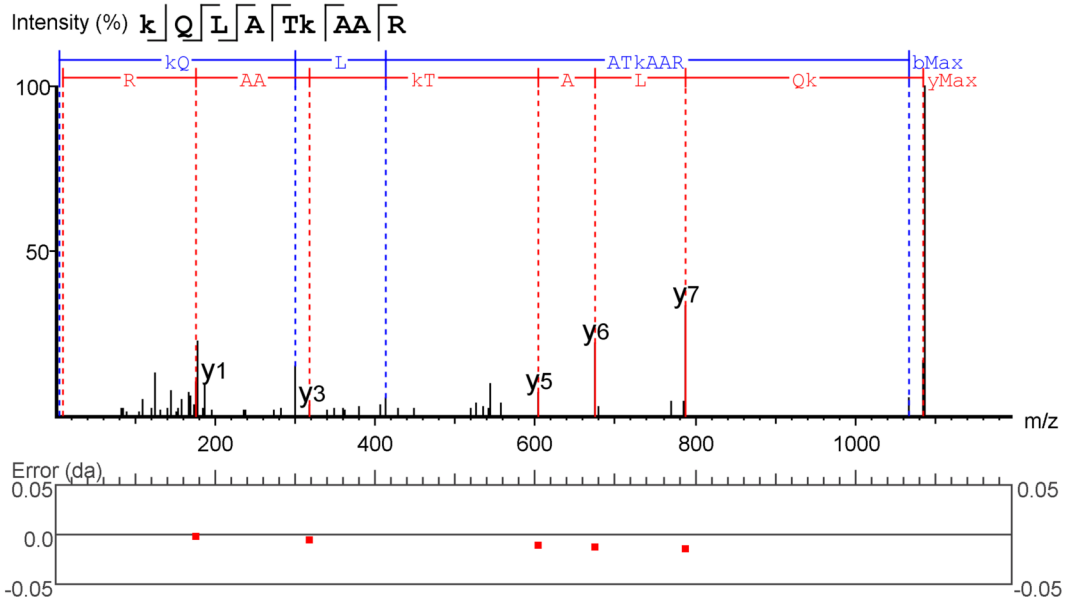
Intensity (%)
k Q L A Tk AA R
kQ
L
ATkAAR
bMax
R
AA
kT
A
L
Qk
yMax
100
50
y1
y3
y5
y6
y7
200
400
600
800
1000
m/z
Error (da)
0.05
0.0
-0.05
0.05
-0.05

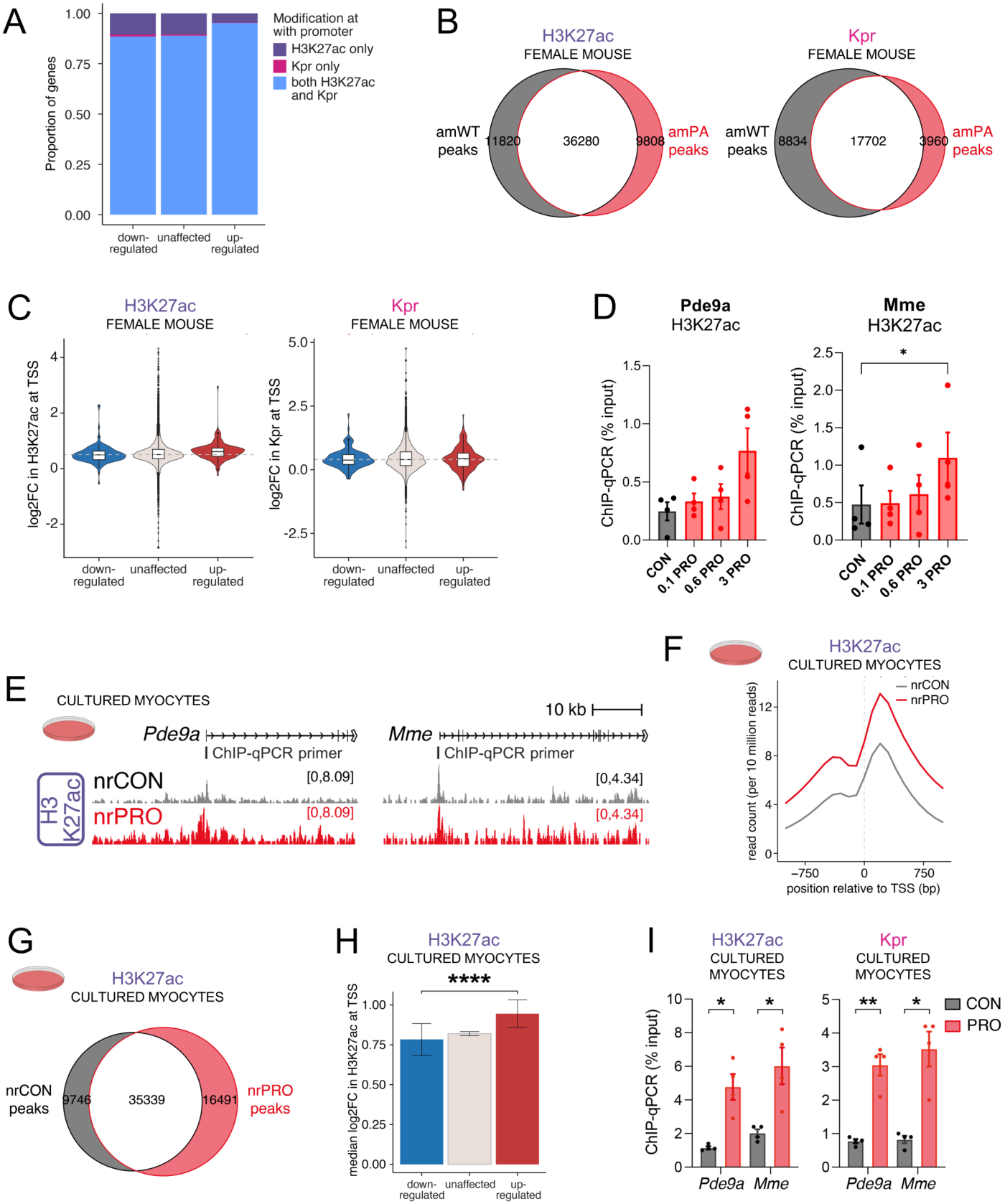
A
Proportion of genes
1.00
0.75
0.50
0.25
0.00
down-regulated
unaffected
up-regulated
Modification at with promoter
H3K27ac only
Kpr only
both H3K27ac and Kpr
B
H3K27ac
FEMALE MOUSE
amWT peaks
11820
36280
9808
amPA peaks
Kpr
FEMALE MOUSE
amWT peaks
8834
17702
3960
amPA peaks
C
H3K27ac
FEMALE MOUSE
log2FC in H3K27ac at TSS
Kpr
FEMALE MOUSE
log2FC in Kpr at TSS
down-regulated
unaffected
up-regulated
D
Pde9a
H3K27ac
ChIP-qPCR (% input)
CON
0.1 PRO
0.6 PRO
3 PRO
Mme
H3K27ac
*
E
CULTURED MYOCYTES
10 kb
Pde9a
ChIP-qPCR primer
Mme
ChIP-qPCR primer
H3K27ac
nrCON
[0,8.09]
nrPRO
[0,8.09]
[0,4.34]
[0,4.34]
F
H3K27ac
CULTURED MYOCYTES
nrCON
nrPRO
read count (per 10 million reads)
−750
0
750
position relative to TSS (bp)
G
H3K27ac
CULTURED MYOCYTES
nrCON peaks
9746
35339
16491
nrPRO peaks
H
H3K27ac
CULTURED MYOCYTES
****
median log2FC in H3K27ac at TSS
down-regulated
unaffected
up-regulated
I
H3K27ac
CULTURED MYOCYTES
ChIP-qPCR (% input)
Pde9a
Mme
Kpr
CULTURED MYOCYTES
CON
PRO